Petroleum Science 20 (2023) 2605–2636

Contents lists available at ScienceDirect

Petroleum Science

journal homepage: www.keaipublishing.com/en/journals/petroleum-science

Review Paper

Gas storage in shale pore system: A review of the mechanism, control and assessment

Yue Feng [a, 1], Xian-Ming Xiao [a, 1, *], En-Ze Wang [b], Ping Gao [a], Chen-Gang Lu [a], Gang Li [a]

[a] School of Energy Resources, China University of Geosciences (Beijing), Beijing, 100083, China
[b] School of Earth and Space Sciences, Peking University, Beijing, 100871, China

ARTICLE INFO

Article history:
Received 13 October 2022
Received in revised form
16 February 2023
Accepted 18 May 2023
Available online 22 May 2023

Edited by Jie Hao and Teng Zhu

Keywords:
Shale gas
Retention mechanism
Multi-component adsorption
Influencing factors
Evaluation method

ABSTRACT

In the past 15 years, the shale gas revolution and large-scale commercial developments in the United States have driven the exploration and development of shale plays worldwide. Among many factors affecting shale gas exploration potential, the gas-bearing properties of shale (quantity, storage state, composition) and their controlling factors are the essential research attracting wide attention in the academic community. This paper reviews the research progress on the retention mechanism, influencing factors, and evaluation methods for resource potential of the shale gas system, and proposes further research directions. Sorption is the main mechanism of gas retention in organic-rich shales; the gas is mainly stored in nanopores of shale in free and sorption states. The presence of water and non-hydrocarbon gases in pores can complicate the process and mechanism of methane (CH_4) sorption, and the related theoretical models still need further development. The *in-situ* gas content and gas-bearing properties of shale are governed by the geological properties (organic matter abundance, kerogen type, thermal maturity, mineral composition, diagenesis), the properties of fluids in pores (water, CH_4, non-hydrocarbon gases), and geological conditions (temperature, pressure, preservation conditions) of the shale itself. For a particular basin or block, it is still challenging to define the main controlling factors, screen favorable exploration areas, and locate sweet spots. Compared to marine shales with extensive research and exploration data, lacustrine and marine-continental transitional shales are a further expanding area of investigation. Various methods have been developed to quantitatively characterize the in-situ gas content of shales, but all these methods have their own limitations, and more in-depth studies are needed to accurately evaluate and predict the in-situ gas content of shales, especially shales at deep depth.

1. Introduction

The progress of horizontal drilling technology, multistage hydraulic fracturing and other engineering techniques has brought about the successful American shale gas revolution, which has gradually put America on the road to energy independence. This has encouraged extensive attention into unconventional resource exploration worldwide (Soeder and Borglum, 2019; Han et al., 2021a; Wang et al., 2022). From the exploration and development achievements of the United States, shale gas has become one of the realistic replacement resources for conventional petroleum resources. In 2021, shale gas production in the United States exceeded 7.638×10^{11} m^3 (Novi Labs, 2022; Zou et al., 2022a); By 2050, it is expected that more than 92% of dry natural gas production in the United States will come from tight and shale gas resources, which can reach 1.11×10^{12} m^3 (U.S. Energy Information Administration, 2022). Inspired by the success of shale gas exploitation in the United States, Canada, Argentina, and China have successively realized the commercial exploration and development of shale gas resources (Fig. 1) (Zou et al., 2021). Systematic research and industrial exploration of shale gas in China started relatively late (Zou et al., 2010), but considerable shale gas resources have been found in many petroliferous basins, with about 4.3×10^5 km^2 favorable for exploration (Gao et al., 2021). In particular, exploration breakthroughs in shallow-middle shale gas reservoirs have been

* Corresponding author.
E-mail address: xmxiao@cugb.edu.cn (X.-M. Xiao).
[1] These authors contribute equally to this work.

https://doi.org/10.1016/j.petsci.2023.05.012

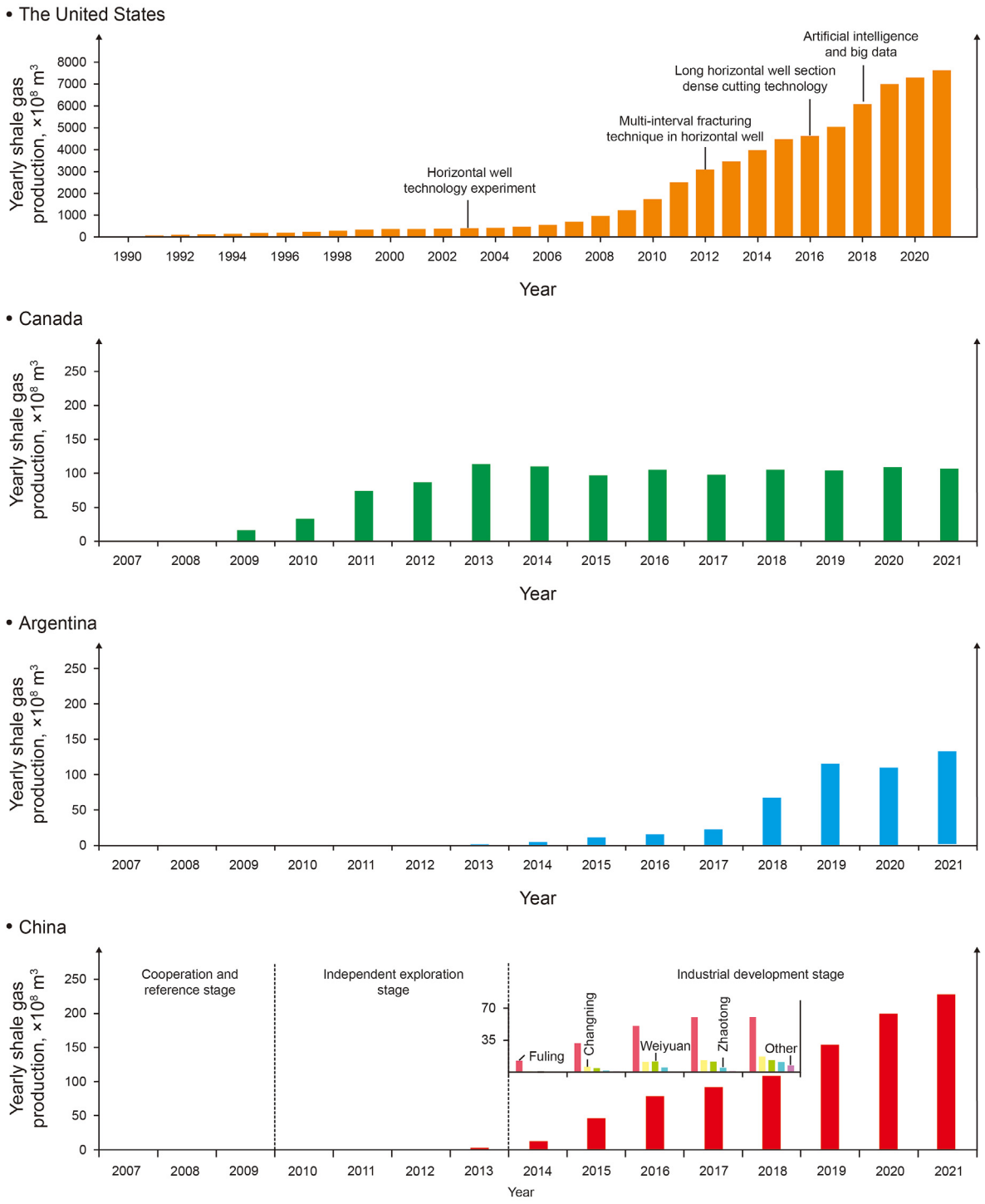

Fig. 1. Annual production trend of shale gas mining countries (the production data of the United States, China, Canada and Argentina are from Gao et al., 2021; Canada Energy Regulator, 2022; Novi Labs, 2022; Secretaría de energía, 2022; Zou et al., 2021, 2022a).

achieved in the Sichuan Basin and its periphery, and the daily shale gas production can reach 3×10^7 m^3 (Ma et al., 2021b). Deep marine shale reservoirs, marine-terrestrial transitional and continental shale systems also have notable exploration and development potential in China where the recoverable resources of continental shale gas are 3.85×10^{12} m^3 (Sun et al., 2021a). The shale gas resource in marine-terrestrial transitional shale systems could reach 1.98×10^{13} m^3 (Yin et al., 2021). Exploration for deep marine shale gas reservoirs (3500–4500 m) is concentrated in and around the Sichuan Basin (Ma et al., 2021b), and the recoverable reserves are expected to reach 9×10^{11} m^3 (Zou et al., 2021). These new exploration targets have become new expansion fields for shale gas (Zou et al., 2021).

Shale gas is extracted directly from organic-rich shale, which distinguishes it from conventional natural gas (Zou et al., 2010). In recent years, research on shale gas has become a hot topic in

petroleum geology, and an increasing number of studies on shales has been performed in which Chinese researchers have made an important contribution (Fig. 2). Especially the gas storage mechanism of organic-rich shale (Chalmers and Bustin, 2010; Hao et al., 2013; Sheng et al., 2014; Wang et al., 2016b; Zhou et al., 2017a, 2017b; Li et al., 2018a; Ju et al., 2019; Tang et al., 2019a; Dang et al., 2020; Klewiah et al., 2020; Zhu et al., 2020; Hu et al., 2021b; Mu et al., 2022), the nanosized pore structure characteristics (Loucks et al., 2012; Rine et al., 2013; Tian et al., 2013; Zolfaghari et al., 2017; Ji et al., 2019; Borjigin et al., 2021), factors influencing gas content in shale (Ross and Bustin, 2008; Bustin et al., 2009; Hao et al., 2013; Xiao et al., 2015; Ma et al., 2018; Yi et al., 2019; Fan et al., 2020; He et al., 2020; Jiang et al., 2020; Sun et al., 2021b), and evaluation of *in-situ* gas-bearing characteristics (Ambrose et al., 2012; Gasparik et al., 2012; Cerri et al., 2015; Pan et al., 2016; Su et al., 2017; Dang et al., 2018; Chen et al., 2019a, 2020b; Yao et al., 2019; Zhou et al., 2022b; Miao et al., 2022) have been the foci of research. This paper summarizes these theoretical understanding and technological developments, focusing not only on the relevant progress, but also suggesting directions for further research, in order to provide a deeper understanding of shale gas geological theory for the benefit of further exploration and development.

2. Retention mechanism of gas in shale

2.1. Occurrence state of shale gas

Clay minerals, brittle minerals, and organic matter (OM) in organic-rich shale contain a variety of nano- and micron-sized storage spaces: Organic pores, inorganic pores (intergranular pores and intragranular pores), mixed pores of OM and inorganic matter, and microfractures (Loucks et al., 2012; Ji et al., 2019; Borjigin et al., 2021). However, the shale gas reservoir is dominated by the nanosized pore system, ranging from a few to hundreds of nanometers (Zou et al., 2012; Tian et al., 2013), furthermore, micropores (< 2 nm) and mesopores (2–50 nm) are the most developed in shale (Kuila and Prasad, 2013; Wang et al., 2014). OM pores are an important shale gas occurrence space, the shapes of pores being various (from circular to angular) (Borjigin et al., 2021), and the size is relatively small. For example, the statistical results of pore size distribution by Rine et al. (2013) show that most organic pores are less than 100 nm; Bai et al. (2013) observed through SEM images that the majority of pores in OM were submicron-sized (5–100 nm); Chen et al. (2013) studied the visualization of microscale pores in kerogens and suggested that the nano-sized pores with pore size less than 100 nm could reach 92.7% of the total

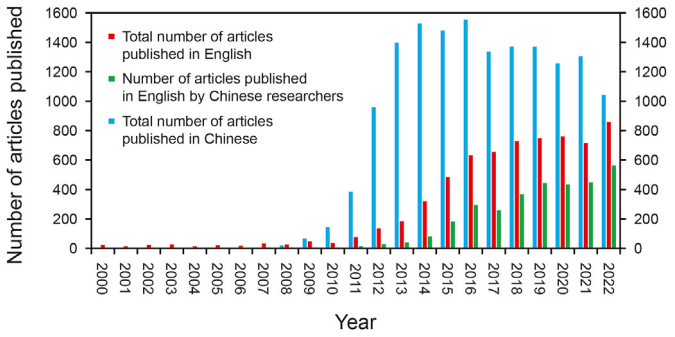

Fig. 2. Statistical histogram of the literature on shale gas research. The data of Chinese articles (blue column) come from China National Knowledge Infrastructure (CNKI), the data of English articles come from ScienceDirect, the red column represents total data, and the green column represents researchers from Chinese research institutions. The search methods are all through title, abstract and keywords.

number of pores; according to the analysis of Kang et al. (2011), OM pore space is mainly composed of micropores and mesopores, with an average size below 4–5 nm; Zolfaghari et al. (2017) suggested that organic pores (with an average pore size of ~3 nm) were smaller than inorganic pores (~10 nm).

There has been a relatively unified understanding of the occurrence states of shale gas: it is stored in large pores and/or microfractures in the free state (Jarvie et al., 2007; Bustin et al., 2009; Zhu et al., 2021b), adsorbed on the surface of OM and inorganic minerals in the sorption state, and dissolved in kerogen, pore water, and retained oil (Loucks et al., 2009; Ross and Bustin, 2009; Hao et al., 2013; Li et al., 2018b; Guo et al., 2020a). Given the low solubility of methane (CH_4) in water (Wang et al., 2011; Zhou et al., 2022a), and the retained oil in shale is basically cracked in high-mature to over-mature stages, gas in commercially developed shale gas reservoirs mainly exists in the free and sorption states (Curtis, 2002; Ross and Bustin, 2008; Wang et al., 2011). However, the ratio of adsorbed to free gas varies greatly in different shale gas plays (Fig. 3), being not only related to gas content of the shale, but is also controlled by various geological and geochemical factors (Wang et., 2011; Hao et al., 2013; Zhang et al., 2019).

2.2. Adsorption mechanism of CH_4

The adsorption on shale, capillary sealing and low-speed diffusion of shale gas from micro retention are the enrichment mechanisms of shale gas (Borjigin et al., 2017). Among them, adsorption is the most essential mechanism of shale gas retention (Rani et al., 2019), which makes it different from tight gas. Nano- and micron-sized pores in shale provide large internal surface area and confined space, which facilitates gas binding to the pore surface (Klewiah et al., 2020), so CH_4 tends to accumulate near the pore wall (Ju et al., 2019). Chen et al. (2017) believes that there is a strong interaction force between CH_4 molecules and OM pores because as the distance between CH_4 molecules and the pore walls is less than 2 nm, CH_4 molecules are in an adsorption state under the influence of the interaction force, which can be attributed to the fact that the heat of adsorption on small pores is higher than that on large pores (Yang et al., 2018). Compared with mesopores and macropores, micropores can provide larger surface area and adsorption potential, thus having stronger CH_4 adsorption capacity. The study of Li et al. (2019a) shows that the proportion of adsorbed gas in pores less than 1 nm can reach 90%.

The adsorption process of shale gas is accompanied by change of entropy and enthalpy of the adsorption system, an exothermic process. Based on the excessively negative adsorption entropy values observed for Woodford kerogen (Zhang et al., 2012), it is considered that there may be a small amount of chemical interaction or chemical adsorption between CH_4 and kerogen in these samples. However, it is generally believed that the main adsorption process of CH_4 on shale is physical adsorption, with no obvious chemical interaction with the solid surface (Xia and Tang, 2012), and is controlled by the physical bond (van der Waals force) between gas and solid molecules (Chen et al., 2019c; Jiang et al., 2021a), the gas-solid interface having low adsorption energy (8–41 kJ/mol gas) (Ho et al., 2014). In order to clarify the mechanism and adsorption process of CH_4 in shale, the thermodynamic parameters of CH_4 adsorption are usually used. The physical (van der Waals force) bonding properties of CH_4 and solid molecules lead to a negative correlation between isosteric heat of adsorption and adsorption entropy, with an increase of adsorbate-adsorbent binding energy (corresponding to ΔH), which leads to the weakening of the fluidity of the adsorbed phase, and thus a more negative standard adsorption entropy is obtained (Gasparik et al., 2014; Li et al., 2018a). This negative correlation is prevalent in

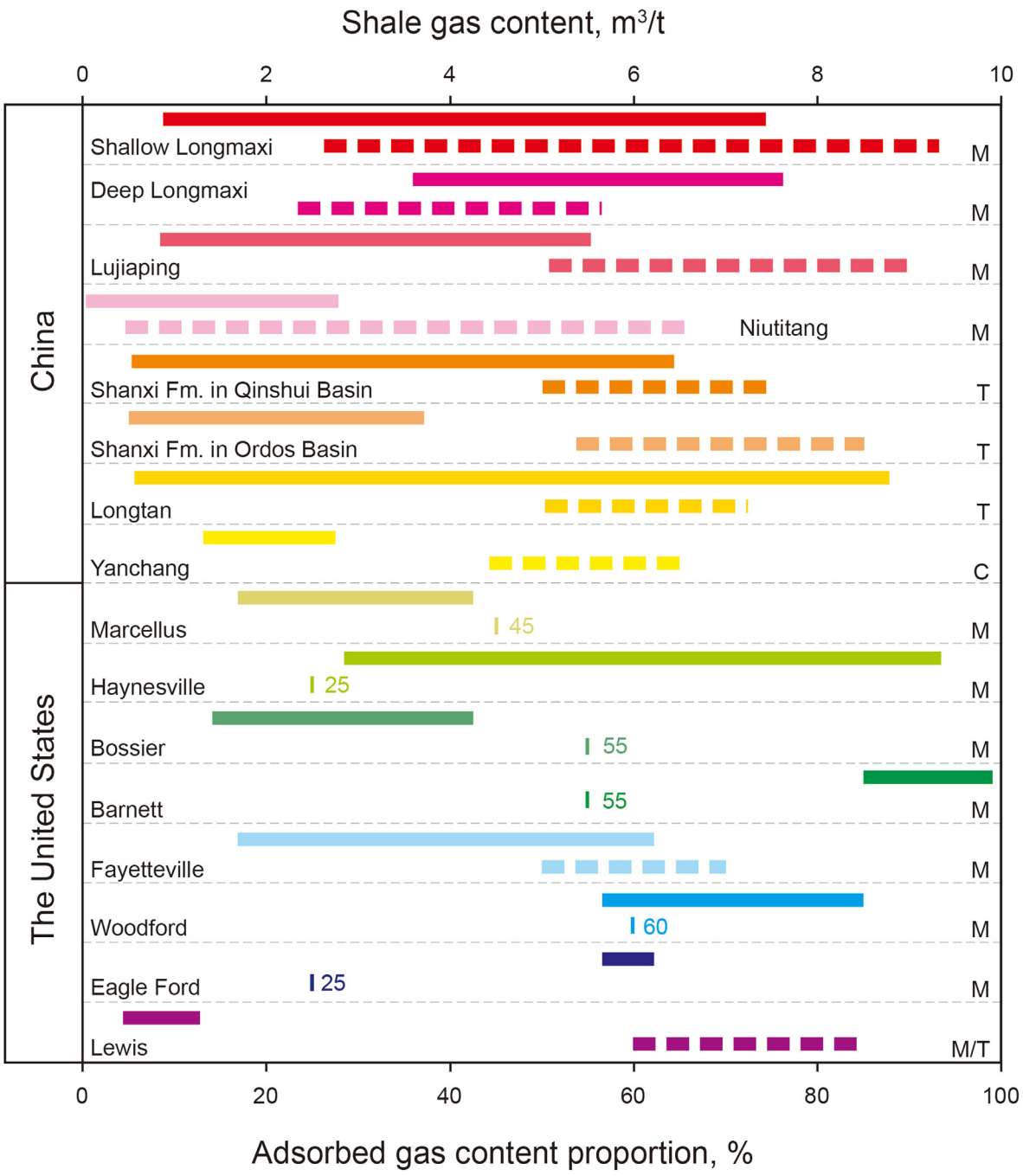

Fig. 3. Shale gas content and proportion of adsorbed gas of typical shale gas reservoirs in China and the United States (data from Curtis, 2002; Jarvie, 2012; Ma et al., 2015; Guo et al., 2019b; Zhang et al., 2019; Li et al., 2020d; Zhai et al., 2020; Shao et al., 2021; Sun et al., 2021b; Zhang et al., 2021). M, T and C represent marine shale, marine-continental transitional shale and continental shale, respectively. The solid line shows the shale gas content, m^3/t; the dotted line shows the proportion of adsorbed gas, %.

clay minerals, kerogen and shales (Li et al., 2018a; Chen et al., 2019c). The relevant data reported at present are summarized in Fig. 4 (Ji et al., 2012, 2015; Zhang et al., 2012; Gasparik et al., 2014; Rexer et al., 2014; Yang et al., 2015; Tian et al., 2016, 2017; Zou et al., 2017; Li et al., 2018a; Shabani et al., 2018; Chen et al., 2019c; Hu and Mischo, 2020; Qiao et al., 2020; Hu et al., 2021b; Huang et al., 2022a). Therefore, the adsorption intensity can be measured by the adsorption heat, and a higher adsorption heat indicates stronger adsorption. Some researchers have pointed out that the adsorption heat of CH_4 on kerogen is greater than that of clay minerals (Ji et al., 2012), although some studies have pointed out that the adsorption heat of some isolated kerogen (8.46–21.90 kJ/mol) in shale is slightly lower than that of clay minerals (9.60–16.60 kJ/mol) (Li et al., 2018a). The dissolution of CH_4 in OM, the small pore size and the hydrophobicity of OM may make organic pores have a stronger gas adsorption capacity than inorganic mineral pores (Ross and Bustin, 2009; Qi et al., 2017; Lawal et al., 2020). In addition, Yang et al. (2018) noted that the adsorption performance of shale shows a parabolic-like trend of decreasing first and then increasing with the evolution of thermal maturity, which is closely related to the evolution of pores, especially micropores.

The critical temperature and pressure of CH_4 are 190.4 K and 4.69 MPa, respectively. Shale gas (including adsorbed gas and free gas) under geological conditions mostly exists as supercritical fluid (Tang et al., 2019a; Hu et al., 2021b). The adsorption of supercritical CH_4 on organic-rich shale is thermodynamically spontaneous, and the degree of disorder of CH_4 gas at the gas/solid interface decreases during the adsorption process. Its physical properties are very different from subcritical CH_4. The adsorption of CH_4 shale under supercritical conditions follows the Gibbs excess adsorption behavior (Dang et al., 2020). There are many opinions about the supercritical adsorption behavior of shale gas. Bi et al. (2017) believed that under actual geological conditions, the adsorption of shale gas is multi-layer adsorption under the action of intermolecular forces. Other researchers have reported that gas can only adsorb at a single molecular layer under supercritical conditions (Borjigin et al., 2017; Hu et al., 2021a). Because multi-layer adsorption can only occur in the case of condensation or liquefaction of adsorbent, multi-layer adsorption does not occur in supercritical adsorption (Zhou et al., 2017a, 2017b). Sheng et al. (2014) pointed out that supercritical CH_4 is adsorbed in ultra-micropores of kerogen in the form of micropore filling in the low-pressure stage, and exists on the surface of kerogen mesopores and clay mineral macropores in the form of monolayer molecular adsorption in the high-pressure stage. Zhou et al. (2017b) believed that the supercritical adsorption mechanism of shale gas should be either monolayer adsorption or pore filling. Mu et al. (2022) analyzed the competition between monolayer adsorption and microporous filling using the composite model, and indicated that increase of pressure makes monolayer adsorption and microporous filling appear in turn. Obviously, the subject requires to be further explored.

2.3. Adsorption mechanism of CH_4 under water-containing conditions

There is a certain amount of water in the pores of a shale reservoir. Unlike non-polar CH_4 molecules, water molecules attach more strongly to polar materials (Xia and Tang, 2012). Compared with CH_4, the existence of polar groups and exchangeable cations means that clay minerals have greater van der Waals and electrostatic forces on water molecules (Li et al., 2019e). When the coverage of water molecules is less than that of single layer, there is fierce competition between water and CH_4 for adsorption positions on the clay surface (Li et al., 2016a). Water molecules can occupy the adsorption sites provided by clay minerals for CH_4 molecules, resulting in the reduction of adsorption capacity for CH_4 (Zhang and Fu, 2018), which is manifested by coexistence of adsorbed gas, free gas and water (Zhao et al., 2018) (Fig. 5a). Furthermore, the water film formed on the pore surface changes the interaction between CH_4 and the pore surface, forming gas-solid interactions, mixed adsorption of gas-liquid-solid interactions, and solid-liquid-gas interface interactions. Since the interaction intensity of gas-liquid is much lower than the force of gas-solid, it would also reduce the adsorption capacity of shale to CH_4 (Li et al., 2016a; Hu et al., 2018c) (Fig. 5b). With the increase of moisture content, the accessible pores are decomposed into many invalid pores by water molecules. Water reduces the CH_4 adsorption surface area through multi-layer adsorption, and the high gas-water capillary at the pore and throat prevents CH_4 from entering the pores (Gong et al., 2020; Han et al., 2021b), mainly showing the adsorption characteristics of solid-liquid interface (Fig. 5c). However, Gao and Xiong (2021) suggested that the hydrophilic difference between clay minerals and OM seems to have a protective effect on OM with adsorption capacity. Some authors believe that water has no effect on CH_4 adsorption of kerogen, for example, Li et al. (2016b) found that due to the existence of hydrophobic repulsion, water would not condense in organic pores, and thus its water saturation can be ignored. In fact, the recognition of water on the surface of kerogen mainly depends on the composition of its heteroatoms (N, S and O), although the water adsorption capacity of kerogen will decrease with increase of maturity (Lawal et al., 2020). Chalmers and Bustin (2010) suggested that the influence of moisture on CH_4 adsorption capacity may be controlled by hydrophobic and hydrophilic adsorption sites in pores (Fig. 5d). The existence of different oxygen-containing functional groups (the order of increasing hydrophilicity is carboxyl group > phenolic hydroxyl group > alcohol hydroxyl group > carbonyl group > ether bond), especially the −COOH and −OH functional groups still existing in over-mature shale, can adsorb water through hydrogen bonding (Dang et al., 2021). If the content of functional groups in OM is high and/or the water content is high, water molecules may “cluster” or even “condense” in the pores of OM (Liu et al., 2017a; Fan et al., 2018), resulting in the reduction of its adsorption capacity for CH_4.

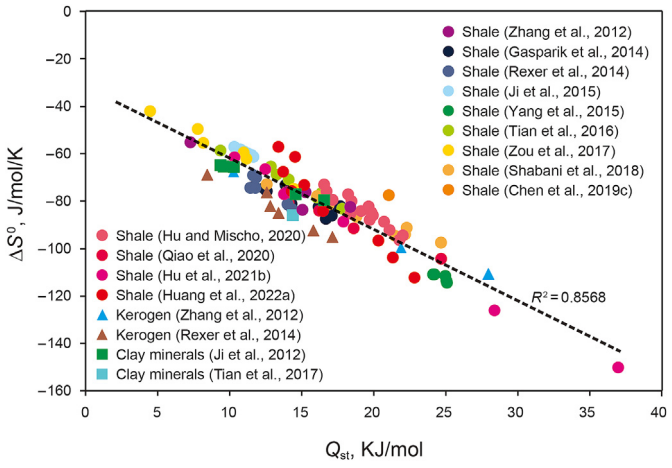

Fig. 4. A possible linear relationship between the standard entropy (ΔS^0) and isosteric heat (Q_{st}) of CH_4. Circles, squares, and triangles represent shale, clay minerals and kerogen, respectively.

Organo-clay composites exist widely in shale systems. In general, clay minerals have the ability to adsorb OM and catalyze hydrocarbon generation, and the OM distributed between clay layers plays a supporting role on protecting primary pores. The pores in organo-clay composites under the protection of rigid mineral skeleton are better developed (Chang et al., 2021). Zhu et al. (2020) believed that clay-organic nanocomposites compared with discrete OM and clay minerals contain more active adsorbent sites for gas. The outer surfaces of organo-clay composites or the inner surfaces of interparticle nanopores can provide sufficient retention space. Moreover, decrease of CH_4 adsorption capacity occurs under higher water content conditions compared with clay minerals free of OM (Gao and Xiong, 2021). In addition, Hu et al. (2021b) found that the organic-inorganic pore surface (trimethylsilane) is hydrophobic, which is more conducive to the adsorption of CH_4 molecules than the isolated organic pore surface.

It can be seen that the adsorption of shale gas could have gas-solid two-phase and gas-liquid-solid three-phase interactions under actual geological conditions. The competitive adsorption of H_2O–CH_4 is influenced by the water content, mineral composition (especially clay mineral content), OM content, pore abundance and pore structure in shale.

2.4. Competitive adsorption of CH_4 and non-hydrocarbon gases

Shale gas contains not only CH_4, but also more or less non-hydrocarbon gases such as carbon dioxide (CO_2) and nitrogen (N_2). The existence of these gases will affect the adsorption of CH_4. CO_2 has the functions of a screen, replacing CH_4, etc. (Wang et al., 2016b). Isothermal adsorption experiments of CO_2 and CH_4 on shale and/or coal samples show that CO_2 always has a higher adsorption capacity than CH_4 (Fig. 6a) (Weniger et al., 2010; Chareonsuppanimit et al., 2012; Heller and Zoback, 2014; Duan et al., 2016; Hwang et al., 2019), which can be attributed to: (1) the smaller size of CO_2 molecules and the better storage capacity in micropores (Kang et al., 2011), (2) the higher ionization potential and polarizability of CO_2 molecules (Wang et al., 2016b), (3) the CO_2 molecule has a strong permanent quadrupole moment and stronger adsorption capacity/affinity (Ortiz Cancino et al., 2017; Takbiri-Borujeni et al., 2017). For example, Huang et al. (2018) noted that the average isosteric heat of CO_2 adsorption (26.1–28.7 kJ/mol) is greater than that of CH_4 adsorption (18.5–20.7 kJ/mol). The thermodynamic analysis of shale by Lu et al. (2021) shows that the adsorption surface energy, free energy and adsorption heat of CO_2 are higher than those of CH_4. The selectivity of shale to binary mixed gases (CH_4 + CO_2) depends on shale composition and/or pore structure (Sun et al., 2021c). Duan et al. (2016) suggested that shale with a high clay mineral content and developed microporous structure may have stronger CO_2 selective adsorption. Řimnáčová et al. (2020) pointed out that the adsorption of CO_2 preferentially depends on the porous structure, but has little to do with the content of OM and clay minerals in shale system.

In contrast, the kinetic diameters of CH_4 and N_2 molecules are relatively large and cannot diffuse in ultra-micropores (< 0.6 nm) (Wang and Tian, 2018). Zhang et al. (2020a) found that CH_4 has a higher adsorption heat than N_2 through activated carbon adsorption experiments, which is attributed to the relatively high polarizability of CH_4 and the greater van der Waals force between CH_4 and the adsorbent surface. More notably, N_2 with low affinity can promote the desorption of CH_4 by reducing the partial pressure of CH_4 (Li and Elsworth, 2019).

The total adsorption capacity of shale for a binary mixed gas (CH_4 + CO_2 or CH_4 + N_2) is between the adsorption capacity of its two constituent pure gases, and the increase in proportion of gas component with stronger adsorption capacity is beneficial to the

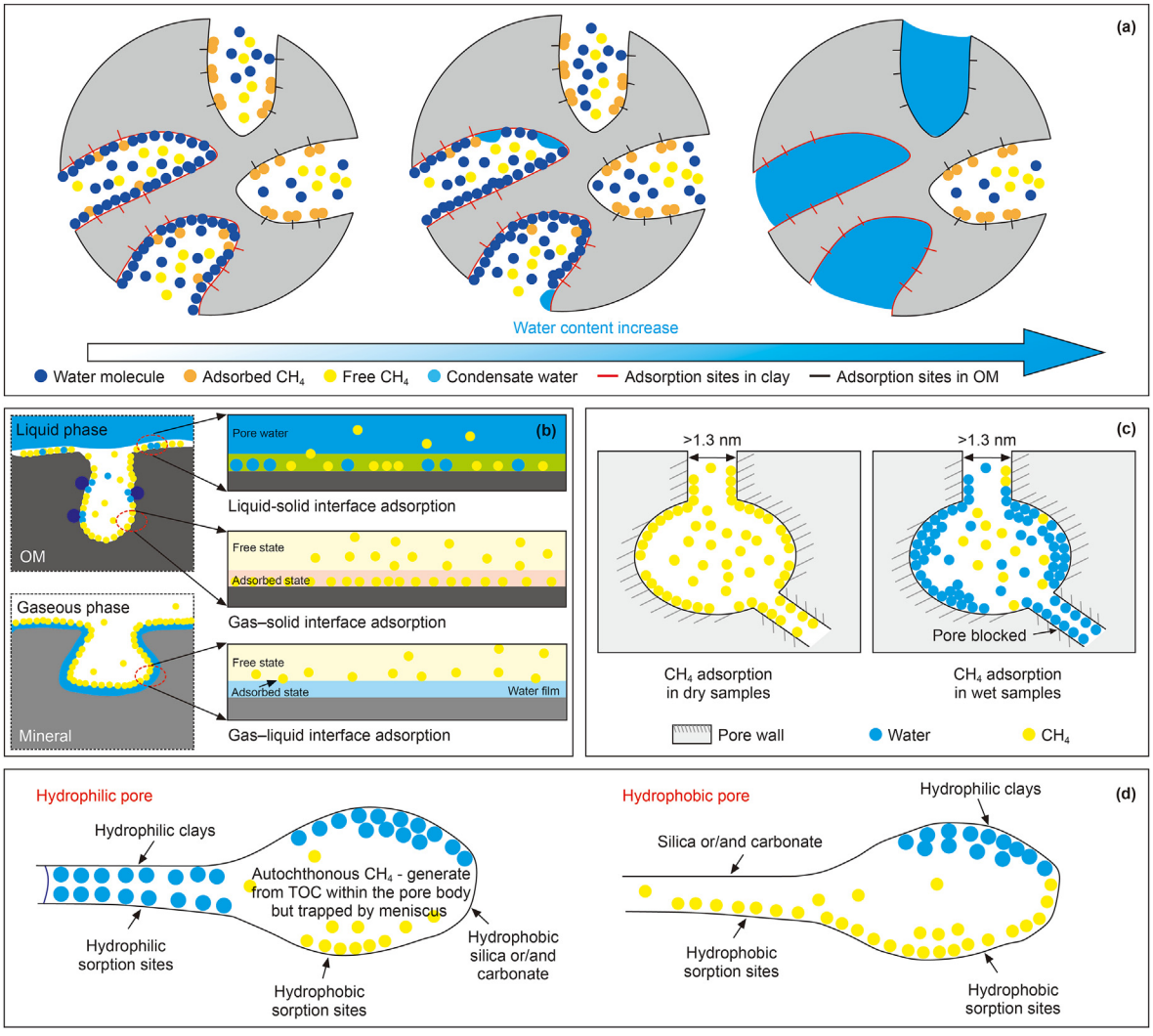

Fig. 5. Schematic diagram of shale gas occurrence under water bearing conditions. (a) Changes of CH_4 and water adsorption in shale pores with increasing water content (modified from Fan et al., 2018); (b) gas-water distribution and interfacial adsorption characteristics in different pores (modified from Li et al., 2020c); (c) differences in CH_4 adsorption between dry and water-bearing pores (modified from Li et al., 2021b); (d) difference in gas-water adsorption characteristics caused by difference in adsorption site properties (modified from Chalmers and Bustin, 2010, AAPG©[2010], reprinted by permission of the AAPG whose permission is required for further use).

increase in the total adsorption capacity (Du et al., 2020; Zhang et al., 2020a) (Fig. 6b). Current research shows that the adsorption capacity of CO_2, CH_4 and N_2 in shale is $CO_2 > CH_4 > N_2$ (Fig. 6a) (Chareonsuppanimit et al., 2012). Therefore, the presence of CO_2 and N_2 will not only affect the total gas adsorption capacity in shale, but also reduce the adsorption capacity of CH_4.

3. Controlling factors of gas retention and storage in shale

The gas bearing properties (quantity, composition and occurrence state) of shale are influenced by various factors. Previous workers have done much research on related issues. We can systematically analyze the influencing factors and restrictive mechanisms of shale gas content from the points of view of geological properties of shale (such as TOC, mineral composition, pore type), moisture content, gas occurrence under geological temperature-pressure conditions, and preservation conditions.

3.1. Influence of shale geological properties on gas bearing properties

3.1.1. OM abundance and type

OM abundance (generally expressed by TOC) is one of the most important parameters in shale oil and gas exploration, and its influence on shale gas is mainly reflected in two aspects: (1) the amount of natural gas generated; (2) it provides a material basis for the generation of organic pores. For shales from different sedimentary environments, the influencing factors and effects of OM abundance are different.

In general, a high OM abundance reflects a great base material and is favorable for hydrocarbon generation. With increasing thermal maturation, OM pores are formed while hydrocarbons are generated. Katz and Arango (2018) proposed that TOC content exerts apparent control over the formation of organic pores. At present, the world's major shale gas producing formations have been deposited in a marine environment, such as the Middle Devonian Marcellus Shale widely distributed in North America, and the Upper Ordovician Wufeng-Lower Silurian Longmaxi shales in China, which are in a high mature to over-mature stage, and in them considerable organic-matter-hosted pores can be observed by SEM (Wei et al., 2019a; Song and Carr, 2020). OM pores may make a major contribution to gas content in some shale samples. For example, Chen et al. (2019b) conducted a quantitative study on the contribution rate of porosity in the Longmaxi shale, observing OM pores contributed nearly half of the porosity in samples with TOC > 4%. With the extensive development of nano pores in OM, therefore, the TOC content is usually positively correlated with pore structure parameters (Fig. 7a and b). Although this correlation may decrease or even reverse under low maturity conditions, the dissolution of residual asphaltene compensates for the decrease in CH_4 adsorption capacity (Ma et al., 2021c). Therefore, the shale gas content is predominately controlled by higher OM abundance, and TOC often exhibits a growing trend with increase of adsorbed gas and total gas contents (Fig. 7c and d). Compared with marine-continental transitional shale and continental shale, marine shale has a better relationship between TOC content and gas content (Fig. 7d), and the correlation line has a larger slope, which can be attributed to its more developed nano-pores and better positive correlation between pore volume (PV), specific surface area (SSA) and TOC content (Fig. 7a and b).

The influence of shale OM abundance in different sedimentary environments on gas content is various (Fig. 7), which may be attributed to the different kerogen types formed in marine, marine-continental transitional, and lacustrine environments. The degree of development of organic-matter-hosted pores is in the order type I> type II > type III of shales with similar thermal maturity (Zhang et al., 2017a; Zeng et al., 2019; Cao et al., 2021). Marine sedimentary environment species are mainly algae, which often form sapropelic kerogen. Humic OM components transformed from higher plants are very common in marine-terrestrial transitional shale due to the influence of marine and river geologic agents (Dong et al., 2021), and type III dominates the kerogen type in marine-terrestrial transitional shale. The organic-rich lacustrine shales deposited in more distal settings within lake systems or in special sedimentary environments (salt lakes, volcanic activities, seawater intrusions, etc.) are more hydrogen-rich, but these shales as a whole have a higher input of terrestrial OM (Katz and Lin, 2014; Zou et al., 2019). At a certain level of maturity, the type of original OM input has a determining control on the pore difference of shales deposited in different sedimentary facies (Gou et al., 2021a; Qiu et al., 2021). Moreover, marine shale has more developed OM pores than that of transitional shale and continental shale (Fig. 8a–f).

Nano pores of various types of macerals/OM in shale develop differently (Loucks et al., 2012; Ko et al., 2018; Luo et al., 2020; Chang et al., 2021). Solid bitumen and/or hydrogen-rich kerogen are the major development sites of organic pores (Curtis et al., 2012; Borjigin et al., 2021; Luo et al., 2021). Sapropelic matter (generally type I kerogen) widely developed in marine shale

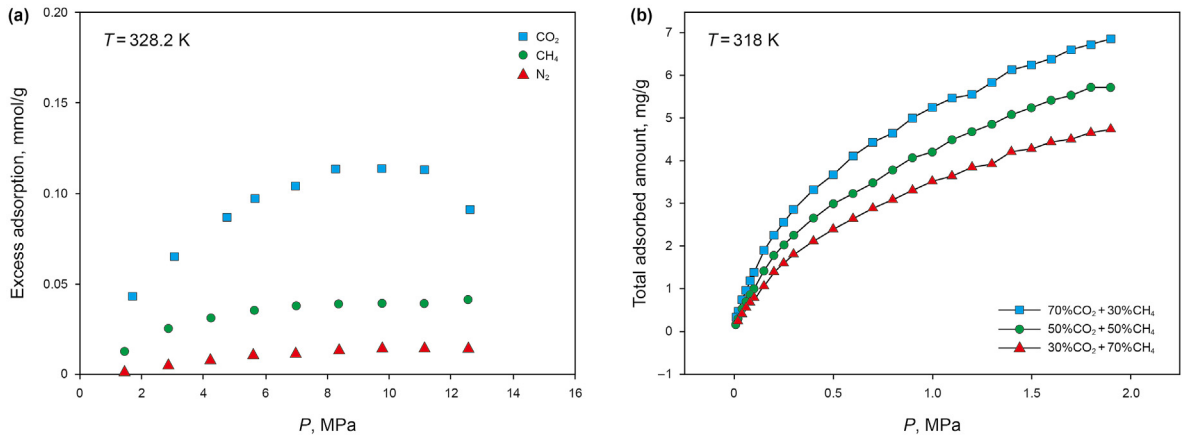

Fig. 6. (a) Comparison of adsorption of CO_2, N_2 and CH_4 by shale (Chareonsuppanimit et al., 2012); (b) comparison of adsorption on shale of mixed gases with different proportions of CO_2 and CH_4 (Duan et al., 2016, reprinted (adapted) with permission from {Duan, S., Gu, M., Du, X.D. et al., 2016. Adsorption equilibrium of CO_2 and CH_4 and their mixture on Sichuan Basin shale. Energy & Fuels. 30 (3), 2248–2256}. Copyright {2016} American Chemical Society).

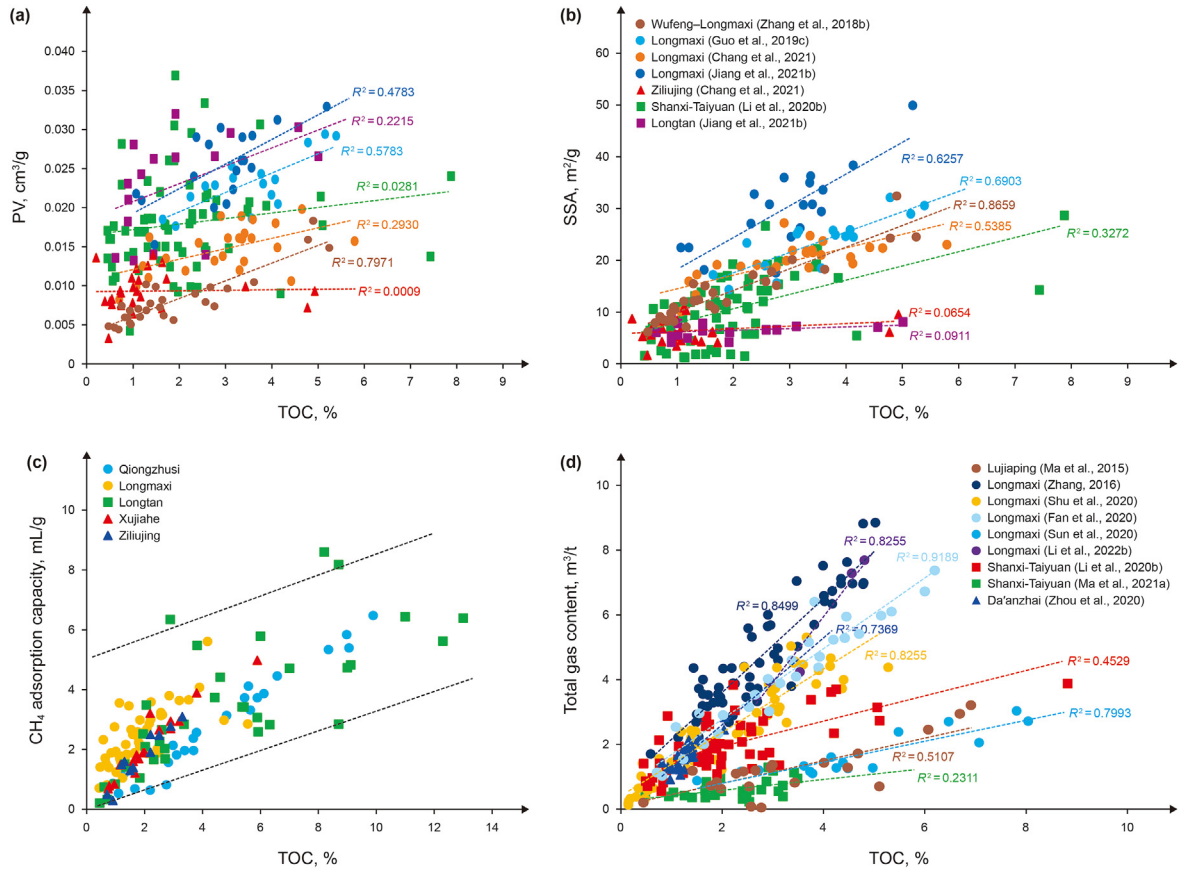

Fig. 7. Relationship between TOC and (a) PV, (b) SSA (data from Zhang et al., 2018; Guo et al., 2019c; Li et al., 2020b; Chang et al., 2021; Jiang et al., 2021b); (c) CH_4 adsorption capacity (modified from Tang et al., 2021); (d) total gas content (data from Ma et al., 2015; Zhang, 2016; Fan et al., 2020; Li et al., 2020b; Shu et al., 2020; Sun et al., 2020; Zhou et al., 2020; Ma et al., 2021a; Li et al., 2022b) of organic-rich shale. Circles, squares, and triangles represent marine shale, marine-continental transitional shale, and continental shale, respectively.

exhibits a high pore-generation ability (Chen et al., 2015), forming a large number of nano pores on the surface under sufficient gas-expansion-force during hydrocarbon generation (e.g. hydrocarbon-bubble pores, Yang et al., 2016a) (Fig. 8a and d), and migrated OM, widely distributed in shale, may also have a well-developed pore system (Ko et al., 2017; Wei et al., 2020a; Zhang et al., 2020b). In general, the organic devolatilization pores are not well-developed in humic OM dominated by vitrinite and chitinite during thermal evolution due to its macromolecule cross-linked structure (Yang et al., 2019). On the contrary, they mainly form microcracks or shrinkage cracks (Fig. 8b and e, i.e. hydrocarbon shrinkage cracks, Yang et al., 2016a). Ardakani et al. (2018) observed with scanning electron microscopy that OM similar to type III kerogen has no obvious pores in its structure with increasing thermal maturity. This is related to the low hydrocarbon generation capacity, underdeveloped migrated OM and poor development of OM pores in shales containing this type of kerogen (Ardakani et al., 2018; Gou et al., 2021a). Continental/marine-continental transitional shale with type II and/or type III kerogen is often dominated by inorganic storage space, and OM pores make little contribution to the total porosity (Gao et al., 2018; Kuang et al., 2020; Xiao et al., 2021). Furthermore, the pore growth in their OM is different in marine, transitional and continental shales, leading to a certain difference in their CH_4 adsorption capacity (Fig. 8g).

3.1.2. Thermal maturity

Maturity not only controls the gas generation, but also changes the reservoir physical properties of shale, thus affecting the gas content. It is generally believed that the process of CH_4 generation from OM in shale ends at approximately vitrinite reflectance $R_o = 3.0\%$ (Chen et al., 2007). With the further increase of maturity, the onset of hydrocarbon destruction occurs (Burnaman and Shelton, 2009) and large amounts of non-hydrocarbon gases may be produced (Krooss et al., 1995; Gai et al., 2020). Obviously, the production of these non-hydrocarbon gases will affect the accumulation of CH_4 in shale. In order to describe the gas generation characteristics in shales more accurately, Gai et al. (2020) applied anhydrous pyrolysis experiments and found that the total N_2 yields began to increase rapidly and CH_4 began to crack when temperature reached 650 °C (equivalent vitrinite reflectance (EqVRo) = 3.4%).

As for the influence of maturity on shale porosity, the general understanding is that when shale maturity enters the wet gas generation stage, the porosity evolution in shale increases first and then decreases (Fig. 9a). There are two main mechanisms that comprehensively control the changes of shale pores: (1) OM pore formation and evolution; (2) inorganic mineral pore formation and destruction. With further increase of maturity, OM generates hydrocarbons and begins to form organic pores, accompanied by dissolution (feldspar and carbonate minerals), and clay mineral recrystallization (such as montmorillonite transformation into illite, etc., Loucks et al., 2012; Kuang et al., 2020), effects that are stronger than the damage to porosity caused by compaction, so overall, porosity gradually increases with the degree of thermal evolution. When the shale enters the highly over-mature stage, carbonization of OM will lead to changes in the OM pore structure

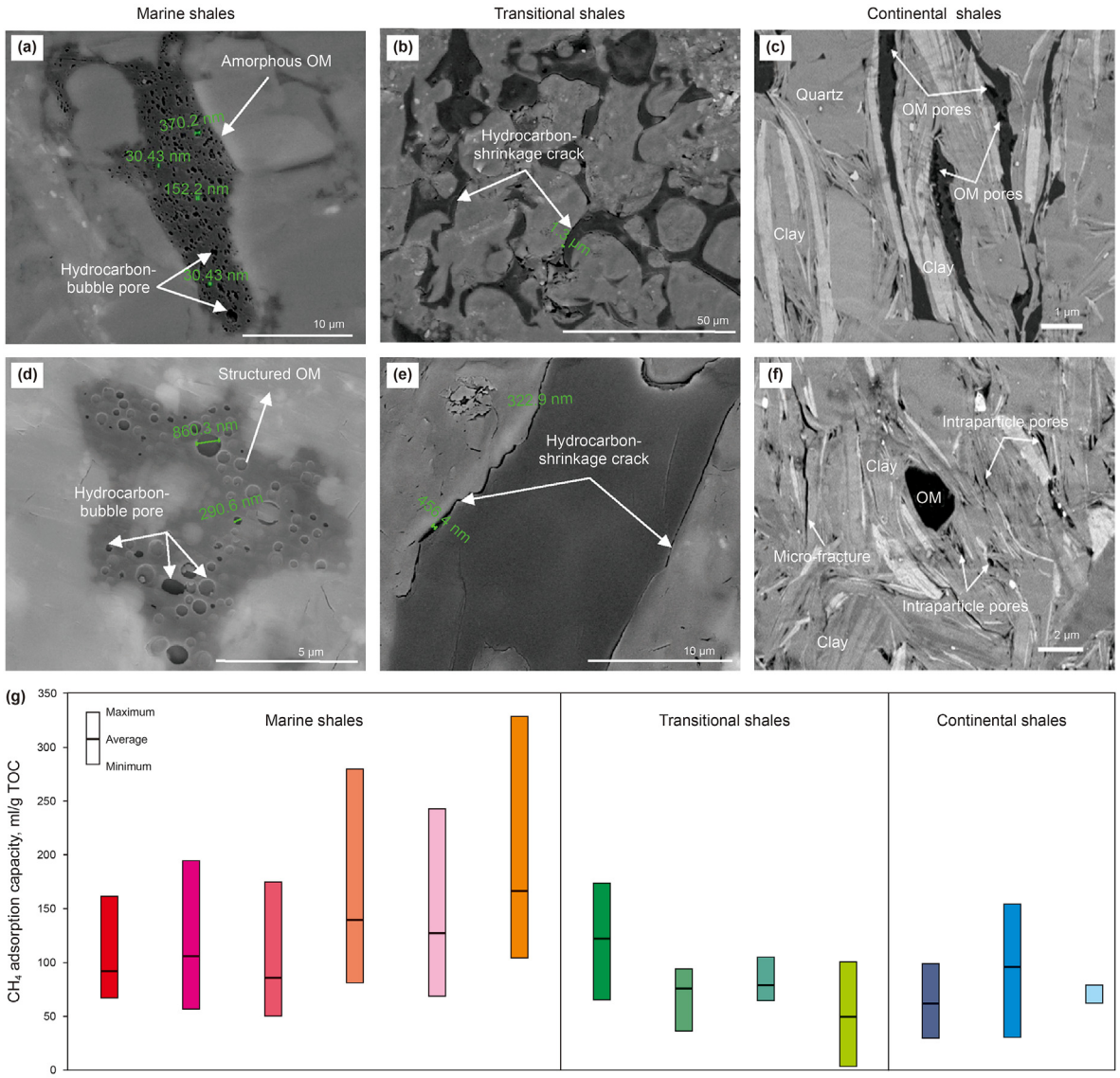

Fig. 8. Comparison of pore development characteristics and adsorption capacity of OM in different types of shale (a-f from Yang et al., 2016a and Gou et al., 2021a, reprinted (adapted) with permission from {Gou, Q.Y., Xu, S., Hao, F. et al., 2021a. Differences in the nanopore structure of organic-rich shales with distinct sedimentary environments and mineral compositions. Energy & Fuels. 35 (20), 16562–16577}. Copyright {2021} American Chemical Society; data in (g) from Li et al., 2016c; Dang et al., 2017; Guo et al., 2017b; Chen et al., 2018; Hu et al., 2018a; Zhang and Fu, 2018; Feng et al., 2019; He et al., 2019; Shi et al., 2019; Yang et al., 2019; Li et al., 2020d; Ma et al., 2020b; Li et al., 2022a). All shale samples were dry, the adsorption experiment temperature was 30 °C, and TOC standardization was performed on the data to eliminate the influence of OM abundance.

(Yang et al., 2016b), the increasing compaction will lead to pore collapse and matrix contraction, which will further destroy the nano-pores (Wei et al., 2019a), and the decrease of both OM-hosted pores and porosity could result from the combined effects of these two mechanisms (Borjigin et al., 2021).

At present, there are still different views on the inflection in the relationship between thermal maturity and porosity. Xiao et al. (2015), based on thermal simulation experiments, combined with geological sample data, proposed that the porosity of marine shale in China would decrease significantly with the further increase of maturity with R_o about 3.5%. Chen et al. (2019b) made comprehensive statistical analysis on multiple sets of porosity and maturity values for marine and continental shales and suggested that porosity reversal would occur when EqVRo was 2.5%–3.0% (Fig. 9a). Wang et al. (2018) studied the marine Longmaxi and Qiongzhusi shales in the Sichuan Basin (China) and found that OM carbonization generally occurs when R_o exceeds 3.5%, when organic pores and clay mineral intergranular pores were substantially reduced or had even disappeared (Fig. 9b). Similar to porosity evolution, pore structure parameters of shale (such as the PV and SSA) are also significantly related to thermal maturity. Chen and Xiao (2014), based on thermal simulation analysis, proposed that with increasing maturity, the micropore PV and SSA in OM-rich shale gradually increase at R_o values below 3.5% and then subsequently decrease.

It should be noted that PV in shale decreases with increase of maturity in the main oil generation stage (Fig. 9c), which may be related to infilling by the generated and retained oil in pores, and kerogen swelling behavior (Mastalerz et al., 2013; Han et al., 2017; Guo et al., 2017a). However, with increase of thermal maturity, the liquid oil and kerogen are further cracked into gaseous hydrocarbons, the asphaltene is ex-solvated, and the large number of OM pores lead to increasing PV and SSA (Loucks et al., 2012; Chen and Xiao, 2014; Guo et al., 2017a). In this process, the influence of

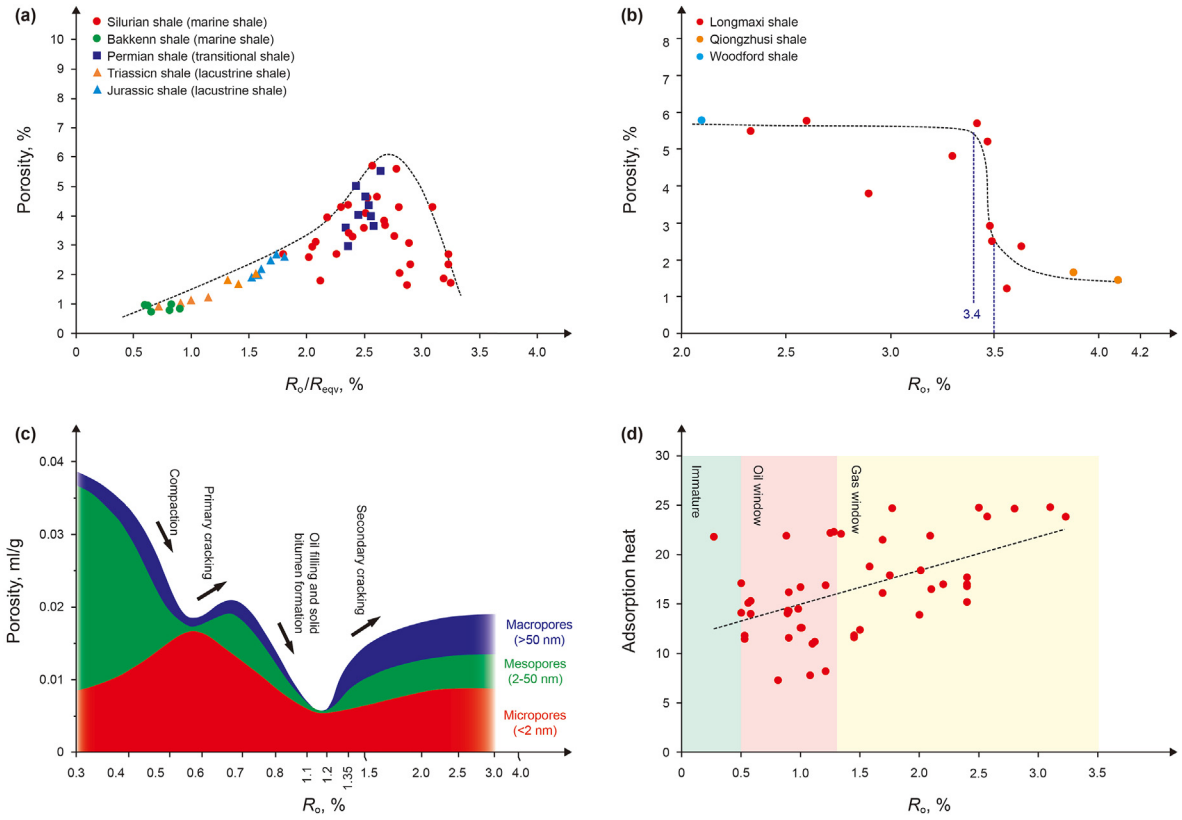

Fig. 9. (a) Relationship between shale porosity and maturity (modified from Chen et al., 2019b; data from Tian et al., 2013; Pan et al., 2015; Yang et al., 2016b; Jiang et al., 2017; Zhang et al., 2017b; Chen et al., 2019b; Liu et al., 2019b); (b) average porosity-Ro correlation in marine organic-rich shales (modified from Wang et al., 2018; data from Jacobi et al., 2009; Wang et al., 2016c; Wang et al., 2018); (c) schematic diagram showing different types of PV change with maturation in shale (modified from Mastalerz et al., 2013, AAPG© [2013], reprinted by permission of the AAPG whose permission is required for further use); (d) the effect of maturity on shale adsorption capacity (modified from Li et al., 2018a; data from Zhang et al., 2012; Gasparik et al., 2014; Rexer et al., 2014; Hu et al., 2015; Yang et al., 2015; Zou et al., 2017; Li et al., 2018a; Shabani et al., 2018).

hydrocarbon expulsion efficiency cannot be ignored, because as it increases, the gas yield will be significantly reduced (Tan et al., 2021), leading to the weakening of OM pore development (Borjigin et al., 2021).

Corresponding to the evolution of porosity and pore structure, maturity has an important impact on the adsorption capacity of shale. After reaching the high over-mature stage, PV and SSA show a decreasing trend, the degree of aromatic polymerization of organic compounds increases and standard enthalpy of sorption has a moderately high value, so its CH_4 adsorption capacity is still higher than that of middle-low maturity shale, as shown in Fig. 9d (Yang et al., 2018; Alafnan et al., 2020; Klewiah et al., 2020). Nonetheless, CH_4 adsorption capacity decreases to a certain extent with higher maturity (for example, EqVRo ≈ 4.0%, Li et al., 2017).

3.1.3. Mineral type and content

Shales are mainly comprised felsic, clay and carbonate minerals. These inorganic components affect shale gas content through their different contributions to pores. Although quartz and carbonate minerals themselves may develop some pores, such as intragranular pores of biogenic quartz and dissolution pores of carbonate minerals, they are mainly skeleton minerals, forming the intergranular pores, which have become essential gas storage spaces (mainly free gas), especially providing protection for the pores of OM and clay minerals. Studies have shown that brittle minerals can support and protect the pores at the edge of brittle mineral particles (Chen et al., 2021c). The existence of rigid matrix skeleton minerals reduces the effective stress on organic particles and is conducive to protection of the OM pores from collapse (Knapp et al., 2020). However, carbonate minerals appear to be less effective than microcrystalline quartz in maintaining porosity, which can be attributed to its numerous sources and relative chemical instability during diagenesis (Knapp et al., 2020), Guo et al. (2019a) studied the Longmaxi Formation shale in the Weiyuan area, Sichuan Basin (China), and showed that shale porosity decreased significantly when the carbonate mineral content was greater than 10%. In addition, quartz of different origins may have different effects on the pore evolution of shale. Although terrigenous quartz can also play a supporting role for pores, it may not be very conducive to the improvement of shale gas reservoir performance due to its potential dilution of OM (Sageman et al., 2003), and occurrences (such as quartz floating in clay skeleton, Xu et al., 2020c). In contrast to the insignificant contribution or even destructive effect of quartz overgrowth and clay matrix-dispersed micro-quartz on shale pores, biogenic quartz plays a constructive role in the development of microscale pores (Xu et al., 2021a). Biogenic quartz can form a continuous rigid siliceous matrix framework characterized by point-to-line contact (Xu et al., 2020c; Li et al., 2021d), which is conducive to hydrocarbon retention (Milliken et al., 2021), forming organic pores in migrated OM (Zhao et al., 2017; Dong et al., 2020) and limiting compaction of pores in ductile OM and clay minerals (Knapp et al., 2020), even after the shale is deeply buried (Delle Piane et al., 2022). For example, deep shale gas reservoirs in the Sichuan Basin (China) have higher surface porosity of organic and inorganic pores than shallower shale strata (Ma et al., 2021b). Therefore, biogenic quartz content is often positively correlated with porosity and gas content (Li et al., 2020d; Guo et al., 2021).

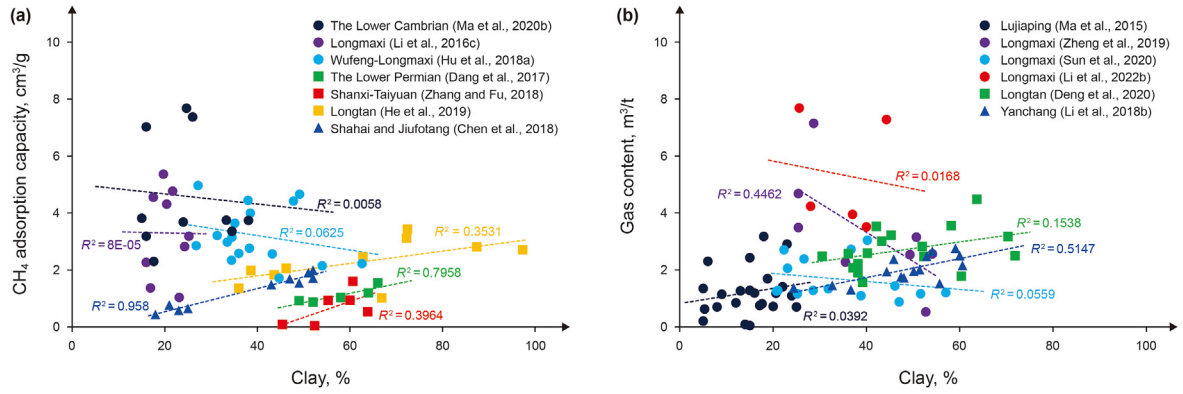

Fig. 10. Relationship between clay mineral content and (a) adsorption capacity (data from Li et al., 2016c; Dang et al., 2017; Chen et al., 2018; Hu et al., 2018a; Zhang and Fu, 2018; He et al., 2019; Ma et al., 2020b) and (b) total gas content (data from Ma et al., 2015; Li et al., 2018b; Zheng et al., 2019; Deng et al., 2020; Sun et al., 2020; Li et al., 2022b) of Chinese gas-bearing shale of different sedimentary facies.

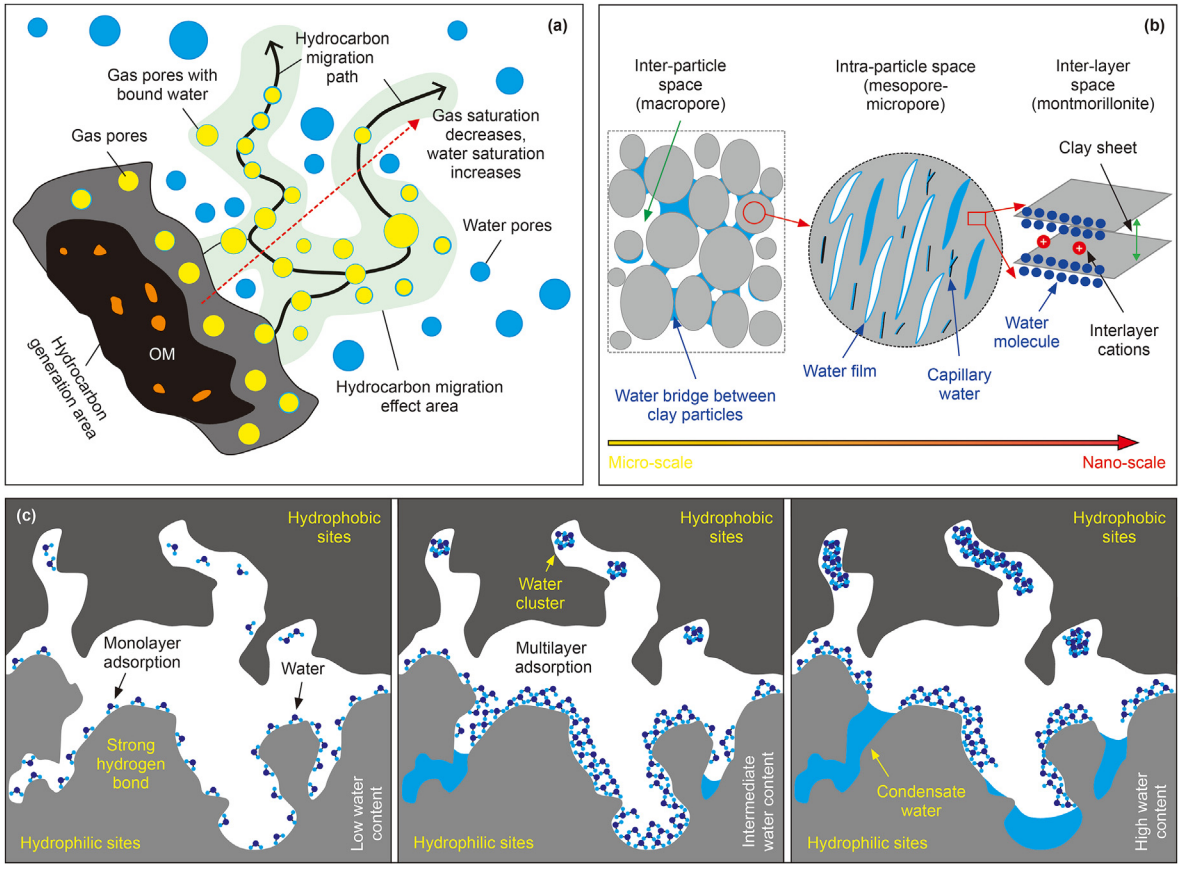

Fig. 11. (a) Fluid distribution pattern in over-mature shale without microfractures (modified from Xu et al., 2019). (b) Water occurrence in three types of pores in clay (modified from Li et al., 2016a). (c) Water distribution in shale pores under different water-bearing conditions (modified from Sang et al., 2019).

Clay minerals play a leading role in the adsorption capacity of inorganic minerals (Xiong et al., 2017; Xiao et al., 2021). The global shale data set suggests that clay may be the main controlling factor for CH_4 adsorption in organic-lean shales with TOC < 2% (Sander et al., 2018). But different types of clay minerals have various adsorption capacities, according to the experimental data of Ji et al. (2012). The gas sorption capacity for clay minerals can be ranked as: montmorillonite ≫ illite/smectite mixed layer > kaolinite > chlorite > illite. However, previous studies have found that the maximum adsorption capacity of marine shale is often negatively correlated with, or is unrelated to clay content (Fig. 10) (Sander et al., 2018; Chen et al., 2021a; Ekundayo et al., 2021). This can be attributed to the negative correlation between clay mineral content and TOC under geological conditions, the advantage of OM in shale adsorption capacity, and the hydrophilicity and/or porosity reduction of clay minerals (Chen et al., 2021c; Sun et al., 2021b). Sun et al. (2020) found that the clay mineral content of marine Longmaxi shale in the Xishui block (Guizhou Province, China) showed a measure of positive correlation with gas-in-place (GIP)/TOC (TOC normalization of GIP), indicating that the pores of clay minerals have a certain

contribution to the in-situ gas volume of marine shale.

For continental and transitional facies shales, clay mineral pores may exert a leading control on porosity, because the nano OM pores are not well developed (Fig. 10). For example, clay minerals-associated pores account for nearly 70% of total porosity in the Lower Jurassic Da'anzhai Member shale (Chen et al., 2019b). Qiao et al. (2020) studied the marine-continental transitional shale of the Ordos Basin (China) and showed that clay minerals control adsorption capacity and porosity, being capable of adsorbing gas on their surface to more than 80%. In addition, marine-continental transitional/continental shales both have strong stratigraphic rhythmicity, and TOC is often proportional to the content of clay minerals (Ma et al., 2018), which magnifies the importance of clay minerals for shale gas enrichment.

3.2. Influence of shale pore water on gas bearing property

Shale reservoirs under in-situ gas accumulation conditions are generally water-bearing and the moisture content is usually quantified by water saturation. The primary water saturation ranges in the Sichuan Basin (China), southern China, Canning Basin (Australia), and Fayetteville Shale (North America) are 25%–75% (Xu et al., 2020a). The occurrence and distribution of water in shale pores are influenced by its composition, the type and structure of pores, and other factors (Zhu et al., 2021a). In the pore system of shale, the isolated pores away from the affected area of hydrocarbon migration are filled with water due to the water displacement of hydrocarbon generation (Xu et al., 2019) (Fig. 11a). Compared with pore size, irreducible water is more closely related to surface chemistry (Seemann et al., 2017), and the existence of clay minerals will affect the distribution of water in shale (Zolfaghari et al., 2017; Mu et al., 2021). Hao et al. (2019) held that water in clay pores exists in the form of a water film or water bridge. Li et al. (2016a), considering the condensation phenomenon, believed that the water in the pores of shale clay occurs in two forms: capillary water in small pores or throats, and water film in larger pores (Fig. 11b). Chen et al. (2019e) believed that the water in micropores exists in the form of volume-filling and surface adsorption, while the water in mesopores and macropores is mainly adsorbed on the surface after reaching the critical value. With the increase of water content, monolayer adsorption occurred, then water molecules adsorbed in multiple layers on hydrophilic pore walls, and water clusters formed in the hydrophobic pore spaces. With further increase of water content, most hydrophilic pores will be gradually filled with condensed water (Sang et al., 2019; Yang et al., 2020) (Fig. 11c). In the non-microporous range, the percentage of water decreases with increase of pore size (Sun et al., 2021b).

Water is distributed differently in assorted pores in shale. Cheng et al. (2018) studied the equilibrium irreducible water content in inorganic and organic pores in overmature Lower Paleozoic organic-rich shale samples from southern China, and found that the former was about twice as high as the latter. Sun et al. (2021b) conducted low-pressure N_2 and CO_2 adsorption experiments on the Lower Silurian Longmaxi shale obtained from the Xishui area, and observed that water accounts for an average of 82% and 41% of the inorganic and organic non-micropore SSAs, and 44% and 18% of PV of inorganic and organic micropores, respectively. Zhu et al. (2021a) found that compared with dry samples, PV and SSA in continental shale samples with 98% relative humidity were reduced by a maximum of 1/2 and 2/3, respectively. Sun et al. (2022) using well-preserved Carboniferous marine-continental transitional shale samples containing primary water in the Qinshui Basin found that the average micropore PV and non-micropore SSA of water-containing samples compared with dry samples were reduced by 50.63% and 70.21%, respectively. The water content of shale is generally positively correlated with the content of clay minerals, but negatively correlated with TOC (Chen et al., 2019e; Sun et al., 2021b). These studies also seem to confirm that organic and inorganic pores have different water wettability and that organic pores are relatively hydrophobic. However, some researchers have found that with increase of TOC content, the equilibrium adsorbed water volume increased significantly (Cheng et al., 2017; Li et al., 2021a). This is because the SSA in these researchers' shale samples is mainly contributed by OM (Li et al., 2019d), and there are hydrophilic points on the surface of organic pores (Wang et al., 2020b). For example, Zhao et al. (2018) showed that kerogen is more inclined to adsorb H_2O than CH_4 through competitive adsorption simulation (at 20 MPa and 298 K). Although the interaction between H_2O and oxygen-containing functional groups is stronger, clay minerals may contribute more to water adsorption because the content of oxygen-containing functional groups is much lower than that of shale clay minerals (Wang et al., 2020b).

It can be seen that water in shale affects not only free gas content but also the adsorbed gas content. The influence of water on free gas is expressed by water saturation in the calculation and is deducted (Ambrose et al., 2012; Ansari et al., 2019). The effects of moisture on CH_4 adsorption have been studied and explored. Three methods are commonly adopted: comparative study on adsorption capacity of as-received and dried shale samples (Fig. 12a and b); CH_4 high-pressure adsorption experiments for moisture-equilibrated samples and dried samples (Fig. 12c); molecular simulation calculations (Fig. 12d). A basic understanding is obtained: an increase in the moisture content suggests a decrease in the adsorption gas capacity (Table 1). Ross and Bustin (2007) did not find that the adsorption capacity of moisture-equilibrated samples decreased continuously with increase of moisture, and suggested that this correlation was masked by the influence of OM and thermal maturity. However, they pointed out that the presence of water would greatly reduce the adsorption capacity of gas. Chalmers and Bustin (2008) found that there seems to be no correlation between water content and CH_4 capacity based on moisture-equilibrated samples, and attributed this to the different adsorption sites occupied by water and CH_4 molecules. Gasparik et al. (2014) found that the sorption capacity of moisture-equilibrated samples (at 97% relative humidity (RH)) was 40%–60% of that of the dry samples. Shale composition makes the reduction of CH_4 adsorption capacity highly variable, mainly due to the loss of active adsorbent sites on clay minerals, and the sorption capacity no longer decreases with increase of water content when the critical moisture content (the critical moisture content is at $\approx$ 50%–75% RH) is reached (Merkel et al., 2015, 2016). Yang et al. (2017) pointed out that the three stages of the adsorption capacity, namely initial decline, sharp decline and slow decline, are the results of the occurrence of the competitive adsorption of CH_4 and water by hydrophilic clay minerals, the blockage of pore space by water molecular clusters and the continuous filling of macropores by a continuous water phase with rising water content. Fan et al. (2018) found that the relationship between CH_4 adsorption capacity and water content can be divided into three stages: linear decline, flat, and convex decline, according to the water content threshold. The appearance of the flat stage is correlated to the fact that the hydrophobic water level is not occupied by water molecules.

3.3. Influence of temperature and pressure on shale gas storage

Overburden stress, as the product of depth, overburden density and gravitational acceleration (Ferrill et al., 2014), is closely associated with the physical properties of shale gas reservoirs, and the porosity subjected to high stress in shale might slump (Gaus et al.,

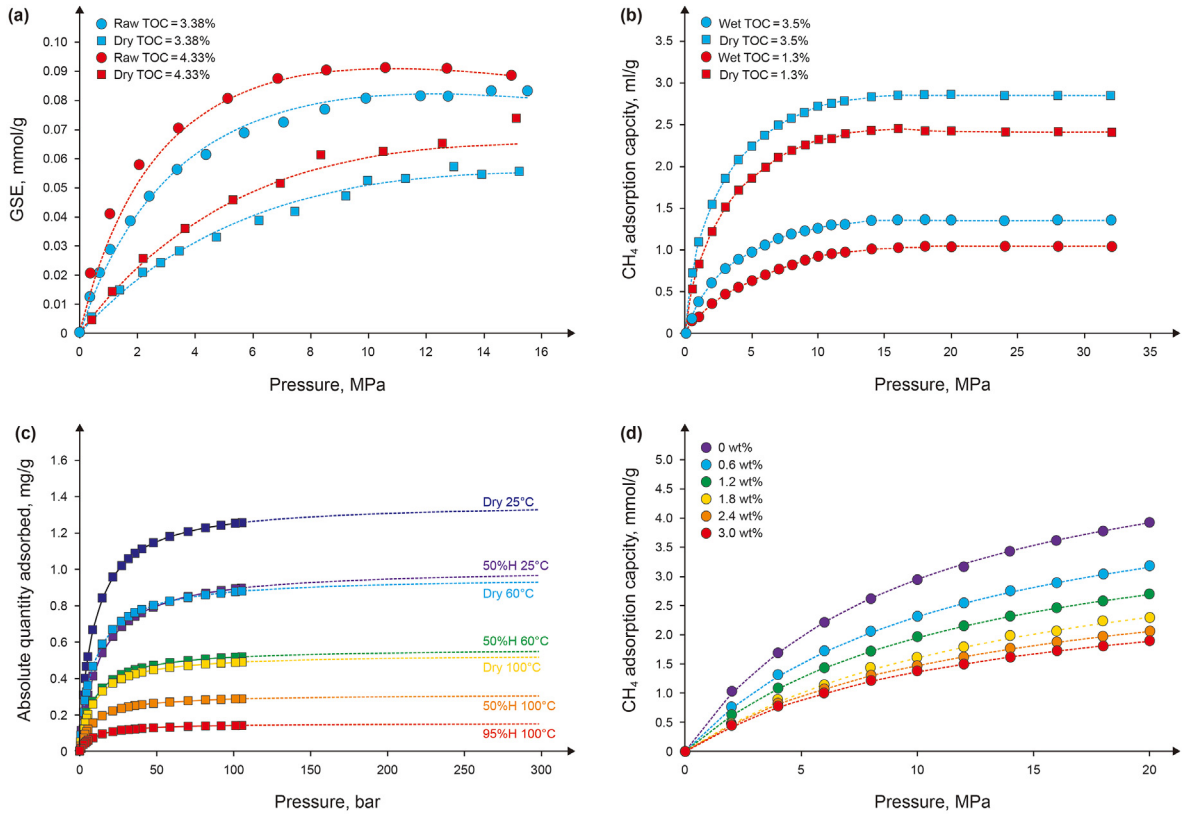

Fig. 12. Comparison of adsorption capacity between aqueous and dry shale. (a) Comparison of isothermal adsorption experimental results between as-received containing primary moisture, and dry marine shale samples (modified from Wang et al., 2020b, reprinted (adapted) with permission from {Wang et al., 2020b. Influences of primary moisture on methane adsorption within Lower Silurian Longmaxi Shales in the Sichuan Basin, China. Energy & Fuels. 34 (9), 10810–10824}. Copyright {2020} American Chemical Society); (b) Comparison of isothermal adsorption experimental results between as-received and dry marine-continental transitional shale samples (modified from He et al., 2019); (c) Comparison of isothermal adsorption experimental results of equilibrium-moisture shale and dry shale (modified from Whitelaw et al., 2019); (d) Molecular simulation results of the effect of water content on CH_4 adsorption in marine type II kerogen ($C_{175}H_{102}O_9N_4S_2$) (modified from Zhao et al., 2018).

2021). The pressure also reduces the adsorption capacity of the adsorbent as the depth increases according to studies (Hol et al., 2011; Gaus et al., 2021). Moreover, free gas content makes a decreasing contribution to GIP when the effect of in-situ stress on pore structure is taken into account (Miao et al., 2022).

The pore-fluid pressure, that is, the pressure acting on the fluid in the formation pore space (Dutta, 2002) has the most direct impact on shale gas accumulation. Thermal simulation experiments show that increased reservoir pressure promotes the development of micropores and fine mesopores (< 10 nm) (Liu et al., 2017b). The content of gas in any state of storage, in general, rises along with increasing pressure (Nie et al., 2009). The increase of pressure can effectively reduce the binding energy required for gas adsorption. Moreover, the increasing rate of gas adsorption capacity decreases due to intense gas-molecular collisions under high pressure, which may lead to slow gas adsorption (Rani et al., 2018). The free gas content of shale increases with increase of pore pressure (Zhou et al., 2014; Pan et al., 2016), and the influence of pore pressure on free gas is greater than that on adsorbed gas (Wei et al., 2019b). Therefore, high pressure is a more positive factor in the accumulation of free gas content than adsorbed gas (Sun et al., 2019). Furthermore, abnormal pressure developed by oil-gas generation, the self-sealing effect, and non-equilibrium compaction in the formation with a vast area of developed shale (Tingay et al., 2013), is beneficial to the preservation of shale gas, for it can offset the compaction effect of partial overlying formation pressure on pores (particularly micropores), and postpone or even alter the decreasing trend of porosity with increase in burial depth (Liu et al., 2021a).

Since CH_4 adsorption is an exothermic process, the tendency of molecules to aggregate near the shale surface leads to weaker physical adsorption at high temperatures. Under the same pressure, the surface coverage of CH_4 on shale decreases with increasing temperature (Wang et al., 2016a). Chalmers and Bustin (2008) pointed out that there is a negative exponential relationship between the CH_4 adsorption capacity of shale and temperature, and higher temperature favors the relative increase of free gas, which is attributed to the temperature dependence of the Langmuir coefficient (Tan et al., 2014).

Temperature and pressure, represented by the burial depth of shale in a comprehensive manner, in general, have an opposite effect on the CH_4 adsorption capacity of shale to some degree (Liu et al., 2021b). Hao et al. (2013) suggested that adsorbed gas in shale is dominated by pressure at shallow depths, that is, the content of adsorbed gas in shale increases with burial depth. By contrast, the content of adsorbed gas in shale is controlled by temperature in deeper strata, which declines as burial depth increases. Patterns of CH_4 adsorption capacity/GIP and depth were established by previous authors under a wide range of conditions (Fig. 13). In general, the increase of fluid overpressure and burial depth is beneficial for shale gas enrichment, especially free gas (Fig. 13) (Xiao et al., 2015; Ma et al., 2020a).

3.4. Preservation conditions

The tectonic intensity of shale gas reservoirs in North America is

Table 1
Comparison of adsorption capacity for shale under moisture and dry conditions.

Research	Formation	Shale type	Method	Variation characteristics of adsorption capacity	Reference
Northeastern British Columbia	Lower Jurassic Gordondale Member and the Poker Chip Shale	Marine shale	Moisture equilibrium experiment; High-pressure CH_4 adsorption experiment	The CH_4 capacity for dry shale = The CH_4 capacity for moisture-equilibrated shale × (1 + 0.30 × moisture content)	Ross and Bustin (2007)
Hils syncline in NW Germany; Southern Scandinavia; N Germany and the Netherlands; US	Mid-Jurassic Posidonia Shale; Lower Paleozoic Alum Shale; Carboniferous shales; Barnett, Eagle Ford and Haynesville shales	Marine shale	Moisture equilibrium experiment; High pressure CH_4 adsorption experiment	Compared with the dry samples, moisture-equilibrated samples showed a 40-60% lower adsorption capacity	Gasparik et al. (2014)
US	Upper Jurassic Bossier and Haynesville shales	Marine shale	Moisture equilibrium experiment; High pressure CH_4 adsorption experiment	Compared with the dry samples, the moisture-equilibrated samples (app. 97% RH) showed a 68% and 78% lower CH_4 adsorption capacity, respectively	Merkel et al. (2015)
UK	Mississippian Bowland Shale	Marine shale	Moisture equilibrium experiment; High pressure CH_4 adsorption experiment	The shales upon moisturizing the sample showed a maximum CH_4 adsorption capacity 27% lower than that of the dry sample. The experiment conditions were then set to 100 °C and 100% RH and the maximum CH_4 adsorption capacity was further reduced by 85%	Whitelaw et al. (2019)
East of Forth Bridge in South Queensferry, Scotland	West Lothian oil-shale formation	Continental shale	Moisture equilibrium experiment; High pressure CH_4 adsorption experiment	The adsorption capacity of moisture-equilibrated (97% RH) samples were 20%–80% of the initial adsorption capacity of the dry samples	Merkel et al. (2016)
Southern Sichuan Basin, Southwest China	The Lower Silurian Longmaxi Formation	Marine shale	Raw shale samples containing the primary moisture; High pressure CH_4 adsorption experiment applied with the Ono-Kondo lattice equation	The primary moisture (0.64%–0.82%) in the shale samples resulted in a significant reduction in the maximum CH_4 adsorption capacity by 12.86%–45.45%	Wang et al. (2020b)
The shale system with type II-D (over-mature) kerogen		Marine shale	The molecular dynamics and Monte Carlo simulation methods	Under variable moist conditions (0.6, 1.2, 1.8, 2.4 and 3.0 wt%), the adsorption capacity of kerogen decreased by 16%, 30%, 40%, 47% and 55%, respectively	Zhao et al. (2018)
The shale system with type II-D (over-mature) kerogen		Marine shale	The grand canonical Monte Carlo and molecular dynamics methods	Under the conditions with P = 30 MPa and T = 298–358 K, the absolute adsorption capacity of CH_4 decreased from 1.2 mmol/g to 0.6 mmol/g as moisture content increased	Gong et al. (2020)
Changning area in the Sichuan Basin, Southwest China	Upper Ordovician Wufeng- Lower Silurian Longmaxi Formations	Marine shale	Moisture equilibrium experiment; High pressure CH_4 adsorption experiment	At a 97% equilibrium relative humidity, the shales showed a 44%–63% lower CH_4 adsorption capacity than the dry shales	Yang et al. (2017)
Changning-Weiyuan area in the Sichuan Basin, Southwest China	The 1st member of Longmaxi Formation	Marine shale	Moisture equilibrium experiment; High pressure CH_4 adsorption experiment	When the moisture content was 10%, 20%, 30%, and 40%, the loss of adsorbed gas content was 23.88%, 37.31%, 41.87%, and 44.59%, respectively	Hu et al., 2018c
Northern Yunnan-Guizhou Depression in the Upper Yangtze Platform, China	Upper Permian Longtan Formation	Marine-continental transitional shale	Raw shale samples containing the primary moisture; High pressure CH_4 adsorption experiment	The CH_4 adsorption capacities of the water-bearing shales were 40%–50% lower than that of the dry samples	He et al. (2019)
Qaidam Basin, Northwest China	Carboniferous System	Marine-continental transitional shale	Reference evaporation experiment with liquid water, simultaneous adsorption of water vapor and CH_4 and pure CH_4 adsorption onto dry shale	The CH_4 adsorption capacity of shale samples that adsorbed both water vapor and CH_4 was 10%–59% lower than the pure CH_4 adsorption capacity of dry shales	Ma and Yu (2021)
Yangquan block, Qinshui Basin, Northern China	Carboniferous System	Marine-continental transitional shale	Raw shale samples containing the primary moisture; High pressure CH_4 adsorption experiment	The maximum absolute adsorption capacity was reduced by 33.05% on average under the condition of water content at 30 °C	Sun et al., 2022
Northeast Sichuan Basin, Southwest China	Da'anzhai member of Lower Jurassic Ziliujing Formation	Continental shale	Moisture equilibrium experiment; High pressure CH_4 adsorption experiment	A 20% increase in relative humidity resulted in an approx. 10% decrease in the maximum CH_4 adsorption capacity of the samples	Chen et al. (2021b)
Sichuan Basin, Southwest China	Qiongzhusi, Longmaxi, Longtan, Xujiahe and Ziliujing Formations	Marine shale, marine-continental transitional shale, and continental shale	Moisture equilibrium experiment; High pressure CH_4 adsorption experiment	Compared with moisture-equilibrated sample (98% RH), the adsorption capacity of dry shale dropped to 28% of the former. In addition, the adsorption capacity of lacustrine shales (such as Xujiahe Formation and Ziliujing Formation) decreased most significantly due to the abundance of clay minerals	Tang et al. (2021)

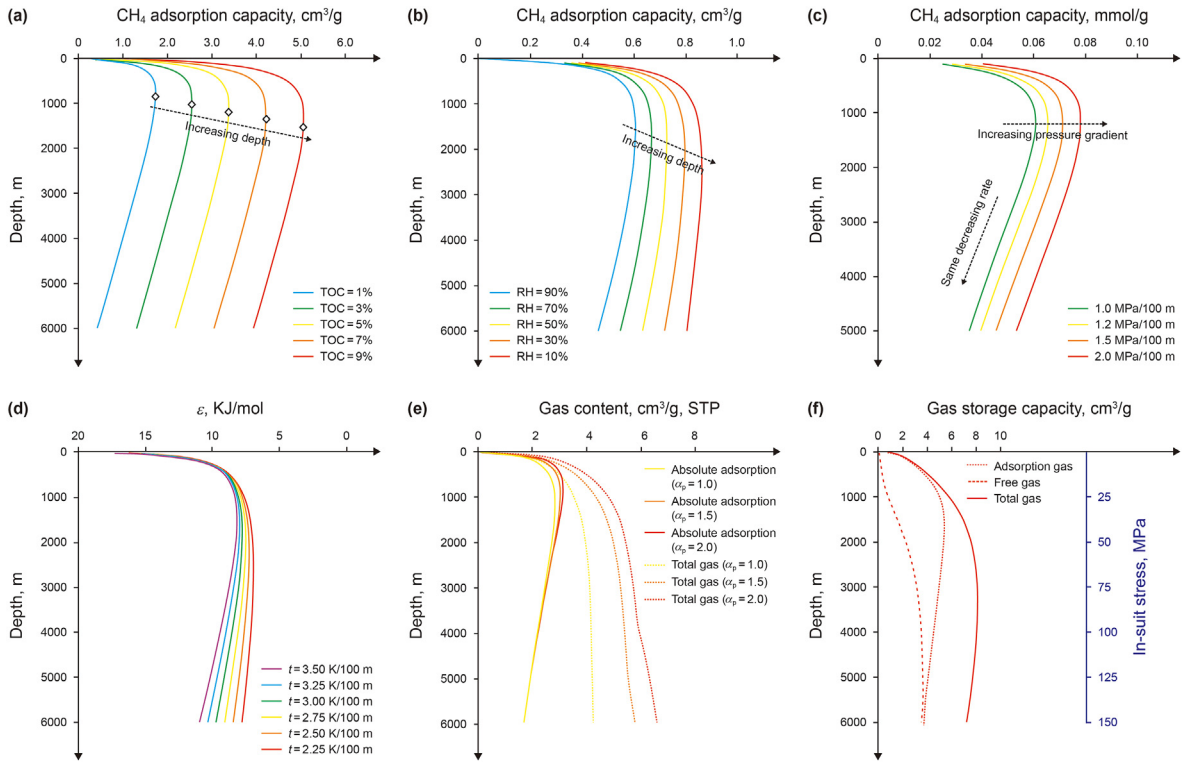

Fig. 13. Geological models of gas content and CH_4 adsorption capacity with depth. (a) different TOC contents (modified from Ji et al., 2015); (b) different relative humidity conditions (modified from Chen et al., 2021b); (c) different hydrostatic pressure gradients (modified from Yang et al., 2015); (d) different ground temperature gradients, ε is the shale adsorption potential, kJ/mol (modified from Huang et al., 2020); (e) different fluid pressure coefficients (modified from Pan et al., 2016); (f) considering in-situ stress (modified from Miao et al., 2022).

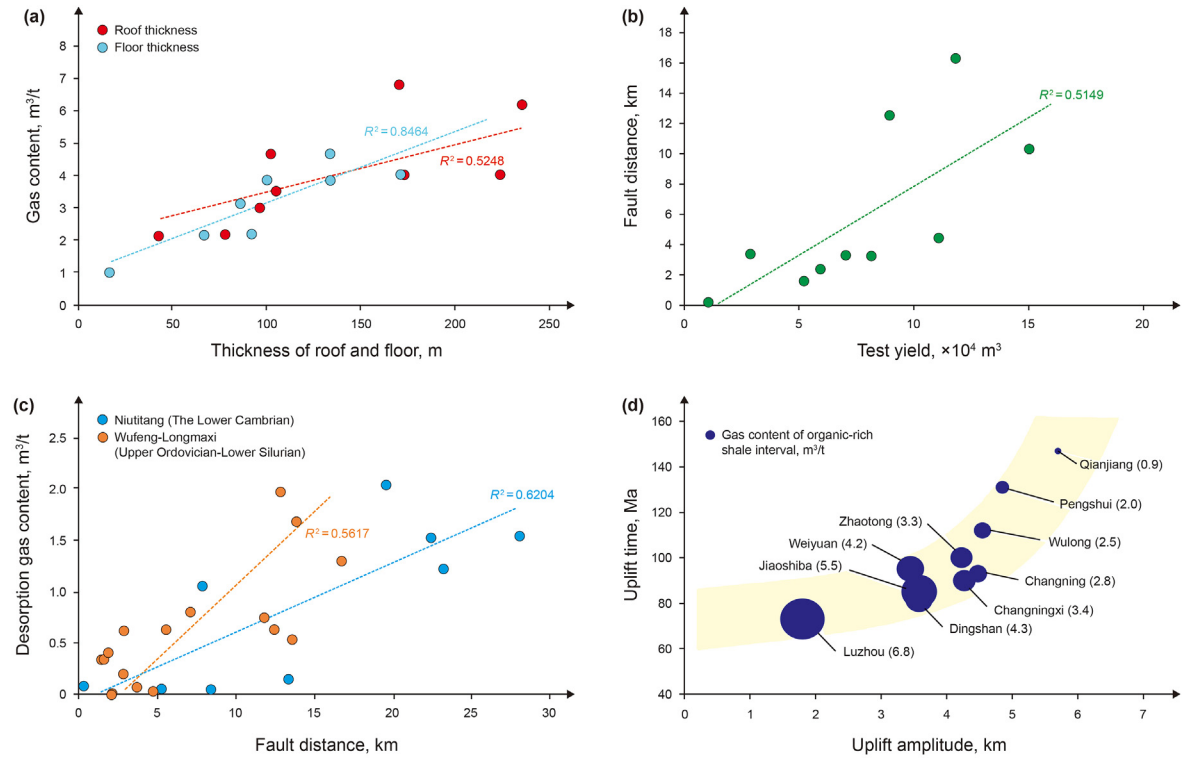

Fig. 14. Relationship between preservation conditions and shale gas content. (a) Relationship between roof and floor thickness and gas content (modified from Jiang et al., 2020); (b) relationship between fault distance and shale gas test production (modified from Feng et al., 2021); (c) correlation analysis between desorption gas content and fault distance (modified from Xu et al., 2021b; Xu et al., 2021c); (d) relationship between gas content of marine shale and uplift time and amplitude in southern China (modified from Jiang et al., 2020).

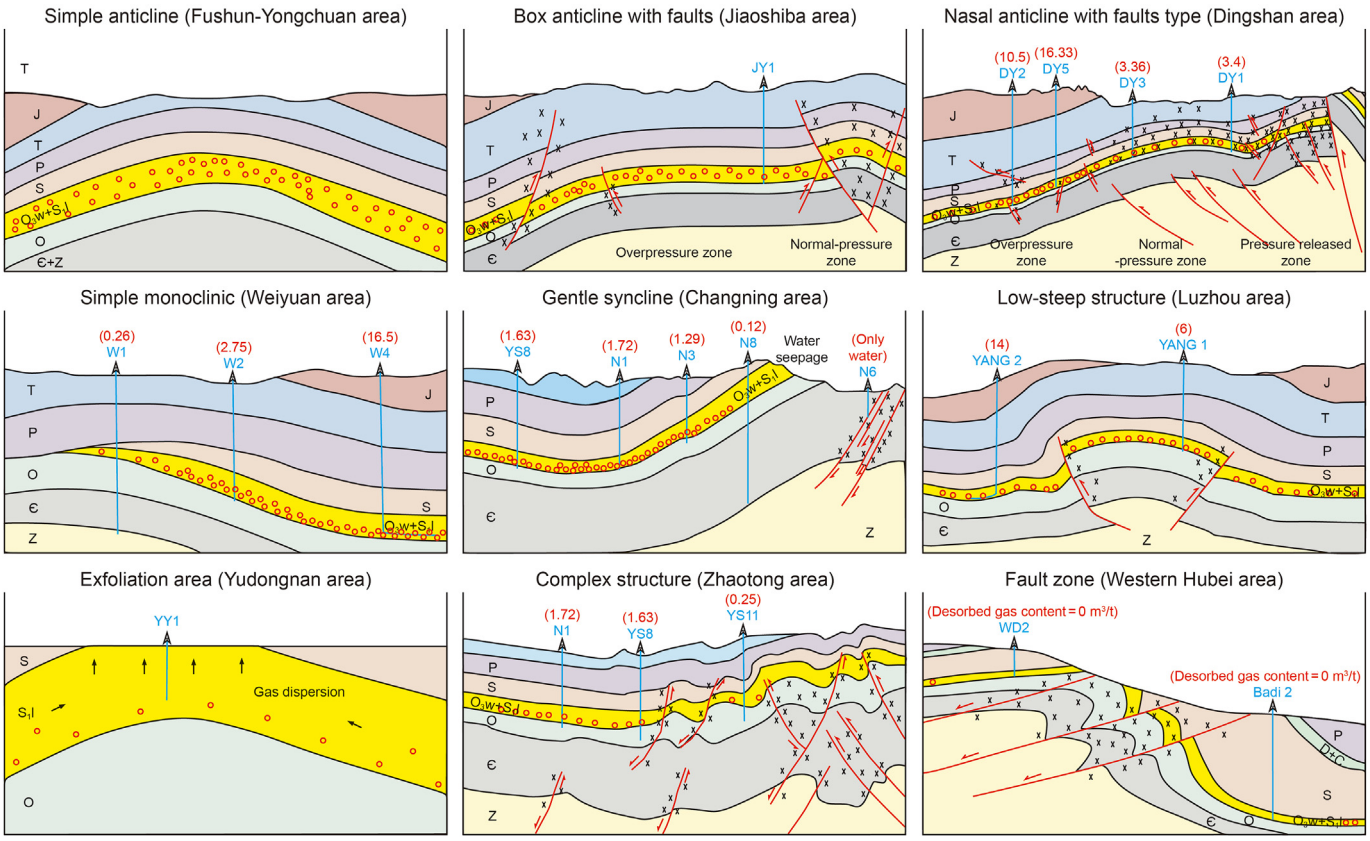

Fig. 15. Structural patterns and gas production of typical shale gas production areas in the Sichuan Basin and its surrounding regions, China (modified from Zhai et al., 2017; Ma, 2018; Wei et al., 2020b; Xu et al., 2021b). In the figure, the black font is the area where the shale gas well is located, the blue font represents the well ID, and unmarked red text in parentheses represents daily production, × 10^4 m^3/d.

relatively weak, therefore, the favorable exploration area for shale gas is widely and continuously distributed, and the gas can be preserved by the self-imperviousness of the shales. Comparatively, Chinese marine shale has experienced complex tectonic activity. There is still a significant difference in gas content despite its similarity in composition and the presence of organic shale compared to its North American counterpart, because preservation conditions are often a key influencing factor.

Roof and floor conditions are the key factors in preventing vertical migration and dispersion of shale gas. The better the quality of the roof and floor, the better the microcosmic sealing capacity (Hu et al., 2014), the shale gas content being positively correlated with the microcosmic sealing capacity of the roof and floor (Cui et al., 2020). In addition, the increase of roof and floor thickness is conducive to improvement of the physical sealing capacity, and shale gas enrichment (Jiang et al., 2020; Tang et al., 2020) (Fig. 14a). For example, the Wufeng-Longmaxi and Qiongzhusi Formations of the Sichuan Basin (China) have similar source rock conditions, but the former has a better roof-floor sealing capacity, resulting in higher gas content (> 3 m^3/t in the Wufeng-Longmaxi Formation (Zou et al., 2020). Regional thick-layer impervious caps are also important for shale gas preservation. Thick-layer caps are not susceptible to seepage caused by a fracture (Fu et al., 2018), and help maintain the regional formation pressure system. For example, the shale gas preservation conditions in the southeastern margin of Dingshan region of the Sichuan Basin (China), the Pengshui region outside the basin and the Wufeng-Longmaxi Formation in the Zhaotong region, which lack a lower-middle Triassic plaster layer cap, have been damaged, resulting in a low or undeveloped overpressure (Jin et al., 2018). The development of small- and mid-scale fractures in shale systems with good preservation conditions is favorable for gas concentration and the formation of high-yielding fracture-type shale gas reservoirs (Hu et al., 2018b). However, the formation of multi-stage, later and large-scale fractures causes damage to shale gas reservoirs (Zeng et al., 2016; Nie et al., 2020), enabling a shale gas escape network to be formed by interconnected fractures, and thus a reduction in gas content (Gou et al., 2021b).

Tectonic deformation will affect the occurrence and enrichment of shale gas. Strong uplift and denudation, high stress and significant deformation are often positively correlated, causing development of fracture systems closely associated with impairment of the preservation conditions, atmospheric water infiltration and other effects, which are reflected in a low formation pressure coefficient and gas content. However, moderate compression and uplift are conducive to the development of micro fractures and bedding fractures in shale, forming shale gas reservoirs with a high pressure coefficient. Xu et al. (2020b) found that the PV and SSA of low-yielding silica-rich shale in the anticlines with strong structural deformation were 34.63% and 22.09% lower than those of high-yielding silica-rich shale, and they proposed that structural deformation would lead to the collapse and merging of organic pores. Hu et al. (2018b) also observed that the more developed the fracture, the larger the fault throw, the more complicated the superimposition relationship along the vertical direction and the shorter the distance to the major fault lead to poorer preservation conditions and lower the gas content (Fig. 14b and c). The preservation conditions for shale gas become favorable when the shale gas system

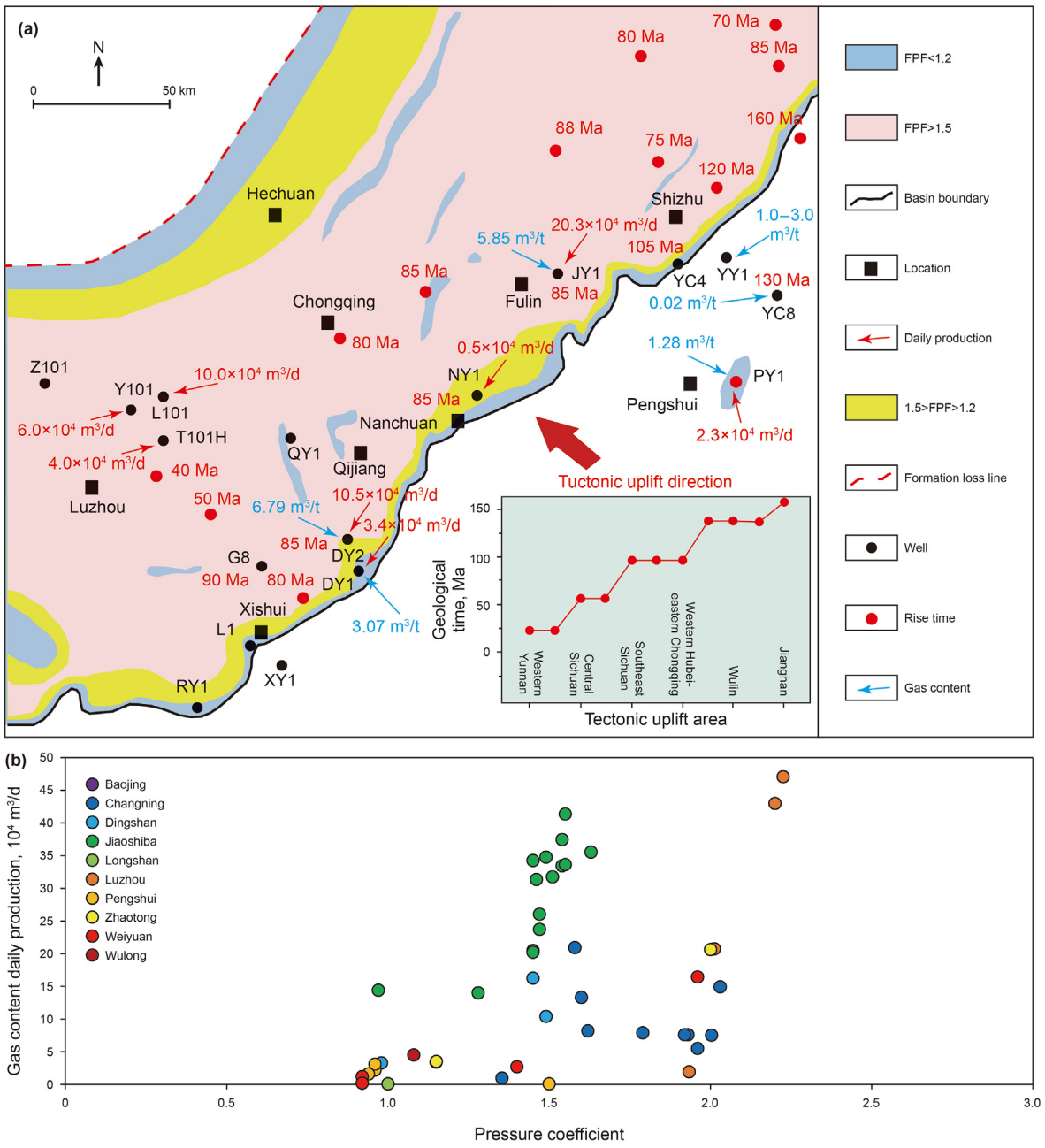

Fig. 16. (a) Distribution of pressure coefficient and gas-bearing characteristics of the Longmaxi Formation in the southeastern Sichuan Basin-western Hunan-Hubei region, China (modified from Fan et al., 2020); (b) relationship between shale gas production and pressure coefficient in the Sichuan Basin and its surrounding regions (modified from Zhai et al., 2017; Guo, 2019; Chen et al., 2020a; Zou et al., 2022b).

lacks caps in the deep or breakthrough regions of a large fault and the fault is impervious. For example, the average gas content in the continental Shahezi Formation and Yingcheng Formation in the Songliao Basin (NE China) is greater than 4 m^3/t due to the favorable preservation conditions that prevent shale gas from escaping in large quantities (Tang et al., 2019b).

The magnitude of tectonic uplift also influences shale gas concentration to a large degree because uplift may reduce reservoir pressure, causing diffusion and loss of shale gas (Katz et al., 2021), or brittle fracture of the shale gas reservoir and overlying cap (Nygård et al., 2006), or re-opening of pre-existing fractures (Guo et al., 2017c), thereby reducing the imperviousness of mud shale and/or the capacity of the impervious layer. To ensure high gas content in shale, it is necessary to maintain relatively low shale gas loss during uplift in sedimentary basins (Li et al., 2019c). The greater the magnitude of uplift, the larger the thickness of eroded strata, the more severe the damage to preservation conditions and the lower shale gas content (Fig. 14d) (Jiang et al., 2020). The microfracture development caused by lateral compression forces in the uplift process may damage the imperviousness of the cap rocks and cause deterioration of preservation conditions of the shale gas (Hou et al., 2021). Studies have reported that moderate uplift (~ 3350–3550 m) leads to few fractures generated and the lateral diffusion of a small amount of gas (~ 0.95–1.72 m^3/t), while tremendous uplift (~ 5350 m) would result in massive fracture development and considerable gas loss by lateral diffusion and vertical dissipation (~ 3.22 m^3/t) (Feng et al., 2022). Moreover, it may further complicate the geological structure, and destroy the

Table 2
An overview of determination of lost gas content in shales.

Method	Calculation formula	Parameter meaning	Method characteristics	Reference
US Bureau of Mines (USBM) method	$V_{Des} = V_L + a\sqrt{t_{Des} + t_L}$	V_{Des} is the cumulative desorption gas volume, m^3; V_L is the negative value of lost gas volume, m^3; t_L is the lost time; t_{Des} is cumulative degassing time in minutes; a is a constant; t_{EX} is the exposed ground time; t_{Lift} is the core lifting time; k is the formation pressure coefficient; ρ_{water} and ρ_{mud} are the density of water and mud filtrate, kg/m^3, respectively	Minimizing the time loss increases the estimation accuracy. Headspace can reduce precision. Therefore, the method may be more suitable for coal seams. In addition, it assumes that environmental changes during coring only have a negligible effect on degassing characteristics	Diamond and Schatzel, 1998; Wei et al. (2015); Li et al., 2022b
Modified USBM method	$V_{Des} = V_L + a\sqrt{t_{Des} + t_{EX} + \frac{\rho_{water} k t_{Lift}}{\rho_{mud}}}$		The improved method modifies the calculation of the time loss. The calculation accuracy of the time loss during core lifting depends on the densities of the water and mud filtrate, as well as the accuracy of the formation pressure coefficient	Su et al. (2017)
Polynomial function method	$V = a_0 + a_1\sqrt{t} + \ldots + a_{n-1}(\sqrt{t})^{n-1} + a_n(\sqrt{t})^n$	V is the cumulative desorption gas volume, mL; t is the sum of the escape time of lost gas and the measured desorption time; a_i is the polynomial fitting coefficient	In the later stages of non-equilibrium diffusion, the volume of gas loss calculated by polynomial regression is closer to the real value	Liu et al. (2019a); Enriquez et al. (2020)
Amoco curve fitting method	$V_D = V_{LD}\left[1 - \frac{6}{\pi^2}\exp\left(-\pi^2\frac{D}{r^2}t\right)\right] - V_L$	V_D, V_{LD}, V_L are the desorption gas volume, the total adsorbed gas volume, and the lost gas volume, ml; t is the time after time zero; D is the diffusion coefficient; r is the diffusion length	For samples with a greater time loss, the calculated value of loss gas is significantly larger, the assumption of a single-porosity media in shale may not hold. The method also focuses on the decline phase of the natural gas desorption curve, which may not be directly related to the core lifting process for deep shale gas reservoir	Zhou et al. (2018); Mahzari et al. (2021)
Calculation model based on instantaneous gas loss and desorption rate when drilling the core during the core-drilling	$V_L = V_{ins} + V_{ris} = \frac{P_i T_0 Z_0}{P_0 T_i Z_i}\Phi(r_{ins}, \infty)V_p S_g + (T_{ris} + T_{exp})\frac{q_{des}}{m}$	V_{ins} and V_{ris} are the instantaneous escape gas volume on ground conditions and the loss gas volume during drilling lifting, m^3/t; P, T, and Z are pressure, temperature and CH_4 correction factors respectively (subscript i represents reservoir conditions, and subscript 0 represents ground conditions); r_{ins} is the minimum capillary radius at which free gas can escape instantaneously, m; $\Phi(r_{ins}, \infty)$ represents the proportion of pore volume with pore throat radius greater than r_{ins}, %; V_p is the total PV of shale, m^3/t; S_g is shale gas saturation, %; m is shale mass, g; T_{ris} is the drilling lifting time, T_{exp} is the exposure time, min; q_{des} is the desorption rate of shale gas, cm^3/min	The method can effectively enhance the accuracy of computing the gas loss and total gas content in shale gas reservoirs under abnormally high pressure	Li and Nie (2019)
Modified Curve Fit (MCF) method based on the bidisperse diffusion model	$Q_{d(t)} = Q_t\left\{\frac{\left[1 - \frac{6}{\pi^2}\exp\left(-\pi^2\frac{tD'_a}{R_a^2}\right)\right]}{1 + \frac{\beta}{3\alpha}} + \frac{\frac{\beta}{3\alpha}\left[1 - \frac{6}{\pi^2}\exp\left(-\pi^2\alpha\frac{tD'_i}{R_i^2}\right)\right]}{1 + \frac{\beta}{3\alpha}}\right\} - Q_l$	$Q_{d(t)}$ is the desorbed gas content at time t, Q_t is the sum of loss gas and desorption gas content, Q_l is the loss gas content, mL/g rock; D'_a and D'_i is the effective macropore diffusivity and the effective micropore diffusivity, respectively, cm^2/s; R_a and R_i are the macrosphere and microsphere radii in cm, respectively; α and β are dimensionless parameters, $\alpha = D_i R_a^2/D_a R_i^2$, $\beta = [3(-\varepsilon_a)\varepsilon_i/\varepsilon_a]D_i R_a^2/D_a R_i^2$ (ε_a and ε_i are the macropore and micropore void fractions, respectively)	The method is theoretically based on a dual-porosity gas diffusion model that is suitable for obtaining the shale gas desorption data over the entire time range, but the model does not fully consider the geological factors that can affect the shale gas diffusion characteristics. And it enjoys a wide range of applications under ratios of free gas versus total gas that are greater than approximately 75%	Dang et al. (2018)
FM (a,b) model	$Q_L = \frac{ab(P_s - P)}{(1 + bP_s)(1 + bP)} + \frac{\left(\frac{P_s}{Z_s}\right) - \left(\frac{P}{Z}\right)}{\left(\frac{P_s}{Z_s}\right)}\left[V_{core}\Phi S_g\frac{T_{sc}}{P_{sc}}\frac{P_s}{Z_s T_s} - 4.2225 \times 10^{-5}\frac{\widehat{M}}{\rho_s B_g}\left(\frac{G_{sL}P}{P + P_L}\right)\right] - Q_M$	Q_L is gas loss volume, and Q_M is the volume of natural gas measured after the core is filled on the ground, mL; a and b are constants related to the physical properties and temperature of the adsorbed gas, respectively, mL and MPa^{-1}; P_s, P and P_{sc} are saturated pressure, the	The model boasts wide applicability and does not require back-calculation of the desorption amount	He et al. (2021)

Table 2 (*continued*)

Method	Calculation formula	Parameter meaning	Method characteristics	Reference
		current core pressure and the ground standard atmospheric pressure, respectively, MPa; T_s and T_{sc} are the formation temperature and the standard temperature, respectively, K; V_{core} is the core volume, mL; S_g is gas saturation in the core; Φ is porosity; Z_s is deviation coefficient under a saturated pressure condition, while Z is under current condition; B_g is gas volume coefficients under current pressure condition; $\widehat{M}$ is the apparent molecular weight of natural gas, g/mol; ρ_s is the adsorption-phase density, g/mL; G_{sL} is the Langmuir storage capacity, mL; P_L is the Langmuir pressure, MPa		
Carbon isotope fractionation (CIF) model	$\begin{cases} Q_{frac}(t_i) = \left[\frac{P(t_{i-1})}{z_{i-1}} - \frac{P(t_i)}{z_i}\right] \frac{V_f \mathrm{V_m}}{RT} \\ Q^*_{frac}(t_i) = \left[\frac{P^*(t_{i-1})}{z_{i-1}} - \frac{P^*(t_i)}{z_i}\right] \frac{V_f \mathrm{V_m}}{RT} \end{cases}$ $\begin{cases} Q_{matrix-free-^{12}C}(t_i) = H_{rock} \times \int_{x=0}^{x=r_{rock}} 2\pi x \Phi \left[\frac{p(x,t_0)}{z(x,t_0)RT} - \frac{p(x,t_i)}{z(x,t_i)RT}\right] dx \times \mathrm{V_m} \\ Q_{matrix-free-^{13}C}(t_i) = H_{rock} \times \int_{x=0}^{x=r_{rock}} 2\pi x \Phi \left[\frac{p^*(x,t_0)}{z(x,t_0)RT} - \frac{p^*(x,t_i)}{z(x,t_i)RT}\right] dx \times \mathrm{V_m} \end{cases}$ $\begin{cases} Q_{matrix-ads-^{12}C}(t_i) = H_{rock} \times \int_{x=0}^{x=r_{rock}} 2\pi x(1-\Phi)[\theta(x,t_0) - \theta(x,t_i)] dx \times \rho_{rock} \times V_L \\ Q_{matrix-free-^{13}C}(t_i) = \mathrm{H_{rock}} \times \int_{x=0}^{x=r_{rock}} 2\pi x(1-\Phi)[\theta^*(x,t_0) - \theta^*(x,t_i)] dx \times \rho_{rock} \times V_L \end{cases}$ $\begin{cases} Q_{k-C_{12}}(t_i) = S_k \times \int_{x=0}^{x=H_k} [C_{k0} - C_k(x,t_i)] dx \times \mathrm{V_m} \\ Q_{k-C_{13}}(t_i) = \mathrm{S_k} \times \int_{x=0}^{x=H_k} [C^*_{k0} - C^*_k(x,t_i)] dx \times \mathrm{V_m} \end{cases}$ $\begin{cases} Q_{cal-^{12}C}(t_i) = Q_{frac}(t_i) + Q_{matrix-free-^{12}C}(t_i) + Q_{matrix-ads-^{12}C}(t_i) + Q_{k-^{12}C}(t_i) \\ Q_{cal-^{13}C}(t_i) = Q^*_{frac}(t_i) + Q_{matrix-free-^{13}C}(t_i) + Q_{matrix-ads-^{13}C}(t_i) + Q_{k-^{13}C}(t_i) \\ Q_{cal}(t_i) = Q_{cal-^{12}C}(t_i) + Q_{cal-^{13}C}(t_i) \end{cases}$	$Q_{frac}(t_i)$ is the amount of free gas degassing from fractures at time i, L; $P(t_{i-1})$ and $P(t_i)$ are the partial pressure of free gas in the fractures at time $i-1$ and i, respectively, Pa; z_{i-1} and z_i are the gas compressibility coefficients for time $i-1$ and i, respectively; Φ is the effective porosity, %; V_f is fracture volume, m^3; V_m is molar gas volume, 22.4 L/mol; R is molar gas constant, 8.314 J/(mol·K); T is temperature, K; x is the distance from the boundary, m; H_{rock} is the height of a cylindrical rock sample; θ is the coverage of adsorbed gas, %; ρ_{rock} is apparent rock density, g/cm^3; V_L is Langmuir volume, cm^3/g; C_k is the gas concentration inside kerogen structural pores, mol/m^3; S_k is active open area of kerogen simplified as plane slice. Asterisked parameters indicate $^{13}CH_4$, while parameters not marked with an asterisk represent $^{12}CH_4$.	The method considers multiple gas flow mechanisms in pores of different scales. Because the boundary conditions can be varied to reflect actual changes in the environment during coring, the CIF model is highly applicable to describing the whole degassing process and evaluating several key parameters, including the GIP, gas adsorption ratio, and in situ Langmuir parameters	Li et al. (2021c); Li et al., 2022b

continuity of the existing fluid pressure system and shale gas reservoir (He et al., 2020). Exploration practices for shale gas reveal that uplift time is associated with loss of shale gas, and the later the uplift time, the more favorable it is for the preservation of shale gas (Fig. 14d) (Yi et al., 2019; He et al., 2020). Although, it should be noted that recent studies have shown that the effect of uplift time on shale gas loss may not be as great as that of intensity of late tectonism (Feng et al., 2022). Additionally, the rapid uplift of shale gas reservoir is unfavorable for the preservation of shale gas, while slow uplift process may not lead to suddenly release of formation fluid (Yang et al., 2021). For example, compared with Sichuan Basin, Western Hubei has the characteristics of rapid uplift rate, and its gas-bearing property is generally poor (Xu et al., 2021b).

Therefore, the coupling of self-sealing ability, physical properties of the roof and floor, reconstruction time, rate and intensity under tectonic action is a significant factor affecting the preservation conditions of shale gas. Fig. 15 shows the structural style and gas production of typical shale gas producing areas in the Sichuan Basin and surrounding areas in China. Different tectonic styles affect the preservation of shale gas, resulting in significantly different shale production. Comparatively, regions with wide and slow, continuously sealed, gradually lifting structures with an appropriate distance from fault zones and/or denudation areas are more ideal for the preservation, accumulation and high yield of shale gas.

The pressure coefficient is a comprehensive index of shale reservoir preservation conditions. The majority of productive shales in the United States are in a closed or semi-closed system during/after peak gas generation and remain in a state of overpressure (Bruns et al., 2016). The normal-pressure shale gas

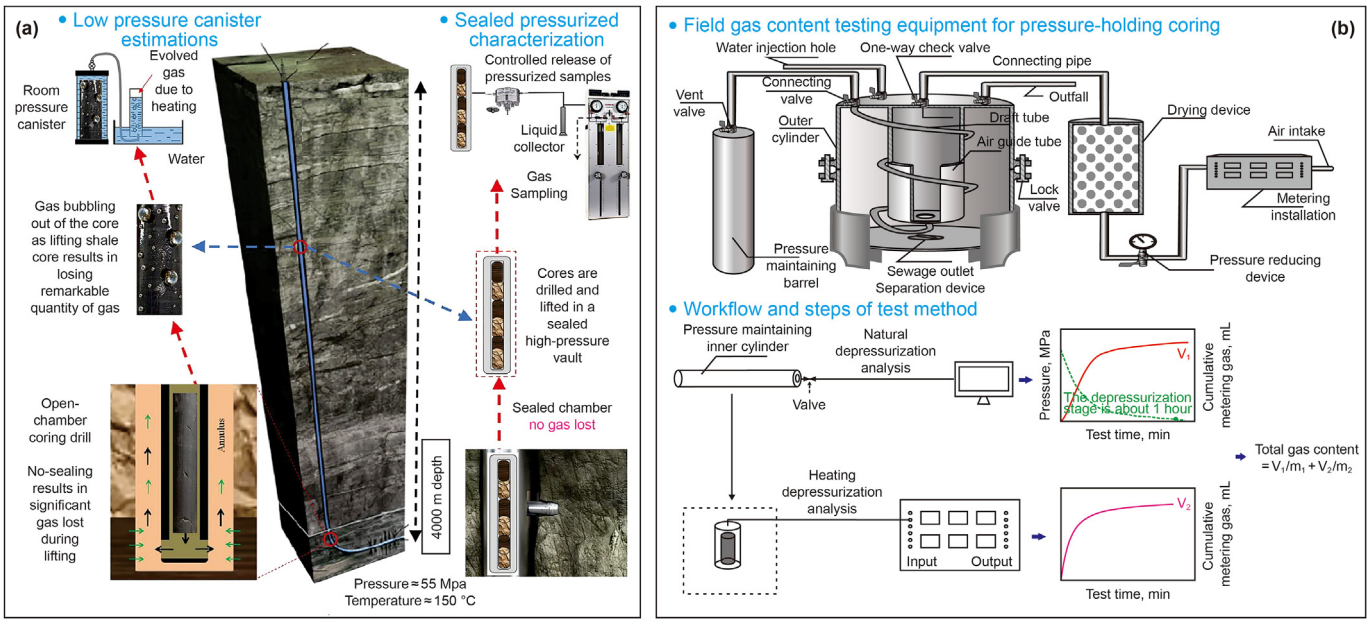

Fig. 17. (a) Comparison between conventional coring, pressure-maintaining coring and subsequent operation (modified from Mahzari et al., 2021); (b) schematic diagram of testing equipment and test procedure for pressure-holding coring of gas shale (modified from Zhou et al., 2022b).

reservoirs and high- and over-pressure shale gas reservoirs share similar sedimentary backgrounds to the Sichuan Basin and its peripheral region in China, but different tectonic reworking in later stages has caused an apparent difference in gas content (Guo et al., 2020c). In the Sichuan Basin, the preservation conditions are generally good, and shale reservoirs generally are in overpressure. The fluid pressure coefficient ranges from 1.2 to 1.6 (Guo et al., 2020b), and in some regions (such as the Luzhou block) can be as high as 2.0 (Ma et al., 2021b). In blocks outside the Sichuan Basin, the preservation conditions are poor due to strong uplift and developed folds/faults, in which the pressure system is normal, or even negative. For example, the fluid pressure coefficient of the Wufeng-Longmaxi Formation of well PYA in the Pengshui area outside the Sichuan Basin is 0.8–1.1 (Wang et al., 2020c) (Fig. 16a). The exploration practices for Longmaxi shale gas show that overpressure indicates high gas content and initial production (Fig. 16b), determining the economy of shale gas development to a great extent.

4. Evaluation method of retained gas in shale

4.1. Field desorption method

GIP evaluation based on analysis data of shale gas basically follows the field test method for coal-bed CH_4. The drilling core is placed into desorption devices as soon as possible, and analytical gas content is obtained through reservoir temperature analysis. Then, the residual gas content is measured by crushing and analyzing the sample. After that, based on the desorption data, the lost gas content is estimated by using different fitting methods. The total gas content consists of desorbed gas, lost gas, and residual gas (Shtepani et al., 2010). For its simple operation and the established specifications in sample collection, handling, and process control (Shi et al., 2019), the desorption method is now the most widely used method in shale gas exploration and development.

The desorbed and residual shale gas contents are both directly measured from experimental data with little error (Li and Nie, 2019), but the calculation of lost gas content is the key (Enriquez et al., 2020), and its accuracy is often questioned (Zhou et al., 2022a). That is because differing from coal gas, the shale gas also consists of free gas and desolated gas and the majority of shale gas is often lost before the desorption test. According to measurements of Chinese researchers, the lost gas content accounts for 40–80% of the total gas content (Wang et al., 2020a). Although multiple mathematical models have been developed to calculate the lost gas content of shale (Table 2), the problem is far from being solved, especially when the shale reservoir is relatively deep. For example, it takes 6–10 h to recover drill core if the shale gas reservoir is in the range from 3000 to 6000 m (Xiong et al., 2020), significantly reducing the accuracy of estimation of dissipated gas (Enriquez et al., 2020; Xiong et al., 2020; Jing et al., 2021; Mahzari et al., 2021).

Due to depressurization of the core during underground transportation and ground processing, the pressure-maintaining coring technology has become a development trend. Cerri et al. (2015) employed controllable pressure coring technology to measure total gas directly. They believed that this eliminated gases and/or liquids lost in traditional coring techniques. Mahzari et al. (2021) reported that the shale gas volume of pressure coring is nearly five times that of conventional desorption methods, and thus lost gas during the core lifting can be obtained more directly, which is of great significance for deep shale gas reservoirs (Fig. 17a). In recent years, Chinese researchers have also been developing pressure-preserving core technology and have conducted a series of tests (Wang et al., 2020a). For example, according to the field test data of Zhou et al. (2022b) in the Zhaotong area, southern Sichuan Basin (China) (Fig. 17b shows the test equipment and process), the average gas content in the pressure-holding coring section can be 2.3 times higher than that of shale in the same layer of an adjacent well obtained by conventional coring.

4.2. Adsorption experiment method

Since the GIP obtained by the field desorption method is influenced by factors such as sampling and testing conditions, manpower, and cost, a high-pressure gas sorption experiment on representative shale samples to calculate the amount of CH_4

Table 3
Summary of adsorption gas calculation models and methods.

Model	Calculation formula	Parameter meaning	Method characteristics	Reference
Langmuir and improved models	$n_{ads}^{excess} = n_L \frac{P}{P+P_L}\left(1-\frac{\rho_{gas}}{\rho_{ads}}\right)$	n_{ads}^{excess} is excess adsorption amount at pressure p; n_L is the maximum Langmuir capacity, mmol/g; P_L is Langmuir pressure, MPa; ρ_{gas} and ρ_{ads} are the bulk gas phase density and the adsorbed phase density, respectively, kg/m^3	The model's assumptions of a homogeneous pore structure, monolayer adsorption, and lack of interaction between gas molecules demonstrate its limited applicability to deep shale gas	Gasparik et al. (2012); Pan et al. (2016)
Dual-site Langmuir equation	$n_e(P,T) = (n_{max} - V_{max}\rho_g)\left[(1-\alpha)\left(\frac{K_1(T)P}{1+K_1(T)P}\right)+\alpha\left(\frac{K_2(T)P}{1+K_2(T)P}\right)\right]$	V_{max} is the volume of the adsorbed phase at maximum adsorption capacity; n_{max} is the maximum adsorption capacity; ρ_g is the bulk gas phase density, kg/m^3; $K(T)$ ($= A_0 \exp\left(-\frac{E_0}{RT}\right)$) is temperature-dependent equilibrium constant, E_0, A_0 and R are adsorption energy, the pre-exponential coefficient and ideal gas content, respectively; α is the fraction of the second type of site ($0< \alpha <1$)	The model supports the inference of adsorption isotherms beyond test data and accurate estimation of the real shale gas volume and relative amount of adsorbed CH_4 under deep geological conditions	Tang et al. (2016); Meng et al. (2020)
Multi-site adsorption model	$n_{ab} = n_{max}\sum_{i=1}^{i=n}\alpha_{(i)}\frac{P}{P+P_{L(i)}}$ $n_{ex} = n_{max}\,(1-\frac{\rho_g}{\rho_l}\bullet e^{\lambda(T-T_b)})$ $\sum_{i=1}^{i=n}\alpha_{(i)}\frac{P}{P+P^0\exp\left(-\frac{\Delta E_{(i)}}{RT}-\frac{\Delta S_m^0}{R}\right)}$	n_{ab}, n_{max} and n_{ex} are the adsorption amount, the maximum adsorption capacity and the excess adsorption amount respectively, mol/g; P, P^0 and $P_{L(i)}$ are the equilibrium pressure, the gas pressure at a reference state (0.1 MPa), the Langmuir constant for each type of adsorption site, MPa; n is the types of the adsorption sites; $\alpha_{(i)}$ is the fraction for each type of adsorption site, %; ρ_g is the bulk gas phase density, and ρ_l is the liquid density at boiling point, $\rho_l = 422.36$ kg/m^3 for CH_4, g/cm^3; $\Delta E_{(i)}$ is the binding energy for each adsorption site, kJ/mol; T_b is the boiling temperature, $T_b = 111.66$ K for CH_4, T is temperature, K; ΔS_m^0 is an apparent entropy for adsorption; R is the gas constant, J/mol/K; λ is the coefficient of thermal expansion, distributed from ~1.5×10^{-3} K^{-1} to ~2.5×10^{-3} K^{-1}	The distribution of adsorption energy in this model is directly related to the pore size distribution of the samples, and the gas resources in a single pore and total gas for a whole shale gas reservoir can be evaluated	Li et al. (2019a)
simplified local-density (SLD) model	$n^{EX} = \frac{A}{2}\int_{Left\ side\ to\ slit}^{Right\ side\ to\ slit}[\rho(z)-\rho_{bulk}]dZ$	n^{EX} is the excess adsorption amount, mmol/g; A is SSA; $\rho(z)$ is the density profile in the slit and ρ_{bulk} is the bulk phase density	The model assumes that the adsorbent comprises rectangular slits. It also considers the changes in the fluid phase and shale petrophysical properties. The model can characterize the original occurrence state of gas in shale	Chareonsuppanimit et al. (2012); Miao et al. (2022)
variable density adsorption (VD) model	$n_{ex} = \rho_{abs}V_a - \rho_g V_a = [\rho_f \ln(dp_g+1) - \rho_g]V_a$	n_{ex} is the excess adsorption; ρ_{abs}, ρ_f and ρ_g are the average adsorbed phase density, a parameter related to the adsorbed phase density, and bulk gas density, mg/cm^3; d is proportional to ρ_{abs}; V_a is the bulk gas density, cm^3/g	The model features easy operation and few unknown parameters. It only requires a single fitting to obtain reasonable adsorption parameters	Kong et al. (2021)
SDR model	$n_{ex}^H = n_o^H\,exp\left\{-D\left(ln\left(\frac{\rho_{ad}^H}{\rho_b^{(H,T,y)}}\right)R(T_o+HT_g)\right)^2\right\}\left(1-\frac{\rho_b^{(H,T,y)}}{\rho_{ad}^H}\right)$ $n_{ab}^H = \frac{n_{ex}^H\rho_{ad}^H}{\rho_{ad}^H-\rho_b^{(H,T,y)}}$	n_{ex}^H, n_o^H, n_{ab}^H are the excess adsorption, the maximum absolute adsorption and the absolute adsorbed gas at a burial depth H, respectively; ρ_{ad}^H is the density of adsorbed phase at a burial depth H; D is a constant related to the pore structure; R is ideal gas content; T is the absolute temperature, K; $\rho_b^{(H,T,y)}$ is the bulk gas density at temperature (T_o+HT_g) and pressure ($0.01\bullet y\bullet H$), H, T_g, T_o and y are burial depth (m), geothermal gradient (K/m), surface temperature (K) and pressure coefficient, respectively	Compared with Langmuir model, density of adsorbed CH_4 resulting from the parameter fit of the SDR-based excess adsorption model is more reasonable that is lower than that of liquid CH_4. In contrast with the DR model (i.e., low-pressure gas adsorption), this model can characterize the high-pressure CH_4 adsorption of shale	Rexer et al. (2013); Pan et al. (2016); Tian et al. (2016)

(*continued on next page*)

Table 3 (*continued*)

Model	Calculation formula	Parameter meaning	Method characteristics	Reference
L-SDR model	$V_{abs} = \begin{cases} V_0\frac{b_1\rho_{gas}}{1+b_1\rho_{gas}}, P<P_t \\ \alpha_1 V_0\frac{b_2\rho_{gas}}{1+b_2\rho_{gas}}+ \\ \alpha_2 V_m \exp\left\{-D\left[\ln\left(\frac{\rho_{ads}}{\rho_{gas}}\right)RT\right]^2\right\} \\ , P>P_t \end{cases}$	V_{abs}, V_0 and V_m are the absolute adsorption volume, the maximum absolute adsorption volume for Langmuir and the maximum absolute adsorption volume for SDR, respectively; b is Langmuir constant; P_t is threshold pressure, P is pressure; D is a constant related to pore structure; ρ_{gas} is the bulk gas density, ρ_{ads} is the adsorbed phase density, g/cm^3; α_1 is the fraction of the Langmuir adsorption volume, and α_2 is the fraction of the SDR adsorption volume; R is universal gas constant; T is temperature, K	The model can describe the supercritical CH_4 adsorption process in shale at different temperatures effectively and accurately	Song et al. (2018)
Improved supercritical D-A adsorption model	$n_{ex} = n_o \exp\left\{-D\left[\ln\left(\frac{RT\rho_a}{16(P-P_w)}\right)\right]^k - \alpha m\right\}\left(1-\frac{16(P-P_w)}{RT\rho_a}\right)$	n_{ex} and n_o are the excess adsorption and the maximum adsorption amount, respectively, mmol/g; D is the pore structure parameter; P is test gas pressure and P_w is water vapor pressure, MPa; R is ideal gas content; T is the absolute temperature, K; ρ_a is the CH_4 adsorbed phase density, g/cm^3; α is the attenuation index of adsorption capacity, dimensionless; m is the moisture content, %	The model corrects the actual gas pressure for CH_4 adsorption in the system and reflects the effect of moisture on the adsorbed gas	Li et al. (2020a)
Ono-Kondo model	$n_{abs} = n_o\frac{2\rho_f\left[1-\exp\left(\frac{\varepsilon_s}{k\bullet T}\right)\right]}{\frac{\rho_f\rho_{ad}}{\rho_{ad}-\rho_f}+\rho_{ad}\exp\left(\frac{\varepsilon_s}{k\bullet T}\right)}$	ρ_f and ρ_{ad} are molar density of free CH_4, molar density of maximum CH_4 adsorption, respectively; ε_s represents the energy of the CH_4-pore interaction; n_0 is the saturated adsorption capacity of the monolayer, and n_{abs} is total CH_4 adsorption capacity; k is the Boltzmann's constant, 1.38×10^{-23} J/K; T is the absolute temperature, K	The model can be derived by strict statistical or thermodynamic methods. Each parameter has a clear physical meaning. It is applicable to subcritical and supercritical adsorption	Bi et al. (2017); Hu et al. (2021a)
Models based on machine learning	(Black-box techniques) The machine learning process begins with data collection and processing, followed by dividing the data into training and test datasets. Then, the training set is used for cross-validation and grid search of hyperparameters, the model is trained with the optimized hyperparameters, and a learning curve is generated. The test dataset is evaluated by various machine learning algorithms, including extreme gradient boosting (XGBoost), artificial neural network (ANN), random forest (RF), support vector machine (SVM), and the optimal algorithm is identified, and finally tested		This method has applicability outside laboratory tests. Rolling data collection allows for continuous refinement of the model, which can significantly reduce time-consuming and labor-intensive work. However, the accuracy and reliability of the data need to be verified. Any extrapolation also needs to be verified when the dataset is rather small. Expanding machine learning data sets or using semi-supervised machine learning can help improve prediction performance	Meng et al. (2020); Huang et al., 2022b
	(White-box supervised intelligent systems) Machine learning can be used with the shale gas database to establish a rigorous and reliable correlation between the amount of adsorbed gas and variables such as temperature, pressure, moisture and TOC based on the gene expression programming (GEP) and group method of data handling (GMDH) methods		This method provides accurate and reliable explicit mathematical expressions for predicting CH_4 adsorption. However, inputting values and operating conditions outside the applicable range may result in inaccurate predictions	Nait Amar et al. (2022)

adsorption has become a widely used alternative method (Liu et al., 2019c). Theoretically, the total gas content of shale can be determined by adding the contents of adsorbed gas, free gas and dissolved gas. Due to the low content of dissolved gas, it can be ignored in practice (Dang et al., 2018; Babatunde et al., 2022; Zhou et al., 2022a). Basically, CH_4 volume density multiplied by effective pore volume (effective pore volume = total pore volume-pore volume occupied by water-adsorbed phase volume) is adopted to evaluate the free gas content (Ambrose et al., 2010, 2012). The properties of adsorbed gas are markedly different from that of free gas, so the traditional equation of state modeling is not suitable for use (Pang et al., 2019). Accurate calculation of adsorbed gas has become a hot spot for research. Many models based on adsorption potential theory, single molecule and multi-molecule adsorption have been developed to characterize the CH_4 adsorption in shales, and these methods exhibit distinct characteristics (Table 3). However, the specific application of these models needs to be further verified. Recently, researchers have used machine learning to predict CH_4 adsorption capacity, because machine learning can provide unbiased, automatic, and complete results, and can significantly accelerate the prediction process of shale gas adsorption capacity under extensive storage conditions (Huang et al., 2022b). Nevertheless, due to the limited number of samples in actual operation, some defects in typical models, the typical models may not be able to play

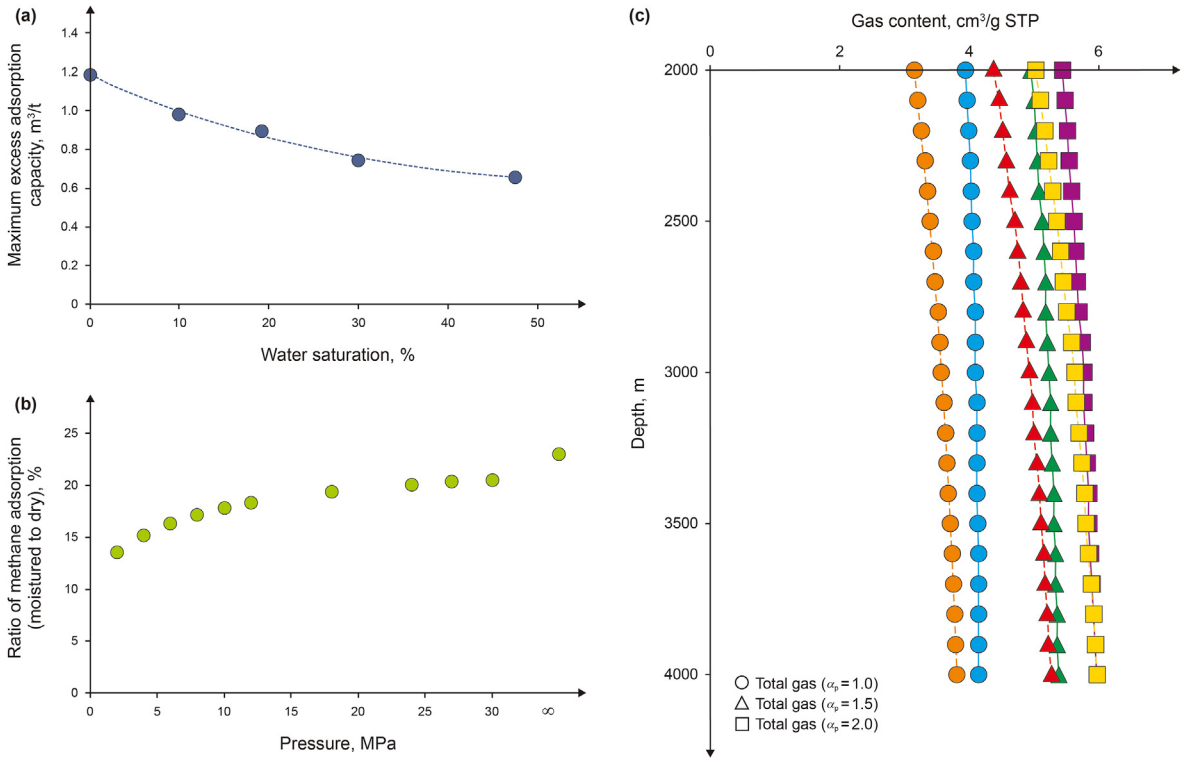

Fig. 18. (a) Relationship between water saturation and maximum excess adsorption capacity (modified from Hu et al., 2018c); (b) relationship between the ratio of methane adsorption and pressure at 30 °C (modified from Huang et al., 2022a); (c) comparison of total gas content under water-bearing and dry conditions (data from Pan et al., 2016). The solid and dotted lines represent the total gas content of dry samples and samples containing water, respectively.

their own advantages and obtain accurate CH_4 adsorption prediction results. Fortunately, the meta-heuristics (e.g., grey wolf optimizer, Syah et al., 2022) can improve the accuracy and effectiveness of typical models. Furthermore, Liu et al. (2022) reported that the ensemble-learning model is expected to solve these problems and obtain reliable prediction results due to its strong generalization ability, which provides a new perspective for CH_4 adsorption prediction.

CH_4 adsorption experiments for shales are generally based on crushed or powdered dried samples under unconstrained conditions (Gaus et al., 2021). Since the shale under geological conditions is water-bearing, this overestimates the adsorbed gas content to some extent. However, how to evaluate the amount of adsorbed gas in geological conditions has always been a challenge (Liu et al., 2019b; Pathi et al., 2022). The first problem is how to obtain and maintain the water-bearing shale under geological conditions, because factors like drilling fluid pollution, water loss or intrusion during sampling, storage and experimental processes can all change the quantity and occurrence of water in shale (Handwerger et al., 2011). The second problem is how to test the adsorbed gas content of water-bearing shale, for although relevant test data have been reported in the literature (Ross and Bustin, 2007; Gasparik et al., 2014; Merkel et al., 2015, 2016; Yang et al., 2017; He et al., 2019; Hu et al., 2018c; Whitelaw et al., 2019; Wang et al., 2020b; Chen et al., 2021b; Ma and Yu, 2021; Tang et al., 2021), they basically avoid one of the most basic problems, that is, the loss of water in the vacuum and heating process of the crushed sample. It is even more difficult to simulate the adsorption under high-temperature reservoir conditions.

Li et al. (2017) proposed a simple method, that is, assuming that water in gas-bearing shale exists only in mineral pores, the OM adsorption can be adopted as the lowest adsorbed gas content in shales. In addition, some researchers have proposed that the adsorption capacity of water-bearing shale and dry shale has a linear relationship, which can be calculated by an empirical value: Ross and Bustin (2007) suggested that the degree of influence of moisture on CH_4 adsorption is taken as 0.3, whereas Yu et al. (2016) concluded that adsorption capacity of water-bearing shale is about 50% of that of dry shale based on previous data, and recommended the use of 50% as the discount factor to obtain the adsorption capacity of shale under actual burial conditions. Additionally, there is an exponential function relationship between the adsorption capacity and water content; the attenuation index of adsorption capacity (λ) can be fitted by experimental data, and adsorption capacity in a realistic shale is equal to the product of $e^{-\lambda_* \text{equilibrium moisture content}}$ and the adsorption capacity of dry shale (Qi et al., 2018).

It is worth further discussing the degree of influence of water on adsorbed gas. Hu et al. (2018c) indicated that with increase of water saturation, its influence on the maximum excess adsorption amount decreased (Fig. 18a). In addition to the amount of water and the properties of the shale itself, the incidence is also affected by the depth of burial (temperature and pressure), as the effect of water on CH_4 weakens with increasing temperature, while increasing pressure reduces the negative influence of water and temperature on CH_4 adsorption (Fig. 18b) (Han et al., 2021b; Huang et al., 2022a). For instance, according to the data of Pan et al. (2016), if the adsorption capacity of water-bearing samples is 50% of that of dry samples, the impact on the total gas content decreases with increase of burial depth, and the reduction of total gas content is mainly distributed in 2.1–12.9% between 2000 and 4000 m (Fig. 18c). It can be seen that for shale with low water saturation, the total gas content calculated by using the adsorbed gas of dry samples is only slightly larger.

Table 4
Summary of other evaluation methods for shale gas content.

Method	Theory principle	Primary parameters	Advantages	Limitation	Reference
Multivariate linear regression analysis method	A regression statistical model can be established according to the relationship between shale gas content and TOC, porosity and other control factors	Internal factors (TOC, porosity, mineral composition, etc.) for shale gas accumulation	The gas-bearing prediction can be carried out by the predecessor model for a single study area, and the main controlling factors of the gas-bearing capacity can be revealed at the same time	The accuracy of the model depends on the various geological parameters used to build it. Fewer parameters reduce the accuracy and applicability of the model	Nie and Zhang (2012)
Numerical model for the dynamic enrichment and evolution process of shale gas	Total shale gas and gas in different occurrence states will change dynamically with the coupling of multiple control factors, which can be characterized by numerical simulation	Burial depth, temperature, formation hydrostatic pressure, maturity, hydrocarbon generating quantity, reservoir porosity, overpressure hydrocarbon expulsion conditions, pore water content and formation water salinity, formation pressure and temperature, TOC, mineral components, other calculation parameters (such as gas solubility, free water volume fraction, etc.)	This model can calculate the shale gas content in the geological history period, obtain the GIP and gas content in different occurrence states	The application of this model needs to meet certain preconditions, including generation products, overpressure and other conditions. At present, it has better applicability for shale systems with type III kerogen	Zhou et al., 2022a
Seismic multiple-attributes analysis method based on neural networks of AI	Gas bearing properties have good correlation with seismic attributes. Parameters such as gas content and attributes are obtained according to logging and seismic data processing. The optimal combination of seismic attributes and the relationship between gas content and each attribute are determined through single attribute and multi-attribute neural network analyses. Based on the optimal attribute number and type, the gas content of the whole three-dimensional data volume is calculated by using the relationship derived from neural network, so as to predict the spatial distribution of gas content.	Well log data (density, P-velocity, S-velocity, gamma ray) and parameters derived from log interpretation (e.g. porosity, TOC content, total gas content, brittleness index, Young's modulus and Poisson's ratio), and seismic elastic parameters	The application of artificial intelligence to determine the optimal combination of elastic parameters and seismic attributes provides a new insight for predicting shale gas content, reveals the main controlling factors of gas content characteristics in a specific study area, and can effectively identify high-quality gas rich reservoirs as well as spatial distribution and variation in the gas content of shale reservoirs	The model accuracy depends on the various geological parameters. The gas-bearing properties for this method are primarily obtained from logging data, from which mainly gas content evaluation depends on the accuracy of logging data processing results	Chen et al. (2019d)
Nuclear magnetic resonance (NMR) method	Mobile hydrogen nucleus or proton in CH_4 can be identified. By measuring NMR T_2 relaxation signal of shale sample, CH_4 in different occurrence states (adsorbed and free) can be determined	T_{2free} (NMR T_2 relaxation signal corresponding to free gas) and T_{2ad} (NMR T_2 relaxation signal corresponding to adsorbed gas)	CH_4 gas in different occurrence states is obtained by NMR test, so as to more directly measure absolute and relative amounts of the adsorbed and free CH_4 in shale	This method has certain requirements for core samples, preferably pressure coring samples. For conventional coring samples, NMR experiments need to be carried out at the reservoir pressure and temperature in order to obtain maximum adsorbed gas content. The free gas content can be estimated from the relationship between them	Yao et al. (2019)
Logging calculation method	The clay minerals, OM content and free gas content in the shale are clarified by logging data, and the total porosity, adsorbed gas and irreducible water porosity can be calculated, from which the total gas content in the shale can be obtained	Adsorbed gas content, irreducible water saturation (S_{wb}), clay mineral content (V_{clay}), TOC content, and logging data for porosity calculation, etc.	The data for this method are easy to obtain from continuous gas content analysis data. Moreover, the model for this method is easy to apply and has good applicability for marine shale with stable deposition and good preservation conditions	The data quality is potentially affected by the model's dependence on samples, as well as the applicability of the logging prediction model	Li et al. (2019b)
Isotopic method	The phenomenon of gas carbon isotope inversion is closely related to the magnitude of secondary cracking of retained oil and wet gases, so $\delta^{13}C_{methane}-\delta^{13}C_{ethane}$ can be used to evaluate the degree of secondary cracking, and then to obtain the gas-bearing properties of shale	$\delta^{13}C_{methane}$, $\delta^{13}C_{ethane}$	The gas content in shale is calculated from the perspective of geochemistry, which provides a new idea and perspective for a shale gas bearing property test	Test indicators are rather expensive to obtain, and they are more fitly applicable to highly mature shale. Because of the difference in the content of retained hydrocarbons and other factors, the correlation between $\delta^{13}C_{methane}-\delta^{13}C_{ethane}$ and gas content in shale may become relatively poor	Chen et al. (2020b)
Basin Modeling method	Shale gas accumulation is not only controlled by factors such as TOC content, thermal evolution degree and mineral content, but also by the tectonic-thermal evolution history. Based on petroleum system modeling (e.g., PetroMod),	Stratigraphic data (lithology, thickness, age), tectonic events (unconformity, denudation, sedimentary discontinuity time), tectonic-thermal evolution restoration boundary conditions (palaeoheat flow, paleowater	This method is easy to operate, and the experimental results are easy to obtain, the coupling relationship among shale structure-thermal evolution, oil and gas composition change and adsorption process can be	The method needs many input parameters and depends on matching the built-in model of the software to actual geological conditions	Chen et al. (2019a)

Table 4 (*continued*)

Method	Theory principle	Primary parameters	Advantages	Limitation	Reference
	the tectonic-thermal evolution history, oil and gas composition change and adsorption process can be simulated, so as to clarify the gas content of the target interval	depth, water-rock interface temperature, etc.), isothermal adsorption data (V_L, P_L, etc.) and geochemical characteristics of source rocks (TOC, hydrogen index, hydrocarbon generation kinetic model)	determined, and the dynamic changes of shale adsorption capacity and gas content in different geological periods can be obtained		

4.3. Other methods

With the exception of the two commonly used methods introduced above, qualitative methods such as gas logging and water immersion test are often used to evaluate gas content in shale gas exploration and development. In particular, in recent years, Chinese researchers have also explored some new assessment methods for shale gas content. Table 4 summarizes the theory principle, primary parameters, practicability and existing problems of these methods. Obviously, there is still a long way to go before these methods can be applied to shale gas evaluation under geological conditions.

5. Summary and further research directions

Gas is stored mainly in free and sorption states in the nanoscale pores of OM-rich shale, which makes it different from coalbed CH_4 and tight gas. The sorption mechanisms of shale under real geological conditions should be highly complex due to the presence of pore water and non-hydrocarbon gases. Many factors and processes influence the CH_4 sorption ability of shale, such as the variation of pore types, the sorption mechanism of supercritical CH_4 under water-bearing conditions, and the competitive sorption processes of CH_4 with water molecules, heavy hydrocarbon gases and non-hydrocarbon gases. All of these factors will affect the adsorption capacity and gas-bearing capacity of shale, especially the competitive adsorption mechanism and influence of water and N_2, and require further attention and research.

The gas content of shale is controlled by a combination of its geological properties (OM abundance, kerogen type, thermal maturity, mineral composition, diagenesis), pore fluid properties (water, CH_4, non-hydrocarbon gases), and geological conditions (temperature, pressure, preservation conditions). The influence of their coupling on shale gas enrichment is still the focus of research. In particular, the differences in mineral composition and OM properties of shales from various depositional environments may lead to significant differences in the influencing factors and constraining mechanisms of gas-bearing properties. Under the broad prospect of green and low-carbon energy, shale gas will make a crucial contribution to meeting clean energy demand, which is particularly significant for China's energy supply and transformation. The fundamental research on deep and ultra-deep marine, marine-continental transitional, and lacustrine shale gas reservoirs needs to be further investigated, and they will be important targets for future expanding exploration and development.

Various methods have been developed for qualitative and quantitative evaluation of shale gas content, with the most commonly used methods being the field desorption method and adsorption experimental methods. Although the field desorption method can directly obtain specific data of gas content in shale, the calculation of lost gas still faces challenges in many aspects, and the reliability of the data has been questioned for shale from deeper burial. The adsorption experimental method is simple and easy to implement, but the available theoretical models should be carefully reviewed for their suitability for specific geological applications, and the calculation results often require validation by shale gas field or development data. Fortunately, the development and application of confinement/pressure-holding coring technology not only allows for the acquisition of realistic shale gas content, but also allows for corrections to existing gas loss calculation models and developing new calculation models. Meanwhile, the improvement of artificial intelligence and data processing technologies will also provide a new means for shale gas evaluation. Combined with geochemical data, the application of geophysical data to regional shale gas content assessment will become the direction of shale gas resource potential evaluation.

Declaration of competing interest

The authors declare that they have no known competing financial interests or personal relationships that could have appeared to influence the work reported in this paper.

Acknowledgments

This study is supported by the National Natural Science Foundation of China (U19B6003-03-01), the Science and Technology Department of Shanxi Province, China (20201101003), and the National Natural Science Foundation of China (42030804). The authors appreciate both editors and reviewers for their precious time and insightful comments and suggestions that greatly improved the manuscript.

References

Alafnan, S., Solling, T., Mahmoud, M., 2020. Effect of kerogen thermal maturity on methane adsorption capacity: a molecular modeling approach. Molecules 25 (16), 3764. https://doi.org/10.3390/molecules25163764.

Ambrose, R.J., Hartman, R.C., Diaz-Campos, M., et al., 2010. New pore-scale considerations for shale gas in place calculations. In: SPE Unconventional Gas Conference, 131772. https://doi.org/10.2118/131772-MS. Pittsburgh, Pennsylvania, USA.

Ambrose, R.J., Hartman, R.C., Diaz-Campos, M., et al., 2012. Shale gas-in-place calculations Part I: new pore-scale considerations. SPE J. 219–229. https://doi.org/10.2118/131772-PA.

Ansari, R., Merletti, G., Gramin, P., et al., 2019. More accurate quantification of free and adsorbed gas in shale reservoirs. Petrophysics 60, 560–584. https://doi.org/10.30632/PJV60N5-2019a2.

Ardakani, O.H., Sanei, H., Ghanizadeh, A., et al., 2018. Do all fractions of organic matter contribute equally in shale porosity? A case study from Upper Ordovician Utica Shale, southern Quebec, Canada. Mar. Petrol. Geol. 92, 794–808. https://doi.org/10.1016/j.marpetgeo.2017.12.009.

Babatunde, K.A., Negash, B.M., Jufar, S.R., et al., 2022. Adsorption of gases on heterogeneous shale surfaces: a review. J. Petrol. Sci. Eng. 208 (Part B), 109466. https://doi.org/10.1016/j.petrol.2021.109466.

Bai, B.J., Elgmati, M., Zhang, H., et al., 2013. Rock characterization of Fayetteville shale gas plays. Fuel 105, 645–652. https://doi.org/10.1016/j.fuel.2012.09.043.

Bi, H., Jiang, Z.X., Li, J.Z., et al., 2017. Ono–Kondo model for supercritical shale gas storage: a case study of Silurian Longmaxi Shale in Southeast Chongqing, China. Energy Fuels 31 (3), 2755–2764. https://doi.org/10.1021/acs.energyfuels.6b03425.

Borjigin, T., Lu, L.F., Yu, L.J., et al., 2021. Formation, preservation and connectivity control of organic pores in shale. Petrol. Explor. Dev. 48 (4), 798–812. https://doi.org/10.1016/S1876-3804(21)60067-8.

Borjigin, T., Shen, B.J., Yu, L.J., et al., 2017. Mechanisms of shale gas generation and accumulation in the Ordovician Wufeng-Longmaxi Formation, Sichuan Basin,

SW China. Petrol. Explor. Dev. 44 (1), 69–78. https://doi.org/10.1016/S1876-3804(17)30009-5.
Bruns, B., Littke, R., Gasparik, M., et al., 2016. Thermal evolution and shale gas potential estimation of the Wealden and Posidonia Shale in NW-Germany and The Netherlands: a 3D basin modelling study. Basin Res. 28, 2–33. https://doi.org/10.1111/bre.12096.
Burnaman, M.D., Shelton, J., 2009. Shale gas play screening and evaluation criteria. China Petrol. Explor. 14 (3), 51–64.
Bustin, R.M., Bustin, A., Ross, D., et al., 2009. Shale gas opportunities and challenges. In: AAPG Annual Convention. San Antonio, Texas, Search and Discovery Articles #40382.
Canada Energy Regulator, 2022. Canada's energy future data appendices. https://doi.org/10.35002/zjr8-8x75.
Cao, T.T., Deng, M., Cao, Q.G., et al., 2021. Pore formation and evolution of organic-rich shale during the entire hydrocarbon generation process: examination of artificially and naturally matured samples. J. Nat. Gas Sci. Eng. 93, 104020. https://doi.org/10.1016/j.jngse.2021.104020.
Cerri, R., Di Martino, S., Balossino, P., et al., 2015. Combined application of pressure coring and desorption analysis for Barnett Shale gas evaluation. In: SPE Middle East Unconventional Resources Conference and Exhibition. Muscat, Oman. https://doi.org/10.2118/SPE-172936-MS.
Chalmers, G.R.L., Bustin, R.M., 2008. Lower Cretaceous gas shales in northeastern British Columbia, Part II: evaluation of regional potential gas resources. Bull. Can. Petrol. Geol. 56 (1), 22–61. https://doi.org/10.2113/gscpgbull.56.1.22.
Chalmers, G., Bustin, M., 2010. The effects and distribution of moisture in gas shale reservoir systems. In: AAPG Annual Convention and Exhibition, New Orleans, Louisiana, Search and Discovery, 80113. https://www.researchgate.net/publication/303445713.
Chang, J.Q., Fan, X.D., Jiang, Z.X., et al., 2021. Differential impact of clay minerals and organic matter on pore structure and its fractal characteristics of marine and continental shales in China. Appl. Clay Sci. 106334. https://doi.org/10.1016/j.clay.2021.106334.
Chareonsuppanimit, P., Mohammad, S.A., Robinson, R.L., et al., 2012. High-pressure adsorption of gases on shales: measurements and modeling. Int. J. Coal Geol. 95, 34–46. https://doi.org/10.1016/j.coal.2012.02.005.
Chen, C., Hu, D.D., Westacott, D., et al., 2013. Nanometer-scale characterization of microscopic pores in shale kerogen by image analysis and pore-scale modeling. Geochem. Geophys. Geosyst. 14, 4066–4075. https://doi.org/10.1002/ggge.20254.
Chen, C.S., Shi, S.Y., Wang, Y.P., 2019a. Adsorption simulation based on PetroMod of high-quality shale segment of Wufeng-Longmaxi Formation in Changning area, Sichuan Basin. Geochimica 48 (6), 602–612. https://doi.org/10.19700/j.0379-1726.2019.06.008 (in Chinese).
Chen, D.Y., Zhang, J.C., Wang, X.M., et al., 2018. Characteristics of lacustrine shale reservoir and its effect on methane adsorption capacity in Fuxin Basin. Energy Fuels 32 (11), 11105–11117. https://doi.org/10.1021/acs.energyfuels.8b01683.
Chen, F.R., Duan, J.B., Zhang, H.R., et al., 2020a. Shale gas resource evaluation based on “pressure coefficient”: a case study of Upper Ordovician Wufeng-Lower Silurian. Petrol. Geol. Exp. 42 (3), 405–414. https://doi.org/10.11781/sysydz202003405 (in Chinese).
Chen, G.H., Li, C., Lu, S.F., et al., 2021a. Critical factors controlling adsorption capacity of shale gas in Wufeng-Longmaxi formation, Sichuan Basin: evidences from both experiments and molecular simulations. J. Nat. Gas Sci. Eng. 88, 103774. https://doi.org/10.1016/j.jngse.2020.103774.
Chen, J., Xiao, X.M., 2014. Evolution of nanoporosity in organic-rich shales during thermal maturation. Fuel 129, 173–181. https://doi.org/10.1016/j.fuel.2014.03.058.
Chen, J.P., Zhao, W.Z., Xiao, Z.Y., et al., 2007. A discussion on the upper limit of maturity for gas generation by marine kerogens and the utmost of gas generative potential: taking the study on the Tarim Basin as an example. Chin. Sci. Bull. 52 (Suppl. 1), 125–132. https://doi.org/10.1007/s11434-007-6015-7.
Chen, L., Jiang, Z.X., Jiang, S., et al., 2021b. Effect of pre-adsorbed water on methane adsorption capacity in shale-gas systems. Front. Earth Sci. 9, 958. https://doi.org/10.3389/feart.2021.757705.
Chen, L., Jiang, Z.X., Liu, K.Y., et al., 2017. Relationship between pore characteristics and occurrence state of shale gas: a case study of Lower Silurian Longmaxi shale in the Upper Yangtze Platform, South China. Interpretation 5 (3), 437–449. https://doi.org/10.1190/INT-2016-0191.1.
Chen, L., Jiang, Z.X., Liu, Q.X., et al., 2019b. Mechanism of shale gas occurrence: insights from comparative study on pore structures of marine and lacustrine shales. Mar. Petrol. Geol. 104, 200–216. https://doi.org/10.1016/j.marpetgeo.2019.03.027.
Chen, L., Zuo, L., Jiang, Z.X., et al., 2019c. Mechanisms of shale gas adsorption: evidence from thermodynamics and kinetics study of methane adsorption on shale. Chem. Eng. J. 361, 559–570. https://doi.org/10.1016/j.cej.2018.11.185.
Chen, S., Zhao, W.Z., Ge, X.M., et al., 2019d. Predicting gas content in high-maturity marine shales using artificial intelligence based seismic multiple-attributes analysis: a case study from the lower Silurian Longmaxi Formation, Sichuan Basin, China. Mar. Petrol. Geol. 101, 180–194. https://doi.org/10.1016/j.marpetgeo.2018.11.043.
Chen, S.B., Gong, Z., Li, X.Y., et al., 2021c. Pore structure and heterogeneity of shale gas reservoirs and its effect on gas storage capacity in the Qiongzhusi Formation. Geosci. Front. 12 (6), 101244. https://doi.org/10.1016/j.gsf.2021.101244.
Chen, Z.H., Wang, T.G., Liu, Q., et al., 2015. Quantitative evaluation of potential organic-matter porosity and hydrocarbon generation and expulsion from mudstone in continental lake basins: a case study of Dongying sag, eastern China. Mar. Petrol. Geol. 66 (Part 4), 906–924. https://doi.org/10.1016/j.marpetgeo.2015.07.027.
Chen, Z.P., Chen, L., Wang, G.C., et al., 2020b. Applying isotopic geochemical proxy for gas content prediction of Longmaxi shale in the Sichuan Basin, China. Mar. Petrol. Geol. 116, 104329. https://doi.org/10.1016/j.marpetgeo.2020.104329.
Chen, Z.Y., Song, Y., Li, Z., et al., 2019e. The occurrence characteristics and removal mechanism of residual water in marine shales: a case study of Wufeng-Longmaxi shale in Changning-Weiyuan area, Sichuan basin. Fuel 253, 1056–1070. https://doi.org/10.1016/j.fuel.2019.05.069.
Cheng, P., Tian, H., Xiao, X.M., et al., 2017. Water distribution in overmature organic-rich shales: implications from water adsorption experiments. Energy Fuels 31 (12), 13120–13132. https://doi.org/10.1021/acs.energyfuels.7b01531.
Cheng, P., Xiao, X.M., Tian, H., et al., 2018. Water content and equilibrium saturation and their influencing factors of the Lower Paleozoic overmature organic-rich shales in the Upper Yangtze Region of Southern China. Energy Fuels 32 (11), 11452–11466. https://doi.org/10.1021/acs.energyfuels.8b03011.
Cui, Z., Yang, W., Wang, Q.Y., et al., 2020. Sealing property of roof and floor of Wufeng Formation-LongmaxiFormation and its influence on shale gas differential enrichmentin Sichuan Basin and its surrounding areas. Mar. Origin Petrol. Geol. 25 (3), 243–252. https://doi.org/10.3969/j.issn.1672-9854.2020.03.006 (in Chinese).
Curtis, J.B., 2002. Fractured shale-gas systems. AAPG Bull. 86 (11), 1921–1938. https://doi.org/10.1306/61EEDDBE-173E-11D7-8645000102C1865D.
Curtis, M.E., Cardott, B.J., Sondergeld, C.H., et al., 2012. Development of organic porosity in the Woodford Shale with increasing thermal maturity. Int. J. Coal Geol. 103, 26–31. https://doi.org/10.1016/j.coal.2012.08.004.
Dang, W., Jiang, S., Zhang, J.C., et al., 2021. A systematic experimental and modeling study of water adsorption/desorption behavior in organic-rich shale with different particle sizes. Chem. Eng. J. 426, 130596. https://doi.org/10.1016/j.cej.2021.130596.
Dang, W., Zhang, J.C., Nie, H.K., et al., 2020. Isotherms, thermodynamics and kinetics of methane-shale adsorption pair under supercritical condition: implications for understanding the nature of shale gas adsorption process. Chem. Eng. J. 383, 123191. https://doi.org/10.1016/j.cej.2019.123191.
Dang, W., Zhang, J.C., Tang, X., et al., 2018. Investigation of gas content of organic-rich shale: a case study from Lower Permian shale in southern North China Basin, central China. Geosci. Front. 9 (2), 559–575. https://doi.org/10.1016/j.gsf.2017.05.009.
Dang, W., Zhang, J.C., Wei, X.L., et al., 2017. Geological controls on methane adsorption capacity of Lower Permian transitional black shales in the Southern North China Basin, Central China: experimental results and geological implications. J. Petrol. Sci. Eng. 152, 456–470. https://doi.org/10.1016/j.petrol.2017.03.017.
Delle Piane, C., Ansari, H., Li, Z.S., et al., 2022. Influence of organic matter type on porosity development in the Wufeng-Longmaxi Shale: a combined microscopy, neutron scattering and physisorption approach. Int. J. Coal Geol. 249, 103880. https://doi.org/10.1016/j.coal.2021.103880.
Deng, E.D., Yi, T.S., Yan, Z.H., et al., 2020. Accumulation condition and shale gas potential of the marine-terrestrial transitional facies:A case study of Jinshacan 1 well of Longtan formation in northern Guizhou. J. China Inst. Min. Technol. 49 (6), 1166–1181. https://doi.org/10.13247/j.cnki.jcumt.001184 (in Chinese).
Diamond, W.P., Schatzel, S.J., 1998. Measuring the gas content of coal: a review. Int. J. Coal Geol. 35 (1–4), 311–331. https://doi.org/10.1016/S0166-5162(97)00040-2.
Dong, D.Z., Qiu, Z., Zhang, L.F., et al., 2021. Progress on sedimentology of transitional facies shales and new discoveries of shale gas. Acta Sedimentol. Sin. 39 (1), 29–45. https://doi.org/10.14027/j.issn.1000-0550.2021.002 (in Chinese).
Dong, T., He, Q., He, S., et al., 2020. Quartz types, origins and organic matter-hosted pore systems in the lower cambrian Niutitang Formation, middle yangtze platform, China. Mar. Petrol. Geol. 123, 104739. https://doi.org/10.1016/j.marpetgeo.2020.104739.
Du, X.D., Cheng, Y.G., Liu, Z.J., et al., 2020. Study on the adsorption of CH_4, CO_2 and various CH_4/CO_2 mixture gases on shale. Alex. Eng. J. 59 (6), 5165–5178. https://doi.org/10.1016/j.aej.2020.09.046.
Duan, S., Gu, M., Du, X.D., et al., 2016. Adsorption equilibrium of CO_2 and CH_4 and their mixture on Sichuan Basin shale. Energy Fuels 30 (3), 2248–2256. https://doi.org/10.1021/acs.energyfuels.5b02088.
Dutta, N.C., 2002. Geopressure prediction using seismic data: current status and the road ahead. Geophysics 67 (6), 2012–2041. https://doi.org/10.1190/1.1527101.
Ekundayo, J.M., Rezaee, R., Fan, C.Y., 2021. Experimental investigation and mathematical modelling of shale gas adsorption and desorption hysteresis. J. Nat. Gas Sci. Eng. 88, 103761. https://doi.org/10.1016/j.jngse.2020.103761.
Enriquez, D.A., Zhang, T.W., Sun, X., et al., 2020. Methane resaturation in Barnett Formation core plugs and new approach for determination of post-coring gas loss. Mar. Petrol. Geol. 118, 104430. https://doi.org/10.1016/j.marpetgeo.2020.104430.
Fan, C.H., Li, H., Qin, Q.R., et al., 2020. Geological conditions and exploration potential of shale gas reservoir in Wufeng and Longmaxi Formation of southeastern Sichuan Basin, China. J. Petrol. Sci. Eng. 191, 107138. https://doi.org/10.1016/j.petrol.2020.107138.
Fan, K.K., Li, Y.J., Elsworth, D., et al., 2018. Three stages of methane adsorption capacity affected by moisture content. Fuel 231, 352–360. https://doi.org/10.1016/j.fuel.2018.05.120.
Feng, D.J., Hu, Z.Q., Li, S.J., et al., 2021. Controlling effect of key preservation

elements on shale gas enrichment in Longmaxi Formation, eastern marginal zone of Sichuan Basin. Geol. Rev. 67 (1), 144–158. https://doi.org/10.16509/j.georeview.2021.01.011 (in Chinese).
Feng, G.J., Zhu, Y.M., Wang, G.G.X., et al., 2019. Supercritical methane adsorption on overmature shale: effect of pore structure and fractal characteristics. Energy Fuels 33 (9), 8323–8337. https://doi.org/10.1021/acs.energyfuels.9b01857.
Feng, Q.Q., Qiu, N.S., Borjigin, T., et al., 2022. Tectonic evolution revealed by thermo-kinematic and its effect on shale gas preservation. Energy 240, 122781. https://doi.org/10.1016/j.energy.2021.122781.
Ferrill, D.A., Morris, A.P., Hennings, P.H., 2014. Faulting and fracturing in shale and self-sourced reservoirs: introduction. AAPG Bull. 98 (11), 2161–2164. https://doi.org/10.1306/intro073014.
Fu, X.F., Wu, T., Lyu, Y.F., et al., 2018. Research status and development trend of the reservoir caprock sealing properties. Oil Gas Geol. 39 (3), 454–471. https://doi.org/10.11743/ogg20180304 (in Chinese).
Gai, H.F., Tian, H., Cheng, P., et al., 2020. Characteristics of molecular nitrogen generation from overmature black shales in South China: preliminary implications from pyrolysis experiments. Mar. Petrol. Geol. 120, 104527. https://doi.org/10.1016/j.marpetgeo.2020.104527.
Gao, F.L., Song, Y., Li, Z., et al., 2018. Lithofacies and reservoir characteristics of the lower cretaceous continental Shahezi shale in the Changling fault depression of Songliao Basin, NE China. Mar. Petrol. Geol. 98, 401–421. https://doi.org/10.1016/j.marpetgeo.2018.08.035.
Gao, S.K., Dong, D.Z., Tao, K., et al., 2021. Experiences and lessons learned from China's shale gas development: 2005–2019. J. Nat. Gas Sci. Eng. 85, 103648. https://doi.org/10.1016/j.jngse.2020.103648.
Gao, Z.Y., Xiong, S.L., 2021. Methane adsorption capacity reduction process of water-bearing shale samples and its influencing factors: one example of Silurian Longmaxi Formation shale from the Southern Sichuan Basin in China. J. Earth Sci. China 32 (4), 946–959. https://doi.org/10.1007/s12583-020-1120-5.
Gasparik, M., Bertier, P., Gensterblum, Y., et al., 2014. Geological controls on the methane storage capacity in organic-rich shales. Int. J. Coal Geol. 123, 34–51. https://doi.org/10.1016/j.coal.2013.06.010.
Gasparik, M., Ghanizadeh, A., Bertier, P., et al., 2012. High-pressure methane sorption isotherms of black shales from The Netherlands. Energy Fuels 26 (8), 4995–5004. https://doi.org/10.1021/ef300405g.
Gaus, G., Fink, R., Amann-Hildenbrand, A., et al., 2021. Experimental determination of porosity and methane sorption capacity of organic-rich shales as a function of effective stress: implications for gas storage capacity. AAPG Bull. 105 (2), 309–328. https://doi.org/10.1306/07212019086.
Gong, L., Shi, J.H., Ding, B., et al., 2020. Molecular insight on competitive adsorption and diffusion characteristics of shale gas in water-bearing channels. Fuel 278, 118406. https://doi.org/10.1016/j.fuel.2020.118406.
Gou, Q.Y., Xu, S., Hao, F., et al., 2021a. Differences in the nanopore structure of organic-rich shales with distinct sedimentary environments and mineral compositions. Energy Fuels 35 (20), 16562–16577. https://doi.org/10.1021/acs.energyfuels.1c02555.
Gou, Q.Y., Xu, S., Hao, F., et al., 2021b. Making sense of micro-fractures to the Longmaxi shale reservoir quality in the Jiaoshiba area, Sichuan Basin, China: implications for the accumulation of shale gas. J. Nat. Gas Sci. Eng. 94, 104107. https://doi.org/10.1016/j.jngse.2021.104107.
Guo, F.G., Wang, S., Feng, Q.H., et al., 2020a. Adsorption and absorption of supercritical methane within shale kerogen slit. J. Mol. Liq. 320 (Part A), 114364. https://doi.org/10.1016/j.molliq.2020.114364.
Guo, H.J., Jia, W.L., Peng, P.A., et al., 2017a. Evolution of organic matter and nanometer-scale pores in an artificially matured shale undergoing two distinct types of pyrolysis: a study of the Yanchang Shale with Type II kerogen. Org. Geochem. 105, 56–66. https://doi.org/10.1016/j.orggeochem.2017.01.004.
Guo, Q.H., Jin, Z.K., Geng, Y.K., et al., 2019a. The characteristics of carbonate minerals in the Longmaxi Formation gas shale and its impact on the reservoir performance in the Sichuan Basin. Nat. Gas Geosci. 30 (5), 616–625. https://doi.org/10.11764/j.issn.1672-1926.2018.12.002 (in Chinese).
Guo, T.L., 2019. A few geological issues in shale gas exploration and development. Petrol. Reserv. Eval. Dev. 9 (5), 14–19. https://doi.org/10.13809/j.cnki.cn32-1825/te.2019.05.002 (in Chinese).
Guo, T.L., He, X.P., Zeng, P., et al., 2020b. Geological characteristics and beneficial development scheme of shale gas reservoirs in complex tectonic regions:a case study of Wufeng-Longmaxi formations in Sichuan Basin and its periphery. Acta Pet. Sin. 41 (12), 1490–1500. https://doi.org/10.7623/syxb202012004 (in Chinese).
Guo, S., Lü, X.X., Song, X., et al., 2017b. Methane adsorption characteristics and influence factors of mesozoic shales in the Kuqa depression, Tarim basin, China. J. Petrol. Sci. Eng. 157, 187–195. https://doi.org/10.1016/j.petrol.2017.07.020.
Guo, T.L., Jiang, S., Zhang, P.X., et al., 2020c. Progress and direction of exploration and development of normally-pressured shale gas from the periphery of Sichuan Basin. Petrol. Geol. Exp. 42 (5), 837–845. https://doi.org/10.11781/sysydz202005837 (in Chinese).
Guo, W., Dong, D.Z., Li, M., et al., 2021. Quartz genesis in organic-rich shale and its indicative significance to reservoir quality: a case study on the first submember of the first Member of Lower Silurian Longmaxi Formation in the southeastern Sichuan Basin and its periphery. Nat. Gas. Ind. 41 (2), 65–74. https://doi.org/10.3787/j.issn.1000-0976.2021.02.008 (in Chinese).
Guo, X.S., Hu, D.F., Li, Y.P., et al., 2017c. Geological factors controlling shale gas enrichment and high production in Fuling shale gas field. Petrol. Explor. Dev. 44 (4), 513–523. https://doi.org/10.1016/S1876-3804(17)30060-5.
Guo, X.S., Hu, D.F., Liu, R.B., et al., 2019b. Geological conditions and exploration potential of Permian marine–continent transitional facies shale gas in the Sichuan Basin. Nat. Gas. Ind. B 6 (3), 198–204. https://doi.org/10.1016/j.ngib.2018.10.002.
Guo, X.W., Qin, Z.J., Yang, R., et al., 2019c. Comparison of pore systems of clay-rich and silica-rich gas shales in the lower Silurian Longmaxi formation from the Jiaoshiba area in the eastern Sichuan Basin, China. Mar. Petrol. Geol. 101, 265–280. https://doi.org/10.1016/j.marpetgeo.2018.11.038.
Han, K.X., Song, X.D., Yang, H.J., 2021a. The pricing of shale gas: a review. J. Nat. Gas Sci. Eng. 89, 103897. https://doi.org/10.1016/j.jngse.2021.103897.
Han, W.C., Li, A.F., Memon, A., et al., 2021b. Synergetic effect of water, temperature, and pressure on methane adsorption in shale gas reservoirs. ACS Omega 6 (3), 2215–2229. https://doi.org/10.1021/acsomega.0c05490.
Han, Y.J., Horsfield, B., Wirth, R., et al., 2017. Oil retention and porosity evolution in organic rich shales. AAPG Bull. 101 (6), 807–827. https://doi.org/10.1306/09221616069.
Handwerger, D.A., Suarez-Rivera, R., Vaughn, K.I., et al., 2011. Improved petrophysical core measurements on tight shale reservoirs using retort and crushed samples. In: SPE Annual Technical Conference and Exhibition. Denver, Colorado, USA, SPE-147456-MS. https://doi.org/10.2118/147456-MS.
Hao, F., Zou, H.Y., Lu, Y., 2013. Mechanisms of shale gas storage: implications for shale gas exploration in China. AAPG Bull. 97, 1325–1346. https://doi.org/10.1306/02141312091.
Hao, Y.Z., Jia, X.T., Lu, Z.W., et al., 2019. Water film or water bridge? Influence of self-generated electric field on coexisting patterns of water and methane in clay nanopores. J. Phys. Chem. C. 123 (36), 22656–22664. https://doi.org/10.1021/acs.jpcc.9b06519.
He, J.B., Tang, J.R., Lu, Z.H., et al., 2021. A method for calculating loss of shale gas during coring based on forward modeling. Energy Sci. Eng. 9, 447–460. https://doi.org/10.1002/ese3.834.
He, Q., Dong, T., He, S., et al., 2019. Methane adsorption capacity of marine-continental transitional facies shales: the case study of the Upper Permian Longtan Formation, northern Guizhou Province, Southwest China. J. Petrol. Sci. Eng. 183, 106406. https://doi.org/10.1016/j.petrol.2019.106406.
He, Z.L., Nie, H.K., Li, S.J., et al., 2020. Differential enrichment of shale gas in upper Ordovician and lower Silurian controlled by the plate tectonics of the Middle-Upper Yangtze, south China. Mar. Petrol. Geol. 118, 104357. https://doi.org/10.1016/j.marpetgeo.2020.104357.
Heller, R., Zoback, M., 2014. Adsorption of methane and carbon dioxide on gas shale and pure mineral samples. J. Unconvent. Oil Gas Resourc. 8, 14–24. https://doi.org/10.1016/j.juogr.2014.06.001.
Ho, T.M., Howes, T., Bhandari, B.R., 2014. Encapsulation of gases in powder solid matrices and their applications: a review. Powder Technol. 259, 87–108. https://doi.org/10.1016/j.powtec.2014.03.054.
Hol, S., Peach, C.J., Spiers, C.J., 2011. Applied stress reduces the CO_2 sorption capacity of coal. Int. J. Coal Geol. 85 (1), 128–142. https://doi.org/10.1016/j.coal.2010.10.010.
Hou, Y.G., Gao, J., Ren, K.X., et al., 2021. Variations of lacustrine shale reservoirs in different deformation zones of Mohe Basin, northeastern China: insights into the impact of thrust nappe structure on shale gas preservation. Mar. Petrol. Geol. 133, 105272. https://doi.org/10.1016/j.marpetgeo.2021.105272.
Hu, D.F., Zhang, H.R., Ni, K., et al., 2014. Main controlling factors for gas preservation conditions of marine shales in southeastern margins of the Sichuan Basin. Nat. Gas. Ind. 34 (6), 17–23. https://doi.org/10.3787/j.issn 1000-0976.2014.06.003 (in Chinese).
Hu, H., Zhang, T.W., Wiggins-Camacho, J.D., et al., 2015. Experimental investigation of changes in methane adsorption of bitumen-free Woodford Shale with thermal maturation induced by hydrous pyrolysis. Mar. Petrol. Geol. 59, 114–128. https://doi.org/10.1016/j.marpetgeo.2014.07.029.
Hu, H.Y., Hao, F., Guo, X.S., et al., 2018a. Investigation of methane sorption of overmature Wufeng-Longmaxi shale in the Jiaoshiba area, eastern Sichuan Basin, China. Mar. Petrol. Geol. 91, 251–261. https://doi.org/10.1016/j.marpetgeo.2018.01.008.
Hu, K., Mischo, H., 2020. High-pressure methane adsorption and desorption in shales from the Sichuan Basin, Southwestern China. Energy Fuels 34 (3), 2945–2957. https://doi.org/10.1021/acs.energyfuels.9b04142.
Hu, K., Tang, J.R., Mischo, H., 2021a. Investigation of supercritical shale gas adsorption in shale based on the Ono-Kondo lattice model. J. China Coal Soc. 46 (8), 2479–2487. https://doi.org/10.13225/j.cnki.jccs.CB21.0783 (in Chinese).
Hu, M., Huang, W.B., Li, J.Y., 2018b. Effects of structural characteristics on the productivity of shale gas wells: a case study on the Jiaoshiba Block in the Fuling Shale gasfield, Sichuan Basin. Nat. Gas. Ind. B 5 (2), 139–147. https://doi.org/10.1016/j.ngib.2018.02.001.
Hu, R.N., Wang, W.H., Tan, J.Q., et al., 2021b. Mechanisms of shale gas adsorption: insights from a comparative study on a thermodynamic investigation of microfossil-rich shale and non-microfossil shale. Chem. Eng. J. 411, 128463. https://doi.org/10.1016/j.cej.2021.128463.
Hu, Z.M., Duan, X.G., He, Y.B., et al., 2018c. Influence of reservoir primary water on shale gas occurrence and flow capacity. Nat. Gas. Ind. 38 (7), 44–51. https://doi.org/10.3787/j.issn.1000-0976.2018.07.006 (in Chinese).
Huang, H.X., Li, R.X., Jiang, Z.X., et al., 2020. Investigation of variation in shale gas adsorption capacity with burial depth: insights from the adsorption potential theory. J. Nat. Gas Sci. Eng. 73, 103043. https://doi.org/10.1016/j.jngse.2019.103043.
Huang, H.X., Li, R.X., Lyu, Z., et al., 2022a. Comparative study of methane adsorption

of Middle-Upper Ordovician marine shales in the western Ordos Basin, NW China: insights into impacts of moisture on thermodynamics and kinetics of adsorption. Chem. Eng. J. 446 (Part 4), 137411. https://doi.org/10.1016/j.cej.2022.137411.

Huang, L., Ning, Z.F., Wang, Q., et al., 2018. Molecular simulation of adsorption behaviors of methane, carbon dioxide and their mixtures on kerogen: effect of kerogen maturity and moisture content. Fuel 211, 159–172. https://doi.org/10.1016/j.fuel.2017.09.060.

Huang, M.C., Xu, H.Y., Yu, H., et al., 2022b. Fast prediction of methane adsorption in shale nanopores using kinetic theory and machine learning algorithm. Chem. Eng. J. 446 (Part 3), 137221. https://doi.org/10.1016/j.cej.2022.137221.

Hwang, J., Joss, L., Pini, R., 2019. Measuring and modelling supercritical adsorption of CO_2 and CH_4 on montmorillonite source clay. Microporous Mesoporous Mater. 273, 107–121. https://doi.org/10.1016/j.micromeso.2018.06.050.

Jacobi, D., Breig, J., LeCompte, B., et al., 2009. Effective geochemical and geomechanical characterization of shale gas reservoirs from the well bore environment: Caney and the Woodford Shale. In: 2009 SPE Annual Technical Conference and Exhibition Held in New Orleans. SPE, Louisiana, USA, pp. 1–20. https://doi.org/10.2118/124231-MS.

Jarvie, D.M., Hill, R.J., Ruble, T.E., et al., 2007. Unconventional shale-gas systems: the Mississippian Barnett Shale of north-central Texas as one model for thermogenic shale-gas assessment. AAPG Bull. 91 (4), 475–499. https://doi.org/10.1306/12190606068.

Jarvie, D.M., 2012. Shale Resource Systems for Oil and Gas: Part 1-Shale-Gas Resource Systems. AAPG Memoir, pp. 89–119. https://doi.org/10.1306/13321446M973489.

Ji, L.M., Zhang, T.W., Milliken, K.L., et al., 2012. Experimental investigation of main controls to methane adsorption in clay-rich rocks. Appl. Geochem. 27 (12), 2533–2545. https://doi.org/10.1016/j.apgeochem.2012.08.027.

Ji, W.M., Hao, F., Schulz, H.M., et al., 2019. The architecture of organic matter and its pores in highly mature gas shales of the lower Silurian Longmaxi Formation in the upper Yangtze platform, south China. AAPG Bull. 103 (12), 2909–2942. https://doi.org/10.1306/04101917386.

Ji, W.M., Song, Y., Jiang, Z.X., et al., 2015. Estimation of marine shale methane adsorption capacity based on experimental investigations of Lower Silurian Longmaxi formation in the Upper Yangtze Platform, south China. Mar. Petrol. Geol. 68 (Part A), 94–106. https://doi.org/10.1016/j.marpetgeo.2015.08.012.

Jiang, S., Tang, X.L., Cai, D.S., et al., 2017. Comparison of marine, transitional, and lacustrine shales: a case study from the Sichuan Basin in China. J. Pet. Sci. Eng. 150, 334–347. https://doi.org/10.1016/j.petrol.2016.12.014.

Jiang, W.B., Cao, G.H., Luo, C., et al., 2021a. A composition-based model for methane adsorption of overmature shales in Wufeng and Longmaxi Formation, Sichuan Basin. Chem. Eng. J. 130766. https://doi.org/10.1016/j.cej.2021.130766.

Jiang, Z.X., Li, X., Wang, X.M., et al., 2021b. Characteristic differences and controlling factors of pores in typical South China shale. Oil Gas Geol. 42 (1), 41–53. https://doi.org/10.11743/ogg20210104 (in Chinese).

Jiang, Z.X., Song, Y., Tang, X.L., et al., 2020. Controlling factors of marine shale gas differential enrichment in southern China. Petrol. Explor. Dev. 47 (3), 661–673. https://doi.org/10.1016/S1876-3804(20)60083-0.

Jin, Z.J., Nie, H.K., Liu, Q.Y., et al., 2018. Source and seal coupling mechanism for shale gas enrichment in upper Ordovician Wufeng formation-lower Silurian Longmaxi Formation in Sichuan Basin and its periphery. Mar. Petrol. Geol. 97, 78–93. https://doi.org/10.1016/j.marpetgeo.2018.06.009.

Jing, G.C., Chen, Z.X., Hui, G., 2021. A novel model to determine gas content in naturally fractured shale. Fuel 306, 121714. https://doi.org/10.1016/j.fuel.2021.121714.

Ju, Y., He, J., Chang, E., et al., 2019. Quantification of CH4 adsorption capacity in kerogen-rich reservoir shales: an experimental investigation and molecular dynamic simulation. Energy 170, 411–422. https://doi.org/10.1016/j.energy.2018.12.087.

Kang, S.M., Fathi, E., Ambrose, R.J., et al., 2011. Carbon dioxide storage capacity of organic-rich shales. SPE J. 16, 842–855. https://doi.org/10.2118/134583-PA.

Katz, B., Gao, L., Little, J., et al., 2021. Geology still matters-Unconventional petroleum system disappointments and failures. Unconv. Resour. 1, 18–38. https://doi.org/10.1016/j.uncres.2021.12.001.

Katz, B., Lin, F., 2014. Lacustrine basin unconventional resource plays: key differences. Mar. Petrol. Geol. 56, 255–265. https://doi.org/10.1016/j.marpetgeo.2014.02.013.

Katz, B.J., Arango, I., 2018. Organic porosity: a geochemist's view of the current state of understanding. Org. Geochem. 123, 1–16. https://doi.org/10.1016/j.orggeochem.2018.05.015.

Klewiah, I., Berawala, D.S., Alexander Walker, H.C., et al., 2020. Review of experimental sorption studies of CO_2 and CH_4 in shales. J. Nat. Gas Sci. Eng. 73, 103045. https://doi.org/10.1016/j.jngse.2019.103045.

Knapp, L.J., Ardakani, O.H., Uchida, S., et al., 2020. The influence of rigid matrix minerals on organic porosity and pore size in shale reservoirs: upper Devonian Duvernay Formation, Alberta, Canada. Int. J. Coal Geol. 103525. https://doi.org/10.1016/j.coal.2020.103525.

Ko, L.T., Loucks, R.G., Ruppel, S.C., et al., 2017. Origin and characterization of Eagle Ford pore networks in the south Texas Upper Cretaceous shelf. AAPG Bull. 101 (3), 387–418. https://doi.org/10.1306/08051616035.

Ko, L.T., Ruppel, S.C., Loucks, R.G., et al., 2018. Pore-types and pore-network evolution in Upper Devonian-Lower Mississippian Woodford and Mississippian Barnett mudstones: insights from laboratory thermal maturation and organic petrology. Int. J. Coal Geol. 190, 3–28. https://doi.org/10.1016/j.coal.2017.10.001.

Kong, X.X., Fan, H.J., Xiao, D.S., et al., 2021. Improved methane adsorption model in shale by considering variable adsorbed phase density. Energy Fuels 35 (3), 2064–2074. https://doi.org/10.1021/acs.energyfuels.0c03501.

Krooss, B.M., Littke, R., Müller, B., et al., 1995. Generation of nitrogen and methane from sedimentary organic matter: implications on the dynamics of natural gas accumulations. Chem. Geol. 126, 291–318. https://doi.org/10.1016/0009-2541(95)00124-7.

Kuang, L.C., Dong, D.Z., He, W.Y., et al., 2020. Geological characteristics and development potential of transitional shale gas in the east margin of the Ordos Basin, NW China. Petrol. Explor. Dev. 47 (3), 435–446. https://doi.org/10.1016/S1876-3804(20)60066-0.

Kuila, U., Prasad, M., 2013. Specific surface area and pore-size distribution in clays and shales. Geophys. Prospect. 61, 341–362. https://doi.org/10.1111/1365-2478.12028.

Lawal, L.O., Olayiwola, T., Abdel-Azeim, S., et al., 2020. Molecular simulation of kerogen-water interaction: theoretical insights into maturity. J. Mol. Liq. 299, 112224. https://doi.org/10.1016/j.molliq.2019.112224.

Li, D.H., Nie, H.K., 2019. A new method to calculate shale gas content based on gas reservoir characterization-A case study of Wells JY1 and PY1 in Sichuan Basin and its surrounding areas. Oil Gas Geol. 40 (6), 1324–1332. https://doi.org/10.11743/ogg20190616 (in Chinese).

Li, J., Chen, Z.X., Wu, K.L., et al., 2018a. A multi-site model to determine supercritical methane adsorption in energetically heterogeneous shales. Chem. Eng. J. 349, 438–455. https://doi.org/10.1016/j.apenergy.2019.113368.

Li, J., Li, X.F., Wang, X.Z., et al., 2016a. Water distribution characteristic and effect on methane adsorption capacity in shale clay. Int. J. Coal Geol. 159, 135–154. https://doi.org/10.1016/j.coal.2016.03.012.

Li, J., Li, X.F., Wu, K.L., et al., 2016b. Water sorption and distribution characteristics in clay and shale: effect of surface force. Energy Fuels 30 (11), 8863–8874. https://doi.org/10.1021/acs.energyfuels.6b00927.

Li, J., Wu, K.L., Chen, Z.X., et al., 2019a. Effects of energetic heterogeneity on gas adsorption and gas storage in geologic shale systems. Appl. Energy 251, 113368. https://doi.org/10.1016/j.apenergy.2019.113368.

Li, J., Wu, Q.Z., Jin, W.J., et al., 2019b. Logging evaluation of free-gas saturation and volume content in Wufeng-Longmaxi organic-rich shales in the Upper Yangtze Platform, China. Mar. Petrol. Geol. 100, 530–539. https://doi.org/10.1016/j.marpetgeo.2018.12.016.

Li, J., Zhao, J.Z., Wei, X.S., et al., 2019c. Origin of abnormal pressure in the upper Paleozoic shale of the Ordos Basin, China. Mar. Petrol. Geol. 110, 162–177. https://doi.org/10.1016/j.marpetgeo.2019.07.016.

Li, J.H., Li, B.B., Ren, C.H., et al., 2020a. An adsorption model for evaluating methane adsorption capacity in shale under various pressures and moisture. J. Nat. Gas Sci. Eng. 81, 103426. https://doi.org/10.1016/j.jngse.2020.103426.

Li, J.Q., Wang, S.Y., Lu, S.F., et al., 2019d. Microdistribution and mobility of water in gas shale: a theoretical and experimental study. Mar. Petrol. Geol. 102, 496–507. https://doi.org/10.1016/j.marpetgeo.2019.01.012.

Li, P., Jiang, Z.X., Zheng, M., et al., 2016c. Estimation of shale gas adsorption capacity of the Longmaxi Formation in the upper Yangtze platform, China. J. Nat. Gas Sci. Eng. 34, 1034–1043. https://doi.org/10.1016/j.jngse.2016.07.052.

Li, P., Zhang, J.C., Rezaee, R., et al., 2021a. Effect of adsorbed moisture on the pore size distribution of marine-continental transitional shales: insights from lithofacies differences and clay swelling. Appl. Clay Sci. 201, 105926. https://doi.org/10.1016/j.clay.2020.105926.

Li, P., Zhang, J.C., Tang, X., et al., 2020b. Assessment of shale gas potential of the lower Permian transitional Shanxi-Taiyuan shales in the southern North China Basin. Aust. J. Earth Sci. 68, 262–284. https://doi.org/10.1080/08120099.2020.1762737.

Li, Q.W., Pang, X.Q., Tang, L., et al., 2018b. Occurrence features and gas content analysis of marine and continental shales: a comparative study of Longmaxi Formation and Yanchang Formation. J. Nat. Gas Sci. Eng. 56, 504–522. https://doi.org/10.1016/j.jngse.2018.06.019.

Li, S.T., Wang, Y., Wang, X.M., et al., 2022a. Pore system and gas adsorption potential of lacustrine Yanchang Mudstone, Ordos Basin, China. Energy Rep. 8, 571–581. https://doi.org/10.1016/j.egyr.2021.11.259.

Li, T.F., Tian, H., Xiao, X.M., et al., 2017. Geochemical characterization and methane adsorption capacity of overmature organic-rich Lower Cambrian shales in northeast Guizhou region, southwest China. Mar. Petrol. Geol. 86, 858–873. https://doi.org/10.1016/j.marpetgeo.2017.06.043.

Li, W., Pang, X.Q., Snape, C., et al., 2019e. Molecular simulation study on methane adsorption capacity and mechanism in clay minerals: effect of clay type, pressure, and water saturation in shales. Energy Fuels 33 (2), 765–778. https://doi.org/10.1021/acs.energyfuels.8b03462.

Li, W., Stevens, L.A., Uguna, C.N., et al., 2021b. Comparison of the impact of moisture on methane adsorption and nanoporosity for over mature shales and their kerogens. Int. J. Coal Geol. 237, 103705. https://doi.org/10.1016/j.coal.2021.103705.

Li, W.B., Li, J.Q., Lu, S.F., et al., 2022b. Evaluation of gas-in-place content and gas-adsorbed ratio using carbon isotope fractionation model: a case study from Longmaxi shales in Sichuan Basin, China. Int. J. Coal Geol. 249, 103881. https://doi.org/10.1016/j.coal.2021.103881.

Li, W.B., Lu, S.F., Li, J.Q., et al., 2021c. Geochemical modeling of carbon isotope fractionation during methane transport in tight sedimentary rocks. Chem. Geol. 566, 120033. https://doi.org/10.1016/j.chemgeo.2020.120033.

Li, X., Jiang, Z.X., Jiang, S., et al., 2021d. Synergetic effects of matrix components and diagenetic processes on pore properties in the Lower Cambrian shale in Sichuan

Basin, South China. J. Nat. Gas Sci. Eng. 94, 104072. https://doi.org/10.1016/j.jngse.2021.104072.
Li, X.F., Feng, D., Zhang, T., et al., 2020c. The role and its application of capillary force in the development of unconventional oil and gas reservoirs and its application. Acta Pet. Sin. 41 (12), 1719–1733. https://doi.org/10.7623/syxb202012024 (in Chinese).
Li, Z.Y., Elsworth, D., 2019. Controls of CO_2–N_2 gas flood ratios on enhanced shale gas recovery and ultimate CO_2 sequestration. J. Petrol. Sci. Eng. 179, 1037–1045. https://doi.org/10.1016/j.petrol.2019.04.098.
Li, Z., Zhang, J.C., Gong, D.J., et al., 2020d. Gas-bearing property of the lower cambrian Niutitang Formation shale and its influencing factors: a case study from the Cengong block, northern Guizhou province, south China. Mar. Petrol. Geol. 120, 104556. https://doi.org/10.1016/j.marpetgeo.2020.104556.
Liu, G., Zhao, Q.P., Gao, C., et al., 2019a. A critical desorption time method to improve the calculation accuracy ofgas loss in shale gas content testing. Nat. Gas. Ind. 39 (2), 71–75. https://doi.org/10.3787/j.issn.1000-0976.2019.02.010 (in Chinese).
Liu, K.Q., Ostadhassan, M., Sun, L.W., et al., 2019b. A comprehensive pore structure study of the Bakken Shale with SANS, N2 adsorption and mercury intrusion. Fuel 245, 274–285. https://doi.org/10.1016/j.fuel.2019.01.174.
Liu, L.M., Tan, S.J., Horikawa, T., et al., 2017a. Water adsorption on carbon - a review. Adv. Colloid Interface Sci. 250, 64–78. https://doi.org/10.1016/j.cis.2017.10.002.
Liu, R.W., Gao, D.P., Li, Q., et al., 2019c. Mechanical frontiers in shale-gas development. Adv. Mech. 49, 1–236. https://doi.org/10.6052/1000-0992-17-020 (in Chinese).
Liu, R.Z., Liu, Y.F., Duan, J.Y., et al., 2022. Ensemble learning directed classification and regression of hydrocarbon fuels. Fuel 324 (Part A), 124520. https://doi.org/10.1016/j.fuel.2022.124520.
Liu, S.G., Jiao, K., Zhang, J.C., et al., 2021a. Research progress on the pore characteristics of deep shale gas reservoirs: an example from the Lower Paleozoic marine shale in the Sichuan Basin. Nat. Gas. Ind. 40 (1), 29–41. https://doi.org/10.3787/j.issn.1000-0976.2021.01.003 (in Chinese).
Liu, W.P., Wu, J., Jiang, H., et al., 2021b. Cenozoic exhumation and shale-gas enrichment of the Wufeng-Longmaxi formation in the southern Sichuan basin, western China. Mar. Petrol. Geol. 125, 104865. https://doi.org/10.1016/j.marpetgeo.2020.104865.
Liu, Y.K., Xiong, Y.Q., Li, Y., et al., 2017b. Effects of oil expulsion and pressure on nanopore development in highly mature shale: evidence from a pyrolysis study of the Eocene Maoming oil shale, south China. Mar. Petrol. Geol. 86, 526–536. https://doi.org/10.1016/j.marpetgeo.2017.06.012.
Loucks, R.G., Reed, R.M., Ruppel, S.C., et al., 2012. Spectrum of pore types and networks in mudrocks and a descriptive classification for matrix–related mudrock pores. AAPG (Am. Assoc. Pet. Geol.) Bull. 96, 1071–1098. https://doi.org/10.1306/08171111061.
Loucks, R.G., Reed, R.M., Ruppel, S.C., et al., 2009. Morphology, genesis, and distribution of nanometer-scale pores in siliceous mudstones of the mississippian barnett shale. J. Sediment. Res. 79 (12), 848–861. https://doi.org/10.2110/jsr.2009.092.
Lu, Y.Y., Zhou, J.P., Xian, X.F., et al., 2021. Research progress and prospect of the integrated supercritical CO_2 enhanced shale gas recovery and geological sequestration. Nat. Gas. Ind. 41 (6), 60–73. https://doi.org/10.3787/j.issn.1000-0976.2021.06.007 (in Chinese).
Luo, Q.Y., Fariborz, G., Zhong, N.N., Wang, Y., Qiu, N.S., Skovsted, C.B., Suchý, V., Hemmingsen Schovsbo, N., Morga, R., Xu, Y.H., Hao, J.Y., Liu, A.J., Wu, J., Cao, W.X., Min, X., Wu, J., 2020. Graptolites as fossil geo-thermometers and source material of hydrocarbons: an overview of four decades of progress. Earth Sci. Rev. 200, 103000. https://doi.org/10.1016/j.earscirev.2019.103000.
Luo, Q.Y., Zhang, L., Zhong, N.N., Wu, J., Goodarzi, F., Sanei, H., Skovsted, C., Suchý, V., Li, M.J., Ye, X.Z., Cao, W.X., Liu, A.J., Min, X., Pan, Y.Y., Yao, L.P., Wu, J., 2021. Thermal evolution behavior of the organic matter and a ray of light on the origin of vitrinite-like maceral in the Mesoproterozoic and Lower Cambrian black shales: insights from artificial maturation. Int. J. Coal Geol. 244, 103813. https://doi.org/10.1016/j.coal.2021.103813.
Ma, L.J., Yu, Q.C., 2021. Experimental investigation into simultaneous adsorption of water vapor and methane onto shales. J. Hydrol. 127200. https://doi.org/10.1016/j.jhydrol.2021.127200.
Ma, R.Y., Zhang, J., Wang, M., et al., 2021a. Micro-pore characteristics and gas-bearing property of marine continental transitional shale reservoirs in the Qinshui basin. J. Henan Polytech. Univ. (Nat. Sci.) 40 (4), 66–77. https://doi.org/10.16186/j.cnki.1673-9787.2019120015 (in Chinese).
Ma, X.H., 2018. Enrichment laws and scale effective development of shale gas in the southern Sichuan Basin. Nat. Gas. Ind. 38 (10), 1–10. https://doi.org/10.3787/j.issn.1000-0976.2018.10.001 (in Chinese).
Ma, X.H., Wang, H.Y., Zhou, S.W., et al., 2021b. Deep shale gas in China: geological characteristics and development strategies. Energy Rep. 7, 1903–1914. https://doi.org/10.1016/j.egyr.2021.03.043.
Ma, X.H., Xie, J., Yong, R., et al., 2020a. Geological characteristics and high production control factors of shale gas reservoirs in Silurian Longmaxi Formation, southern Sichuan Basin, SW China. Petrol. Explor. Dev. 47 (5), 901–915. https://doi.org/10.1016/S1876-3804(20)60105-7.
Ma, Y., Ardakani, O.H., Zhong, N.N., et al., 2020b. Possible pore structure deformation effects on the shale gas enrichment: an example from the Lower Cambrian shales of the Eastern Upper Yangtze Platform, South China. Int. J. Coal Geol. 217, 103349. https://doi.org/10.1016/j.coal.2019.103349.
Ma, Y., Pan, J.L., Fu, D.L., et al., 2021c. The organic geochemistry, pore structure and methane adsorption/storage capacity of lacustrine shales from the Cretaceous Madongshan Formation, Liupanshan Basin, China. J. Nat. Gas Sci. Eng. 96, 104287. https://doi.org/10.1016/j.jngse.2021.104287.
Ma, Y., Zhong, N.N., Li, D.H., et al., 2015. Organic matter/clay mineral intergranular pores in the Lower Cambrian Lujiaping Shale in the north-eastern part of the upper Yangtze area, China: a possible microscopic mechanism for gas preservation. Int. J. Coal Geol. 137, 38–54. https://doi.org/10.1016/j.coal.2014.11.001.
Ma, Y.S., Cai, X.Y., Zhao, P.R., 2018. China's shale gas exploration and development: understanding and practice. Petrol. Explor. Dev. 45 (4), 589–603. https://doi.org/10.1016/S1876-3804(18)30065-X.
Mahzari, P., Mitchell, T.M., Jones, A.P., et al., 2021. Direct gas-in-place measurements prove much higher production potential than expected for shale formations. Sci. Rep. 11, 10775. https://doi.org/10.1038/s41598-021-90160-3.
Mastalerz, M., Schimmelmann, A., Drobniak, A., et al., 2013. Porosity of devonian and mississippian new albany shale across a maturation gradient: insights from organic petrology, gas adsorption, and mercury intrusion. AAPG Bull. 97 (10), 1621–1643. https://doi.org/10.1306/04011312194.
Meng, M., Zhong, R.Z., Wei, Z.L., 2020. Prediction of methane adsorption in shale: classical models and machine learning based models. Fuel 278, 118358. https://doi.org/10.1016/j.fuel.2020.118358.
Merkel, A., Fink, R., Littke, R., 2015. The role of pre-adsorbed water on methane sorption capacity of Bossier and Haynesville shales. Int. J. Coal Geol. 147 (1), 1–8. https://doi.org/10.1016/j.coal.2015.06.003.
Merkel, A., Fink, R., Littke, R., 2016. High pressure methane sorption characteristics of lacustrine shales from the Midland Valley Basin, Scotland. Fuel 182, 361–372. https://doi.org/10.1016/j.fuel.2016.05.118.
Miao, F., Wu, D., Liu, X.Y., et al., 2022. Methane adsorption on shale under in situ conditions: gas-in-place estimation considering in situ stress. Fuel 308, 121991. https://doi.org/10.1016/j.fuel.2021.121991.
Milliken, K.L., Zhang, T.W., Chen, J.P., et al., 2021. Mineral diagenetic control of expulsion efficiency in organic-rich mudrocks, Bakken formation (Devonian-Mississippian), Williston basin, North Dakota, U.S.A. Mar. Petrol. Geol. 127, 104869. https://doi.org/10.1016/j.marpetgeo.2020.104869.
Mu, Y., Hu, Z.M., Chang, J., et al., 2021. Effect of water occurrence on shale seepage ability. J. Petrol. Sci. Eng. 204, 108725. https://doi.org/10.1016/j.petrol.2021.108725.
Mu, Z.Q., Ning, Z.F., Ren, C.Y., 2022. Methane adsorption on shales and application of temperature-related composite models based on dual adsorption modes. J. Petrol. Sci. Eng. 208 (Part A), 109379. https://doi.org/10.1016/j.petrol.2021.109379.
Nait Amar, M., Larestani, A., Lv, Q.C., et al., 2022. Modeling of methane adsorption capacity in shale gas formations using white-box supervised machine learning techniques. J. Petrol. Sci. Eng. 208 (Part B), 109226. https://doi.org/10.1016/j.petrol.2021.109226.
Nie, H.K., He, Z.L., Wang, R.Y., et al., 2020. Temperature and origin of fluid inclusions in shale veins of Wufeng-Longmaxi Formations, Sichuan Basin, south China: implications for shale gas preservation and enrichment. J. Petrol. Sci. Eng. 193, 107329. https://doi.org/10.1016/j.petrol.2020.107329.
Nie, H.K., Tang, X., Bian, R.K., 2009. Controlling factors for shale gas accumulation and prediction of potential development area in shale gas reservoir of South China. Acta Pet. Sin. 30 (4), 484–491 (in Chinese).
Nie, H.K., Zhang, J.C., 2012. Shale gas accumulation conditions and gas content calculation: a case study of Sichuan Basin and its periphery in the Lower Paleozoic. Acta Geol. Sin. 86 (2), 349–361 (in Chinese).
Novi Labs, 2022. US-Update through January 2021. https://shaleprofile.com/blog/us/us-update-through-january-2021/.
Nygård, R., Gutierrez, M., Bratli, R.K., et al., 2006. Brittle–ductile transition, shear failure and leakage in shales and mudrocks. Mar. Petrol. Geol. 23 (2), 201–212. https://doi.org/10.1016/j.marpetgeo.2005.10.001.
Ortiz Cancino, O.P., Pino Pérez, D., Pozo, M., et al., 2017. Adsorption of pure CO_2 and a CO_2/CH_4 mixture on a black shale sample: manometry and microcalorimetry measurements. J. Petrol. Sci. Eng. 159, 307–313. https://doi.org/10.1016/j.petrol.2017.09.038.
Pan, L., Xiao, X.M., Tian, H., et al., 2015. A preliminary study on the characterization and controlling factors of porosity and pore structure of the Permian shales in Lower Yangtze region, Eastern China. Int. J. Coal Geol. 146, 68–78. https://doi.org/10.1016/j.coal.2015.05.005.
Pan, L., Xiao, X.M., Tian, H., et al., 2016. Geological models of gas in place of the Longmaxi shale in Southeast Chongqing, south China. Mar. Petrol. Geol. 73, 433–444. https://doi.org/10.1016/j.marpetgeo.2016.03.018.
Pang, W.Y., He, Y.Q., Yan, C.H., et al., 2019. Tackling the challenges in the estimation of methane absolute adsorption in kerogen nanoporous media from molecular and analytical approaches. Fuel 242, 687–698. https://doi.org/10.1016/j.fuel.2019.01.059.
Pathi, V.S., Kurison, C., Hakami, A.M., et al., 2022. Limited storage and recovery of adsorbed gas in shale reservoirs - insights from experiments and production modeling. Fuel Commun. 10, 100039. https://doi.org/10.1016/j.jfueco.2021.100039.
Qi, R.R., Ning, Z.F., Zhang, S., et al., 2018. Prediction model of shale gas content with the consideration of moisture and multicomponent gas. J. China Coal Soc. 43 (9), 2553–2561. https://doi.org/10.13225/j.cnki.jccs.2017.1837 (in Chinese).
Qi, Y., Ju, Y.W., Jia, T.R., et al., 2017. Nanoporous structure and gas occurrence of organic-rich shales. J. Nanosci. Nanotechnol. 17 (9), 6942–6950. https://doi.org/10.1166/jnn.2017.14466.
Qiao, J.Q., Littke, R., Zieger, L., et al., 2020. Controls on gas storage characteristics of Upper Paleozoic shales from the southeastern Ordos Basin. Mar. Petrol. Geol.

117, 104377. https://doi.org/10.1016/j.marpetgeo.2020.104377.
Qiu, Z., Song, D.J., Zhang, L.F., et al., 2021. The geochemical and pore characteristics of a typical marine-continental transitional gas shale: a case study of the Permian Shanxi Formation on the eastern margin of the Ordos Basin. Energy Rep. 7, 3726–3736. https://doi.org/10.1016/j.egyr.2021.06.056.
Rani, S., Padmanabhan, E., Prusty, B.K., 2019. Review of gas adsorption in shales for enhanced methane recovery and CO_2 storage. J. Petrol. Sci. Eng. 175, 634–643. https://doi.org/10.1016/j.petrol.2018.12.081.
Rani, S., Prusty, B.K., Pal, S.K., 2018. Adsorption kinetics and diffusion modeling of CH_4 and CO_2 in Indian shales. Fuel 216, 61–70. https://doi.org/10.1016/j.fuel.2017.11.124.
Rexer, T.F.T., Benham, M.J., Aplin, A.C., et al., 2013. Methane adsorption on shale under simulated geological temperature and pressure conditions. Energy Fuels 27 (6), 3099–3109. https://doi.org/10.1021/ef400381v.
Rexer, T.F., Mathia, E.J., Aplin, A.C., et al., 2014. High-pressure methane adsorption and characterization of pores in Posidonia shales and isolated kerogens. Energy Fuels 28 (5), 2886–2901. https://doi.org/10.1021/ef402466m.
Římnáčová, D., Weishauptová, Z., Přibyl, O., et al., 2020. Effect of shale properties on CH_4 and CO_2 sorption capacity in Czech Silurian shales. J. Nat. Gas Sci. Eng. 80, 103377. https://doi.org/10.1016/j.jngse.2020.103377.
Rine, J.M., Smart, E., Dorsey, W., et al., 2013. Comparison of porosity distribution within selected North American shale units by SEM examination of argon-ion-milled samples. In: Camp, W., Diaz, E., Wawak, B. (Eds.), Electron Microscopy of Shale Hydrocarbon Reservoirs, vol. 102. American Association of Petroleum Geologists Memoir, pp. 137–152. https://doi.org/10.1306/13391710M1023588.
Ross, D.J.K., Bustin, R.M., 2007. Shale gas potential of the lower Jurassic Gordondale member, northeastern British Columbia. Can. B. Can. Petrol. Geol. 55 (1), 51–75. https://doi.org/10.2113/gscpgbull.55.1.51.
Ross, D.J.K., Bustin, R.M., 2008. Characterizing the shale gas resource potential of Devonian-Mississippian strata in the western Canada sedimentary basin: application of an integrated formation evaluation. AAPG Bull. 92, 87–125. https://doi.org/10.1306/09040707048.
Ross, D.J.K., Bustin, R.M., 2009. The importance of shale composition and pore structure upon gas storage potential of shale gas reservoirs. Mar. Petrol. Geol. 26 (6), 916–927. https://doi.org/10.1016/j.marpetgeo.2008.06.004.
Sageman, B.B., Murphy, A.E., Werne, J.P., et al., 2003. A tale of shales: the relative roles of production, decomposition, and dilution in the accumulation of organic-rich strata, Middle-Upper Devonian, Appalachian basin. Chem. Geol. 195 (1–4), 229–273. https://doi.org/10.1016/S0009-2541(02)00397-2.
Sander, R., Pan, Z.J., Connell, L.D., et al., 2018. Controls on methane sorption capacity of Mesoproterozoic gas shales from the Beetaloo Sub-basin, Australia and global shales. Int. J. Coal Geol. 199, 65–90. https://doi.org/10.1016/j.coal.2018.09.018.
Sang, G., Liu, S., Elsworth, D., 2019. Water vapor sorption properties of Illinois shales under dynamic water vapor conditions: experimentation and modeling. Water Resour. Res. 55, 7212–7228. https://doi.org/10.1029/2019WR024992.
Secretaría de energía, 2022. Sesco + tight shale gas production Chapter IV basin Division. http://datos.minem.gob.ar/dataset/produccion-de-petroleo-y-gas-tablas dinamicas/archivo/ad1b9472-a370-47e7-8de3-b742495ec7f1.
Seemann, T., Bertier, P., Krooss, B.M., et al., 2017. Water Vapour Sorption on Mudrocks, vol. 454. Geological Society London Special Publications, pp. 201–233. https://doi.org/10.1144/SP454.8.
Shabani, M., Moallemi, S.A., Krooss, B.M., et al., 2018. Methane sorption and storage characteristics of organic-rich carbonaceous rocks, Lurestan province, southwest Iran. Int. J. Coal Geol. 186, 51–64. https://doi.org/10.1016/j.coal.2017.12.005.
Shao, L.Y., Yang, Z.Y., Fang, C., et al., 2021. Permo-Carboniferous marine-terrestrial transitional facies coal measures shale gas geological conditions and exploration potential in Qinshui Basin. Coal Geol. China 33 (10), 1–10. https://doi.org/10.3969/j.issn.1674-1803.2021.10.01 (in Chinese).
Sheng, M., Li, G.S., Chen, L.Q., et al., 2014. Mechanisms analysis of shale-gas supercritical adsorption and modeling of isorption adsorption. J. China Coal Soc. 39 (S1), 179–183. https://doi.org/10.13225/j.cnki.jccs.2013.0474 (in Chinese).
Shi, W.R., Wang, X.Z., Zhang, C.M., et al., 2019. Experimental study on gas content of adsorption and desorption in Fuling shale gas field. J. Petrol. Sci. Eng. 180, 1069–1076. https://doi.org/10.1016/j.petrol.2019.06.021.
Shtepani, E., Noll, L.A., Elrod, L.W., et al., 2010. A new regression-based method for accurate measurement of coal and shale gas content. SPE Reservoir Eval. Eng. 13, 359–364. https://doi.org/10.2118/115405-PA.
Shu, Y., Lu, Y.C., Chen, L., et al., 2020. Factors influencing shale gas accumulation in the lower Silurian Longmaxi formation between the north and South Jiaoshiba area, Southeast Sichuan Basin, China. Mar. Petrol. Geol. 111, 905–917. https://doi.org/10.1016/j.marpetgeo.2019.06.029.
Soeder, D.J., Borglum, S.J., 2019. 2 - unconventional tight oil and shale gas resources. In: Soeder, D.J., Borglum, S.J. (Eds.), The Fossil Fuel Revolution: Shale Gas and Tight Oil. Elsevier, New York, pp. 31–61. https://doi.org/10.1016/B978-0-12-815397-0.00003-3.
Song, L.S., Carr, T.R., 2020. The pore structural evolution of the Marcellus and Mahantango shales, Appalachian Basin. Mar. Petrol. Geol. 114, 104226. https://doi.org/10.1016/j.marpetgeo.2020.104226.
Song, X., Lü, X.X., Shen, Y.Q., et al., 2018. A modified supercritical Dubinin–Radushkevich model for the accurate estimation of high pressure methane adsorption on shales. Int. J. Coal Geol. 193, 1–15. https://doi.org/10.1016/j.coal.2018.04.008.
Su, J., Shen, Y.C., Hao, J., et al., 2017. Shale gas content calculation of the triassic Yanchang Formation in the southeastern Ordos Basin, China. Energies 10. https://doi.org/10.3390/en10121949.
Sun, C.X., Nie, H.K., Dang, W., et al., 2021a. Shale gas exploration and development in China: current status, geological challenges, and future directions. Energy Fuels 35 (8), 6359–6379. https://doi.org/10.1021/acs.energyfuels.0c04131.
Sun, J., Xiao, X.M., Cheng, P., 2022. Methane absorption of coal-measure shales with and without pore water from the Qinshui Basin, North China: based on high-pressure methane absorption experiments. Int. J. Coal Geol. 263, 104116. https://doi.org/10.1016/j.coal.2022.104116.
Sun, J., Xiao, X.M., Wei, Q., et al., 2021b. Occurrence of irreducible water and its influences on gas-bearing property of gas shales from shallow Longmaxi Formation in the Xishui area, Guizhou, southern China. Front. Earth Sci. 9, 654136. https://doi.org/10.3389/feart.2021.654136.
Sun, J., Xiao, X.M., Wei, Q., et al., 2020. Gas in place and its controlling factors of the shallow Longmaxi shale in the Xishui area, Guizhou, China. J. Nat. Gas Sci. Eng. 77, 103272. https://doi.org/10.1016/j.jngse.2020.103272.
Sun, J.Y., Chen, C., Hu, W.F., et al., 2021c. Asymmetric competitive adsorption of CO_2/CH_4 binary mixture in shale matrix with heterogeneous surfaces. Chem. Eng. J. 422, 130025. https://doi.org/10.1016/j.cej.2021.130025.
Sun, Z., Shi, J.T., Yang, Z.P., et al., 2019. Evaluation about adsorption gas and free gas content inside shale matrix under a wide range of atmosphere conditions. In: Abu Dhabi International Petroleum Exhibition & Conference. UAE, Abu Dhabi. https://doi.org/10.2118/197176-ms.
Syah, R., Towfighi Naeem, M.H., Daneshfar, R., et al., 2022. On the prediction of methane adsorption in shale using grey wolf optimizer support vector machine approach. Petroleum 8 (2), 264–269. https://doi.org/10.1016/j.petlm.2021.12.002.
Takbiri-Borujeni, A., Kazemi, M., Sun, T., et al., 2017. Effect of kerogen type and maturity on performance of carbon dioxide storage in shale. In: SPE Annual Technical Conference and Exhibition San Antonio, Texas, USA, SPE-187360-MS. https://doi.org/10.2118/187360-MS.
Tan, J.Q., Liu, J.L., Kang, X., et al., 2021. Experimental gas generation of organic-rich shales at different oil expulsion efficiencies: implications for shale gas evaluation. Energy Fuels 35 (7), 5925–5940. https://doi.org/10.1021/acs.energyfuels.1c00141.
Tan, J.Q., Weniger, P., Krooss, B., et al., 2014. Shale gas potential of the major marine shale formations in the Upper Yangtze Platform, South China, Part II: methane sorption capacity. Fuel 129, 204–218. https://doi.org/10.1016/j.fuel.2014.03.064.
Tang, L., Song, Y., Jiang, S., et al., 2020. Sealing mechanism of the roof and floor for the Wufeng-Longmaxi shale gas in the Southern Sichuan Basin. Energy Fuels 34 (6), 6999–7018. https://doi.org/10.1021/acs.energyfuels.0c00983.
Tang, X., Ripepi, N., Rigby, S., et al., 2019a. New perspectives on supercritical methane adsorption in shales and associated thermodynamics. J. Ind. Eng. Chem. 78, 186–197. https://doi.org/10.1016/j.jiec.2019.06.015.
Tang, X., Ripepi, N., Stadie, N.P., et al., 2016. A dual-site Langmuir equation for accurate estimation of high pressure deep shale gas resources. Fuel 185, 10–17. https://doi.org/10.1016/j.fuel.2016.07.088.
Tang, X.L., Wu, W., Zhong, G.H., et al., 2021. Characteristics and origin of methane adsorption capacity of marine, transitional, and lacustrine shales in Sichuan Basin, China. Geofluids, 6674815. https://doi.org/10.1155/2021/6674815.
Tang, Y., Yang, R.Z., Zhu, J.F., et al., 2019b. Analysis of continental shale gas accumulation conditions in a rifted basin: a case study of Lower Cretaceous shale in the southern Songliao Basin, northeastern China. Mar. Petrol. Geol. 101, 389–409. https://doi.org/10.1016/j.marpetgeo.2018.12.002.
Tian, H., Li, T.F., Zhang, T.W., et al., 2016. Characterization of methane adsorption on overmature Lower Silurian-Upper Ordovician shales in Sichuan Basin, southwest China: experimental results and geological implications. Int. J. Coal Geol. 156, 36–49. https://doi.org/10.1016/j.coal.2016.01.013.
Tian, H., Pan, L., Xiao, X.M., et al., 2013. A preliminary study on the pore characterization of Lower Silurian black shales in the Chuandong Thrust Fold Belt, southwestern China using low pressure N_2 adsorption and FE-SEM methods. Mar. Petrol. Geol. 48, 8–19. https://doi.org/10.1016/j.marpetgeo.2013.07.008.
Tian, Y.Y., Yan, C.H., Jin, Z.H., 2017. Characterization of methane excess and absolute adsorption in various clay nanopores from molecular simulation. Sci. Rep. 7 (1), 12040. https://doi.org/10.1038/s41598-017-12123-x.
Tingay, M.R.P., Morley, C.K., Laird, A., et al., 2013. Evidence for overpressure generation by kerogen-to-gas maturation in the northern Malay Basin. AAPG Bull. 97 (4), 639–672. https://doi.org/10.1306/09041212032.
U.S. Energy Information Administration, 2022. Outlook for energy markets through 2050: U.S. dry natural gas production. https://www.eia.gov/outlooks/aeo/.
Wang, E.Z., Feng, Y., Guo, T.L., et al., 2022. Oil content and resource quality evaluation methods for lacustrine shale: a review and a novel three-dimensional quality evaluation model. Earth Sci. Rev. 232, 104134. https://doi.org/10.1016/j.earscirev.2022.104134.
Wang, F.Y., He, Z.Y., Meng, X.H., et al., 2011. Occurrence of shale gas and prediction of Original Gas In-place (OGIP). Nat. Gas Geosci. 22 (3), 501–510 (in Chinese).
Wang, H.Y., Zhou, S.W., Liu, D.X., et al., 2020a. Progress and prospect of key experimental technologies for shale gas geological evaluation. Nat. Gas. Ind. 40 (6), 1–17. https://doi.org/10.3787/j.issn.1000-0976.2020.06.001 (in Chinese).
Wang, J.J., Wang, B.E., Li, Y.J., et al., 2016a. Measurement of dynamic adsorption–diffusion process of methane in shale. Fuel 172, 37–48. https://doi.org/10.1016/j.fuel.2015.12.069.
Wang, M., Lun, Z.M., Zhao, C.P., et al., 2020b. Influences of primary moisture on methane adsorption within lower Silurian Longmaxi shales in the Sichuan Basin, China. Energy Fuels 34 (9), 10810–10824. https://doi.org/10.1021/acs.energyfuels.0c01932.

Wang, R.Y., Nie, H.K., Hu, Z.Q., et al., 2020c. Controlling effect of pressure evolution on shale gas reservoirs: a case study of the Wufeng–Longmaxi Formation in the Sichuan Basin. Nat. Gas. Ind. 40 (10), 1–11. https://doi.org/10.3787/j.issn.1000-0976.2020.10.001 (in Chinese).

Wang, X., Tian, H., 2018. Characteristics of competitive adsorption of multicomponent gases on shales: status and prospects. Geochimica 47 (3), 229–239. https://doi.org/10.19700/j.0379-1726.2018.03.001 (in Chinese).

Wang, X.Q., Zhai, Z.Q., Jin, X., et al., 2016b. Molecular simulation of CO_2/CH_4 competitive adsorption in organic matter pores in shale under certain geological conditions. Petrol. Explor. Dev. 43 (5), 841–848. https://doi.org/10.1016/S1876-3804(16)30100-8.

Wang, Y., Zhu, Y.M., Chen, S.B., et al., 2014. Characteristics of the nanoscale pore structure in Northwestern hunan shale gas reservoirs using field emission scanning electron microscopy, high-pressure mercury intrusion, and gas adsorption. Energy Fuels 28 (2), 945–955. https://doi.org/10.1021/ef402159e.

Wang, Y.M., Li, X.J., Chen, B., et al., 2018. Lower limit of thermal maturity for the carbonization of organic matter in marine shale and its exploration risk. Petrol. Explor. Dev. 45 (3), 402–411. https://doi.org/10.1016/S1876-3804(18)30045-4.

Wang, Y.M., Li, X.J., Dong, D.Z., et al., 2016c. Development mechanism of fracture pores in marine shale and its geological significance. Nat. Gas Geosci. 27 (9), 1602–1610. http://www.nggs.ac.cn/CN/10.11764/j.issn.1672-1926.2016.09.1602 (in Chinese).

Wei, M.M., Zhang, L., Xiong, Y.Q., et al., 2019a. Main factors influencing the development of nanopores in over-mature, organic-rich shales. Int. J. Coal Geol. 212, 103233. https://doi.org/10.1016/j.coal.2019.103233.

Wei, Q., Yan, B., Xiao, X.M., 2015. Research progress on the desorption methods of shale gas. Nat. Gas Geosci. 26 (9), 1657–1665. http://www.nggs.ac.cn/CN/10.11764/j.issn.1672-1926.2015.09.1657 (in Chinese).

Wei, S.L., He, S., Pan, Z.J., et al., 2019b. Models of shale gas storage capacity during burial and uplift: application to Wufeng-Longmaxi shales in the Fuling shale gas field. Mar. Petrol. Geol. 109, 233–244. https://doi.org/10.1016/j.marpetgeo.2020.104303.

Wei, S.L., He, S., Pan, Z.J., et al., 2020a. Characteristics and evolution of pyrobitumen-hosted pores of the overmature Lower Cambrian Shuijingtuo Shale in the south of Huangling anticline, Yichang area, China: evidence from FE-SEM petrography. Mar. Petrol. Geol. 116, 104303. https://doi.org/10.1016/j.marpetgeo.2020.104303.

Wei, X.F., Liu, Z.J., Wang, Q., et al., 2020b. Analysis and thinking of the difference of Wufeng-Longmaxi shale gas enrichment conditions between Dingshan and Jiaoshiba areas in southeastern Sichuan Basin. Nat. Gas Geosci. 31 (8), 1041–1051. http://www.nggs.ac.cn/CN/10.11764/j.issn.1672-1926.2020.02.011 (in Chinese).

Weniger, P., Kalkreuth, W., Busch, A., et al., 2010. High-pressure methane and carbon dioxide sorption on coal and shale samples from the Paraná Basin, Brazil. J. Int. J. Coal Geol. 84 (3–4), 190–205. https://doi.org/10.1016/j.coal.2010.08.003.

Whitelaw, P., Uguna, C.N., Stevens, L.A., et al., 2019. Shale gas reserve evaluation by laboratory pyrolysis and gas holding capacity consistent with field data. Nat. Commun. 10, 3659. https://doi.org/10.1038/s41467-019-11653-4.

Xia, X.Y., Tang, Y.C., 2012. Isotope fractionation of methane during natural gas flow with coupled diffusion and adsorption/desorption. Geochem. Cosmochim. Acta 77, 489–503. https://doi.org/10.1016/j.gca.2011.10.014.

Xiao, D.S., Lu, S.F., Shao, M.L., et al., 2021. Comparison of marine and continental shale gas reservoirs and their gas-bearing properties in China: the examples of the Longmaxi and Shahezi shales. Energy Fuels 35 (5), 4029–4043. https://doi.org/10.1021/acs.energyfuels.0c04245.

Xiao, X.M., Wei, Q., Gai, H.F., et al., 2015. Main controlling factors and enrichment area evaluation of shale gas of the Lower Paleozoic marine strata in south China. Petrol. Sci. 12 (4), 573–586. https://doi.org/10.1007/s12182-015-0057-2.

Xiong, J., Liu, X.J., Liang, L.X., et al., 2017. Adsorption of methane in organic-rich shale nanopores: an experimental and molecular simulation study. Fuel 200, 299–315. https://doi.org/10.1016/j.fuel.2017.03.083.

Xiong, W., Gong, Q.S., Duan, X.G., et al., 2020. Pressure building-up methodology to measure gas content of shale samples. J. Petrol. Sci. Eng. 186, 106678. https://doi.org/10.1016/j.petrol.2019.106678.

Xu, H., Zhou, W., Hu, Q.H., et al., 2019. Fluid distribution and gas adsorption behaviors in over-mature shales in southern China. Mar. Petrol. Geol. 109, 223–232. https://doi.org/10.1016/j.marpetgeo.2019.05.038.

Xu, H., Zhou, W., Hu, Q.H., et al., 2021a. Quartz types, silica sources and their implications for porosity evolution and rock mechanics in the Paleozoic Longmaxi Formation shale, Sichuan Basin. Mar. Petrol. Geol. 128, 105036. https://doi.org/10.1016/j.marpetgeo.2021.105036.

Xu, H.Y., Yu, H., Fan, J.C., et al., 2020a. Two-phase transport characteristic of shale gas and water through hydrophilic and hydrophobic nanopores. Energy Fuels 34 (4), 4407–4420. https://doi.org/10.1021/acs.energyfuels.0c00212.

Xu, L.L., Wen, Y.R., Zhang, Y.L., et al., 2021b. Gas-bearing characteristics and preservation conditions of upper Ordovician Wufeng-lower Silurian Longmaxi shale in western Hubei. Petrol. Geol. Exp. 43 (3), 395–405. https://doi.org/10.11781/sysydz202103395 (in Chinese).

Xu, L.L., Zhou, X.H., Chen, W., et al., 2021c. A study on shale gas preservational conditions of the lower cambrian Niutitang Formation in the western Hubei. Mar. Origin Petrol. Geol. 26 (2), 113–122. https://doi.org/10.3969/j.issn.1672-9854.2021.02.003 (in Chinese).

Xu, S., Gou, Q.Y., Hao, F., et al., 2020b. Shale pore structure characteristics of the high and low productivity wells, Jiaoshiba shale gas field, Sichuan Basin, China: dominated by lithofacies or preservation condition? Mar. Petrol. Geol. 114, 104211. https://doi.org/10.1016/j.marpetgeo.2019.104211.

Xu, Z.H., Zheng, M.J., Liu, Z.H., et al., 2020c. Petrophysical properties of deep Longmaxi Formation shales in the southern Sichuan Basin, SW China. Petrol. Explor. Dev. 47 (6), 1100–1110. https://doi.org/10.11698/PED.2020.06.04.

Yang, C., Xiong, Y.Q., Zhang, J.C., et al., 2019. Comprehensive understanding of OM-hosted pores in transitional shale: a case study of Permian Longtan shale in South China based on organic petrographic analysis, gas adsorption, and X-ray diffraction measurements. Energy Fuels 33 (9), 8055–8064. https://doi.org/10.1021/acs.energyfuels.9b01410.

Yang, C., Zhang, J.C., Han, S.B., et al., 2016a. Classification and the developmental regularity of organic-associated pores (OAP) through a comparative study of marine, transitional, and terrestrial shales in China. J. Nat. Gas Sci. Eng. 36, 358–368. https://doi.org/10.1016/j.jngse.2016.10.044.

Yang, F., Hu, B.Y., Xu, S., et al., 2018. Thermodynamic characteristic of methane sorption on shales from oil, gas, and condensate windows. Energy Fuels 32 (10), 10443–10456. https://doi.org/10.1021/acs.energyfuels.8b02140.

Yang, F., Ning, Z.F., Wang, Q., et al., 2016b. Pore structure characteristics of lower Silurian shales in the southern Sichuan Basin, China: insights to pore development and gas storage mechanism. Int. J. Coal Geol. 156 (15), 12–24. https://doi.org/10.1016/j.coal.2015.12.015.

Yang, F., Ning, Z.F., Zhang, R., et al., 2015. Investigations on the methane sorption capacity of marine shales from Sichuan Basin, China. Int. J. Coal Geol. 146, 104–117. https://doi.org/10.1016/j.coal.2015.05.009.

Yang, F., Xie, C.J., Ning, Z.F., et al., 2017. High-pressure methane sorption on dry and moisture-equilibrated shales. Energy Fuels 31 (1), 482–492. https://doi.org/10.1021/acs.energyfuels.6b02999.

Yang, P., Yu, Q., Mou, C.L., et al., 2021. Shale gas enrichment model and exploration implications in the mountainous complex structural area along the southwestern margin of the Sichuan Basin: a new shale gas area. Nat. Gas. Ind. B 8 (5), 431–442. https://doi.org/10.1016/J.NGIB.2021.08.002.

Yang, R., Jia, A.Q., He, S., et al., 2020. Water adsorption characteristics of organic-rich Wufeng and Longmaxi shales, Sichuan Basin (China). J. Pet. Sci. Eng. 193, 107387. https://doi.org/10.1016/j.petrol.2020.107387.

Yao, Y.B., Liu, J., Liu, D.M., et al., 2019. A new application of NMR in characterization of multiphase methane and adsorption capacity of shale. Int. J. Coal Geol. 201, 76–85. https://doi.org/10.1016/j.coal.2018.11.018.

Yi, J.Z., Bao, H.Y., Zheng, A.W., et al., 2019. Main factors controlling marine shale gas enrichment and high-yield wells in South China: a case study of the Fuling shale gas field. Mar. Petrol. Geol. 103, 114–125. https://doi.org/10.1016/j.marpetgeo.2019.01.024.

Yin, K.G., Zhang, C., Shan, C.A., et al., 2021. Geological characteristics and resource potential of the transitional shale gas in the Zhaotong National shale gas demonstration area. Nat. Gas. Ind. 41 (S1), 30–35. https://doi.org/10.3787/j.issn.1000-0976.2021.S1.004 (in Chinese).

Yu, L.J., Fan, M., Borjigin, T., et al., 2016. Shale gas occurrence under burial conditions. Petrol. Geol. Exp. 38 (4), 438–444+452. https://doi.org/10.11781/sysydz201604438 (in Chinese).

Zeng, L.B., Lyu, W.Y., Li, J., et al., 2016. Natural fractures and their influence on shale gas enrichment in Sichuan Basin, China. J. Nat. Gas Sci. Eng. 30, 1–9. https://doi.org/10.1016/j.jngse.2015.11.048.

Zeng, W.T., Ding, W.L., Zhang, J.C., et al., 2019. Analyses of the characteristics and main controlling factors for the micro/nanopores in Niutitang shale from China's southeastern Chongqing and northern Guizhou regions. Earth Sci. Front. 26 (3), 220–235. https://doi.org/10.13745/j.esf.sf.2018.10.1 (in Chinese).

Zhai, G.Y., Wang, Y.F., Bao, S.J., et al., 2017. Major factors controlling the accumulation and high productivity of marine shale gas and prospect forecast in Southern China. Earth Sci. 42 (7), 1057–1068. https://doi.org/10.3799/dqkx.2017.085 (in Chinese).

Zhai, G.Y., Wang, Y.F., Liu, G.H., et al., 2020. Enrichment and accumulation characteristics and prospect analysis of the Permian marine conticental multiphase shale gas in China. Sediment. Geol. Tethyan Geol. 40 (3), 102–117. https://doi.org/10.19826/j.cnki.1009-3850.2020.07003 (in Chinese).

Zhang, H.R., 2016. Gas content of the Silurian shale in the SE Sichuan Basin and its controlling factors. Nat. Gas. Ind. 36 (8), 36–42. https://doi.org/10.3787/j.issn.1000-0976.2016.08.005 (in Chinese).

Zhang, J.H., Wang, P., Li, X.F., et al., 2020a. Equilibrium adsorption and kinetic diffusion mechanism of CH_4/N_2 on coconut shell-based activated carbon. J. China Coal Soc. 45 (S1), 427–435. https://doi.org/10.13225/j.cnki.jccs.2019.1824 (in Chinese).

Zhang, J.K., He, S., Yan, X.L., et al., 2017a. Structural characteristics and thermal evolution of nanoporosity in shales. J. China Univ. Petrol. (Ed. Nat. Sci.) 41 (1), 11–24. https://doi.org/10.3969/j.issn.1673-5005.2017.01.002 (in Chinese).

Zhang, J.Z., Li, X.Q., Zou, X.Y., et al., 2019. Characterization of the full-sized pore structure of coal-bearing shales and its effect on shale gas content. Energy Fuels 33 (3), 1969–1982. https://doi.org/10.1021/acs.energyfuels.8b04135.

Zhang, L.C., Lu, S.F., Jiang, S., et al., 2018. Effect of shale lithofacies on pore structure of the Wufeng-Longmaxi shale in Southeast Chongqing, China. Energy Fuels 32 (6), 6603–6618. https://doi.org/10.1021/acs.energyfuels.8b00799.

Zhang, M., Fu, X.H., 2018. Study of the characteristics of marine–terrigenous facies shale from the Permo-carboniferous system in the Guxian block, southwest Qinshui Basin. Energy Fuels 32 (2), 1096–1109. https://doi.org/10.1021/acs.energyfuels.7b02556.

Zhang, S.R., Dong, D.Z., Liao, Q.S., et al., 2021. Geological characteristics and resource prospect of deep marine shale gas in the southern Sichuan Basin. Nat. Gas. Ind. 41 (9), 35–45. https://doi.org/10.3787/j.issn.1000-0976.2021.09.004 (in

Chinese).
Zhang, T.W., Ellis, G.S., Ruppel, S.C., et al., 2012. Effect of organic-matter type and thermal maturity on methane adsorption in shale-gas systems. Org. Geochem. 47, 120–131. https://doi.org/10.1016/j.orggeochem.2012.03.012.
Zhang, W.T., Hu, W.X., Borjigin, T., et al., 2020b. Pore characteristics of different organic matter in black shale: a case study of the Wufeng-Longmaxi Formation in the Southeast Sichuan Basin, China. Mar. Petrol. Geol. 111, 33–43. https://doi.org/10.1016/j.marpetgeo.2019.08.010.
Zhang, W.Z., Xie, L.Q., Yang, W.W., et al., 2017b. Micro fractures and pores in lacustrine shales of the upper triassic Yanchang Chang 7 member, Ordos Basin, China. J. Pet. Sci. Eng. 156, 194–201. https://doi.org/10.1016/j.petrol.2017.03.044.
Zhao, J.H., Jin, Z.J., Jin, Z.K., et al., 2017. Mineral types and organic matters of the Ordovician-Silurian Wufeng and Longmaxi Shale in the Sichuan Basin, China: implications for pore systems, diagenetic pathways, and reservoir quality in fine-grained sedimentary rocks. Mar. Petrol. Geol. 86, 655–674. https://doi.org/10.1016/j.marpetgeo.2017.06.031.
Zhao, T.Y., Li, X.F., Ning, Z.F., et al., 2018. Molecular simulation of methane adsorption on type II kerogen with the impact of water content. J. Petrol. Sci. Eng. 161, 302–310. https://doi.org/10.1016/j.petrol.2017.11.072.
Zheng, X.W., Zhang, B.Q., Sanei, H., et al., 2019. Pore structure characteristics and its effect on shale gas adsorption and desorption behavior. Mar. Petrol. Geol. 100, 165–178. https://doi.org/10.1016/j.marpetgeo.2018.10.045.
Zhou, D.H., Sun, C.X., Liu, Z.B., et al., 2020. Geological characteristics of continental shale gas reservoir in the Jurassic Da'anzhai member in the northeastern Sichuan Basin. China Petrol. Explor. 25 (5), 32–42. https://doi.org/10.3969/j.issn.1672-7703.2020.05.005 (in Chinese).
Zhou, N.W., Lu, S.F., Zhang, P.F., et al., 2022a. Continental shale gas dynamic enrichment and evolution over geological time. Int. J. Coal Geol. 251, 103914. https://doi.org/10.1016/j.coal.2021.103914.
Zhou, Q., Xiao, X.M., Tian, H., et al., 2014. Modeling free gas content of the lower Paleozoic shales in the Weiyuan area of the Sichuan Basin, China. Mar. Petrol. Geol. 56, 87–96. https://doi.org/10.1016/j.marpetgeo.2014.04.001.
Zhou, S.W., Wang, H.Y., Xue, H.Q., et al., 2018. Comparative analysis of calculation methods for lost gas in the field-test of shale gas content. China Sci. Paper 13 (21), 2453–2460 (in Chinese).
Zhou, S.W., Wang, H.Y., Xue, Q.H., et al., 2017a. Discussion on the supercritical adsorption mechanism of shale gas based on Ono-Kondo lattice model. Earth Sci. 42 (8), 1421–1430. https://doi.org/10.3799/dqkx.2017.543 (in Chinese).
Zhou, S.W., Wang, H.Y., Xue, Q.H., et al., 2017b. Supercritical methane adsorption on shale gas: mechanism and model. Chin. Sci. Bull. 62 (35), 4189–4200. https://doi.org/10.1360/N972017-00151 (in Chinese).
Zhou, S.W., Zhang, J.H., Zou, C., et al., 2022b. A new method for testing shale gas content based on pressure-holding coring technology. J. China Coal Soc. 47 (4), 1637–1646. https://doi.org/10.13225/j.cnki.jccs.2021.0249 (in Chinese).
Zhu, D.Y., Jiang, Z.X., Jiang, S., et al., 2021a. Water-bearing characteristics and their influences on the reservoir capacity in terrestrial shale reservoirs: a case study of the lower Jurassic Ziliujing Formation in the Northeast Sichuan Basin, China. Mar. Petrol. Geol. 123, 104738. https://doi.org/10.1016/j.marpetgeo.2020.104738.
Zhu, H.J., Huang, C., Ju, Y.W., et al., 2021b. Multi-scale multi-dimensional characterization of clay-hosted pore networks of shale using FIBSEM, TEM, and X-ray micro-tomography: implications for methane storage and migration. Appl. Clay Sci. 213, 106239. https://doi.org/10.1016/j.clay.2021.106239.
Zhu, H.J., Ju, Y.W., Huang, C., et al., 2020. Microcosmic gas adsorption mechanism on clay-organic nanocomposites in a marine shale. Energy 197, 117256. https://doi.org/10.1016/j.energy.2020.117256.
Zolfaghari, A., Dehghanpour, H., Xu, M.X., 2017. Water sorption behaviour of gas shales: II. Pore size distribution. Int. J. Coal Geol. 179, 187–195. https://doi.org/10.1016/j.coal.2017.05.009.
Zou, J., Rezaee, R., Liu, K.Q., 2017. Effect of temperature on methane adsorption in shale gas reservoirs. Energy Fuels 31 (11), 12081–12092. https://doi.org/10.1021/acs.energyfuels.7b02639.
Zou, C.N., Dong, D.Z., Wang, S.J., et al., 2010. Geological characteristics, formation mechanism and resource potential of shale gas in China. Petrol. Explor. Dev. 37 (6), 641–653 (in Chinese).
Zou, C.N., Yang, Z., Sun, S.S., et al., 2020. Exploring petroleum inside source kitchen": shale oil and gas in Sichuan Basin. Sci. China Earth Sci. 63, 934–953. https://doi.org/10.1007/s11430-019-9591-5.
Zou, C.N., Yang, Z., Tao, S.Z., et al., 2012. Nano-hydrocarbon and the accumulation in coexisting source and reservoir. Petrol. Explor. Dev. 39 (1), 15–32. https://doi.org/10.1016/S1876-3804(12)60011-1.
Zou, C.N., Zhao, Q., Cong, L.Z., et al., 2021. Development progress, potential and prospect of shale gas in China. Nat. Gas. Ind. 41 (1), 1–14. https://doi.org/10.3787/j.issn.1000-0976.2021.01.001 (in Chinese).
Zou, C.N., Zhao, Q., Wang, H.Y., et al., 2022a. The main characteristics of marine shale gas and the theory & technology of exploration and development in China. Nat. Gas. Ind. 42 (8), 1–13. https://doi.org/10.3787/j.issn.1000-0976.2022.08.001 (in Chinese).
Zou, C.N., Zhu, R.K., Chen, Z.-Q., et al., 2019. Organic-matter-rich shales of China. Earth Sci. Rev. 189, 51–78. https://doi.org/10.1016/j.earscirev.2018.12.002.
Zou, X.Y., Li, X.Q., Wang, Y., et al., 2022b. Reservoir characteristics and gas content of Wufeng-Longmaxi Formations deep shale in southern Sichuan Basin. Nat. Gas Geosci. 33 (4), 654–665. https://doi.org/10.11764/j.issn.1672-1926.2021.10.004 (in Chinese).